Structural and biochemical analysis of the RicAFT complex

Dissertation zur Erlangung des Doktorgrades
der Naturwissenschaften
(Dr. rer. nat.)

dem Fachbereich Chemie
der Philipps-Universität Marburg vorgelegt

Von

Gregor Hoffmann
Master of Science
Geboren am 9. September 1993

in Hann. Münden, Deutschland

Marburg Januar, 2021

Die Untersuchungen zur vorliegenden Arbeit wurden von Januar 2018 bis Dezember 2020 am LOEWE Zentrum für synthetische Mikrobiologie (SYNMIKRO) der Philipps-Universität Marburg unter der Leitung von Prof. Dr. Gert Bange durchgeführt.

Vom Fachbereich der Chemie der Philipps-Universität Marburg (Hochschulkennziffer 1180) als Dissertation angenommen am: 18.02.2021

Erstgutachter:	Prof. Dr. Gert Bange
Zweitgutachter:	Prof. Dr. Peter Graumann
Weitere Komiteemitglieder:	Prof. Dr. Martin Thanbichler
	Prof. Dr. Andreas Seubert

Tag der Disputation: 03.03.2021

Acknowledgements

First of all, I want to thank my supervisor Prof. Dr. Gert Bange for the great opportunity to learn and hone my skills during this work. The fruitful discussions provided valuable insights and encouraged further ideas for this work. Thank you very much Gert, for this atmosphere enabling me to prosper and develop myself.

Additionally, I am incredibly grateful for the whole LOEWE center, for the mutual support and great teamwork. Discussions and conversations were very exhilarating between the various groups.

Dr. Jan Schuller and Dr. Thomas Heimerl are to highlight for their help with negative staining and the cryo-EM experiments and subsequent structure determination. Your support and advice were very much appreciated!

The collaboration for the mass photometry data with Dr. Georg Hochberg and Niklas Steube was very fruitful and their input invaluable for this work.

Dr. Timo Glatter is also thanked for his help in the analysis of the CoIP experiments.

I also do not want to forget my dear colleagues of the Bange group. You always provided support, help and entertainment. The discussions and time spent together over the last three years will always be a memory to behold. Stay as you are and everyone contributed a little to this final work!

Moreover, I want to thank Dr. Wieland Steinchen for his help with the HDX data and its evaluation.

Special thanks go to Patty and Flo, for all the valuable lessons taught and keeping up with me. I learned a lot from you and always appreciated your suggestions for improvement.

However, there are also people outside the lab, that supported me, and I feel indebted to thank. Larissa, thank you for your advice and comfort. Robin and Marvin thanks for keeping me motivated and also provide me with some distraction. Jana and Adi and the others, you know who I mean, thanks for always being there for me and your support.

Lastly, I want to thank my family for believing in me and their continuous support. Mom and dad, thanks for allowing me to pursue my goals.

To all the people I mentioned and to the ones I forgot, thank you very much for your company along the road so far!

Summary

The regulation of protein amounts in the cell is of utmost importance, as imbalance can lead to cell death. Hence, the protein levels are meticulously balanced by a vast network of regulation. This network penetrates all levels of regulation, from transcription to translation and post-translational modification. Messenger RNA (mRNA) maturation is a regulatory process at the post-transcriptional level and enables the cell to adapt to environmental changes quickly and resourcefully. In *Bacillus subtilis*, a soil-dwelling model organism, a large margin of mRNA maturation is carried out by the endoribonuclease RNase Y. However, the precise regulation of the maturation is still not well understood and only some factors involved in the regulation of RNase Y are known, such as the RicAFT complex. This complex is associated with the RNase Y *in vivo* and controls the maturation and degradation of a plethora of different mRNAs. Additionally, the complex is vital for the switch between lifestyles, as a dysfunctional complex leads to various phenotypes: flat and unstructured biofilms, dysfunctional sporulation, and loss of genetic competence. Additionally, the RicAFT complex could be involved in a regulatory cascade of proteins that activates all these processes, essentially regulating the same processes possibly in two different pathways. The switching between these lifestyles is vital for bacteria to survive in an everchanging environment.

Hence, the RicAFT complex is a prime target for research, as it is conserved in Bacilli and many aspects of its role and function are unknown. Therefore, a biochemical and structural analysis of the complex is essential for understanding its function, which this work strives to achieve. Henceforth, various biochemical methods are employed to unravel its structure and its interaction sites. The complex is comprised of three proteins: RicA, RicF and RicT. These are not encoded in one operon yet form a stable complex. Their mechanism of interaction is unknown, as is the structure of the whole complex. However, it is known that the complex coordinates two [4Fe-4S] cluster and binds FADH, their role is yet to be determined. In this work, a comprehensive overview and biochemical analysis of the complex and its interactions is given.

Zusammenfassung

Die Regulation von Proteinmengen ist von höchster Wichtigkeit in Zellen, denn ein Ungleichgewicht könnte zum Zelltod führen. Daher werden Proteinmengen durch ein großes Netzwerk mit vielen Kontrollinstanzen sehr genau reguliert. Dieses Netzwerk reicht durch alle Ebenen der Regulation, von der Transkription über Translation, hin zu posttranslationalen Modifikationen. Die Maturierung der Boten-RNA (mRNA) ist ein posttranskriptionaler Prozess und ermöglicht der Zelle eine schnelle und ressourcenschonende Anpassung an wechselnde Umweltbedingungen. In *Bacillus subtilis*, ein im Boden vorkommendes Modelbakterium, wird ein großer Teil der mRNA Maturierung durch die RNase Y durchgeführt. Jedoch ist die genaue Regulation dieser Maturierung unbekannt. Trotzdem sind Faktoren bekannt, die diese zum Teil bewirken, wie der RicAFT Komplex. *In vivo* ist er mit der RNase Y assoziiert und reguliert die Reifung vieler unterschiedlicher mRNAs. Zudem ist er essenziell für den Wechsel zwischen verschiedenen Lebensarten des Bakteriums. Wenn er nicht vollständig ist, führt dies zu zahlreichen Phänotypen: flache und unstrukturierte Biofilme, keine funktionierende Sporulation und ein Verlust der genetischen Kompetenz. Weiterhin ist der RicAFT Komplex direkt involviert in einer Kaskade von Proteinen, die den Wechsel zu diesen Lebensstilen veranlassen. Somit reguliert der Komplex diese Wechsel auf zwei unterschiedlichen regulatorischen Ebenen und diese Veränderung der Lebensstile ist absolut lebensnotwendig in einer sich ständig wechselnden Umwelt. Daher ist der RicAFT Komplex ein hervorragendes Ziel zur Forschung, da viele Aspekte seiner Rolle und Funktion noch unverstanden sind und der Komplex in den Bacilli konserviert ist. Vor allem eine biochemische und strukturelle Beschreibung des Komplexes ist unabdingbar zum Verständnis seiner Funktion, was in diese Arbeit versucht wird zu erreichen. Daher wurden verschiedene biochemische Methoden angewandt, um mehr von seiner Struktur und dessen Interaktionen zu erfahren. Der Komplex setzt sich aus drei einzelnen Proteinen zusammen: RicA, RicF und RicT. Diese sind nicht in einem Operon konserviert, bilden jedoch einen stabilen Komplex. Wie sie interagieren ist aber unbekannt, wie auch die Struktur des kompletten Komplexes. Es ist nur bekannt, dass zwei [4Fe-4S] Komplexe durch diesen koordiniert werden, sowie dass der Proteinkomplex FADH bindet, ihre Funktionen sind jedoch unbekannt. Daher wird diese Arbeit versuchen einen verständlichen Überblick mit einer biochemischen Analyse des Komplexes und seiner Interaktionen zu geben.

Table of Contents

Chapter Page

List of Abbreviations

Abbreviations

Abbreviation	Meaning
% (v/v)	% (volume/volume)
% (w/v)	% (weight/volume)
ad	up to
ADP	adenosine diphosphate
Amp	ampicillin
AMP	adenosine monophosphate
APS	ammonium peroxydisulfate
ATP	adenosine triphosphate
AU	absorption unit
B.	*Bacillus*
bp	base pairs
BSA	bovine serum albumin
BS^3	(bis(sulfosuccinimidyl)suberate)
cDNA	complementary DNA
Cm	chloramphenicol
CoA	coenzyme A
Cryo-EM	cryo-electron microscopy
CV	column volume
DMSO	dimethyl sulfoxide
DNA	deoxyribonucleic acid
dNTP	deoxyribonucleotide
E.	*Escherichia*
e.g.	exempli gratia
EDTA	ethylenediaminetetraacetic acid
et al.	*et alia*; and others
EV	empty vector
Fwd.	forward
HF	high fidelity
HDX	$^1H/^2H$ exchange mass spectrometry
IPTG	isopropyl β-D-1-thiogalactopyranoside
ISC	Iron-sulfur cluster
Kan	kanamycin
LB	lysogeny broth
MALS	multi angle light scattering
mRNA	messenger RNA
MR	molecular replacement
MS	mass spectrometry
MW	molecular weight
Na	sodium
OD_x	optical density at a certain wavelength λ= x nm
p	plasmid
PBS	phosphate buffered saline

PCR	polymerase chain reaction
PDB	protein data bank
PEP	phosphoenolypyruvate
pH	*potentia Hydrogenii*
P_i	inorganic pyrophosphate
RBS	ribosomal binding site
Rev.	reverse
RNA	ribonucleic acid
rpm	revolutions per minute
rRNA	ribosomal RNA
RT	room temperature
X S	X sedimentation coefficient
SAM	S-adenosyl methionine
SEC	size exclusion chromatography
SDS-PAGE	sodium dodecyl sulfate polyacrylamide gel electrophoresis
SOB	super optimal broth
T4	T4 phage
TAE	TRIS-acetic acid-EDTA
Taq	*Thermus aquaticus*
TCA	tricarboxylic acid cycle
TEM	transmission electron microscopy
TRIS	Tris(hydroxymethyl)aminomethane
tRNA	transfer RNA
UTR	untranslated region
UV	ultraviolet
wt	wild type
λ	lambda / wavelength
σ	sigma

Nucleotides

Abbreviation	Meaning
A	adenine
C	cytosine
G	guanine
T	thymine
U	uracil

Prefixes

Abbreviation	Meaning
k	Kilo (10^{3})
m	milli (10^{-3})
µ	micro (10^{-6})
n	nano (10^{-9})
p	pico (10^{-12})

Units

Abbreviation	Meaning
°C	degree Celsius
A	Ampere
bar	Bar
Da	Dalton
g	Gram
h	Hour
l	Liter
m	Meter
min	Minute
s	Second
mol	Mol
M	Molar
V	Volt

1. INTRODUCTION

1.1. mRNA regulation in Gram-positive bacteria

DNA (deoxyribonucleic acid) is the most basic conveyor of genetic information. Nonetheless, RNA (ribonucleic acid) is the keystone in the transfer of genetic information to the protein level. In this process, RNA is involved in every step from DNA transcription to its translation into proteins (Lodish *et al.*, 2000). First, transcription leads to the formation of messenger RNA (mRNA), this information is then decoded by the interplay of transfer RNA (tRNA) and ribosomal RNA (rRNA) in the ribosome, leading to the synthesis of proteins.

rRNA and tRNA are both subject to massive modifications and/or processing prior their utilization, rRNAs undergo processing before their incorporation into the ribosome, e.g. the trimming of the 5S RNA in *Bacillus subtilis* (Sogin and Pace, 1974). tRNAs are massively modified during their maturation and these modifications are a significant factor for the translation fidelity (Miller *et al.*, 1976; Weissenbach and Grosjean, 1981). A common site for modifications is residue 37 due to its influence on residue 36, which is the third reside of the anticodon. In *B. subtilis* the modification is dependent on the base preceding it, for instance, a i^6A (isopentyl modification at the C6 position of the adenosine) or a ms^2i^6A (thiomethylation at the C2 position of the adenosine) is the most frequent

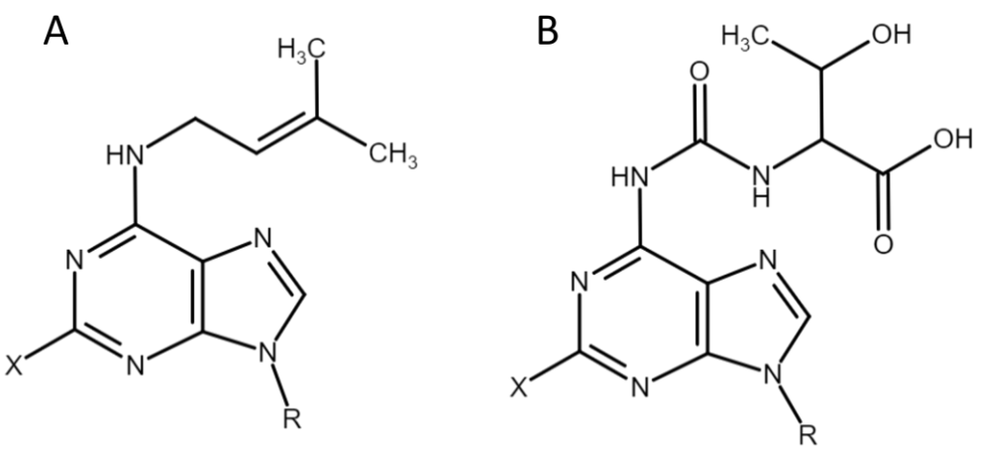

Figure 1: Adenine modifications in tRNA.
A) i^6A when X=H and ms^2i^6A when X= SCH_3. B) t^6A when X= H and ms^2t^6A when X= SCH^3 (modified from Anton *et al*., 2010).

modification if base 36 is an adenine, while a t^6A or ms^2t^6A is most prevalent adaptation if it is an uracil, see Figure 1 (Nishimura and Schimmel, 1979; Czerwoniec *et al.*, 2009).

Similar modifications are known for mRNA in bacteria; however, their regulation and repercussions are unknown at wide.

Although this form of post-transcriptional processing of mRNA in bacteria is not well studied, it adds another layer to the regulation for rapid adaptation and therefore, can be a deciding factor in cell fate. *B. subtilis* is a research model organism for Gram-positive bacteria as the bacterium can switch between various lifestyles: swarming motility, biofilm formation, or sporulation. The switching between these states is accompanied by major shifts in mRNA production and maturation (Branda *et al.*, 2001; Earl *et al.*, 2008; van Dijl and Hecker, 2013; Vlamakis *et al.*, 2013; Hölscher *et al.*, 2015). To study the proceedings by which these switches are occurring is of utmost importance since biofilm formation and sporulation are associated with pathogenicity, persistence, and drug resistance in Gram-positive bacteria, posing an increasing risk for human health (Costerton, 1999; Mah and O'Toole, 2001; Davies, 2003; Kolter and Greenberg, 2006; Hall-Stoodley and Stoodley, 2009; Cutting and Ricca, 2014).

1.1.1. Maturation of mRNA

RNAs have varying lifetimes, while *B. subtilis* rRNAs and tRNAs have lifespans between hours and days (Kimura and Waldor, 2019; Schostag *et al.*, 2020) mRNAs generally exist for about five minutes at optimal growth conditions (Hambraeus *et al.*, 2003). These time frames can be altered by cleavage within a polycistronic mRNA transcript, generating different translation patterns of genes in one operon (DeLoughery *et al.*, 2018).

Polycistronic mRNA can be processed via cleavage within the strand performed by endoribonucleases such as RNase Y (Rny) or RNase E. Other mechanisms involve removal of the triphosphate head from the 5'-end and ensuing degradation by a 5'-exoribonuclease such as RNase J1 or by a 3'-exoribonuclease. Other mRNA decay initiators exist in *B. subtilis*, including RNase III, an endonuclease specifically cleaving double stranded RNAs (Mari and Bechhofer, 1993; Oguro *et al.*, 1998; Huntzinger *et al.*, 2005; Stead *et al.*, 2011; Durand *et al.*, 2012; Durand *et al.*, 2015). A schematic overview of the various RNases and their function is given in Figure 2.

The major endoribonuclease involved in mRNA maturation in *B. subtilis* is RNase Y, which is responsible for the maturation of about a quarter of all mRNAs (Lehnik-Habrink *et al.*, 2011; Durand *et al.*, 2012; Figaro *et al.*, 2013). RNase Y is thought to form the so-called degradosome, in which it associates with metabolic enzymes such as enolase, CshA, phosphofructokinase, and PNPase, required for certain RNA degradation events (Commichau *et al.*, 2009; Lehnik-Habrink *et al.*, 2010; Salvo *et al.*, 2016). In *B. subtilis* the mRNA degradation activity of RNase Y is tightly controlled by the so-called Y-complex (RicAFT) (DeLoughery *et al.*, 2016). Disruption of the RicAFT complex has a major influence on the transcriptome of *B. subtilis* and causes distinct phenotypes, which will be discussed later (1.2, DeLoughery *et al.*, 2018).

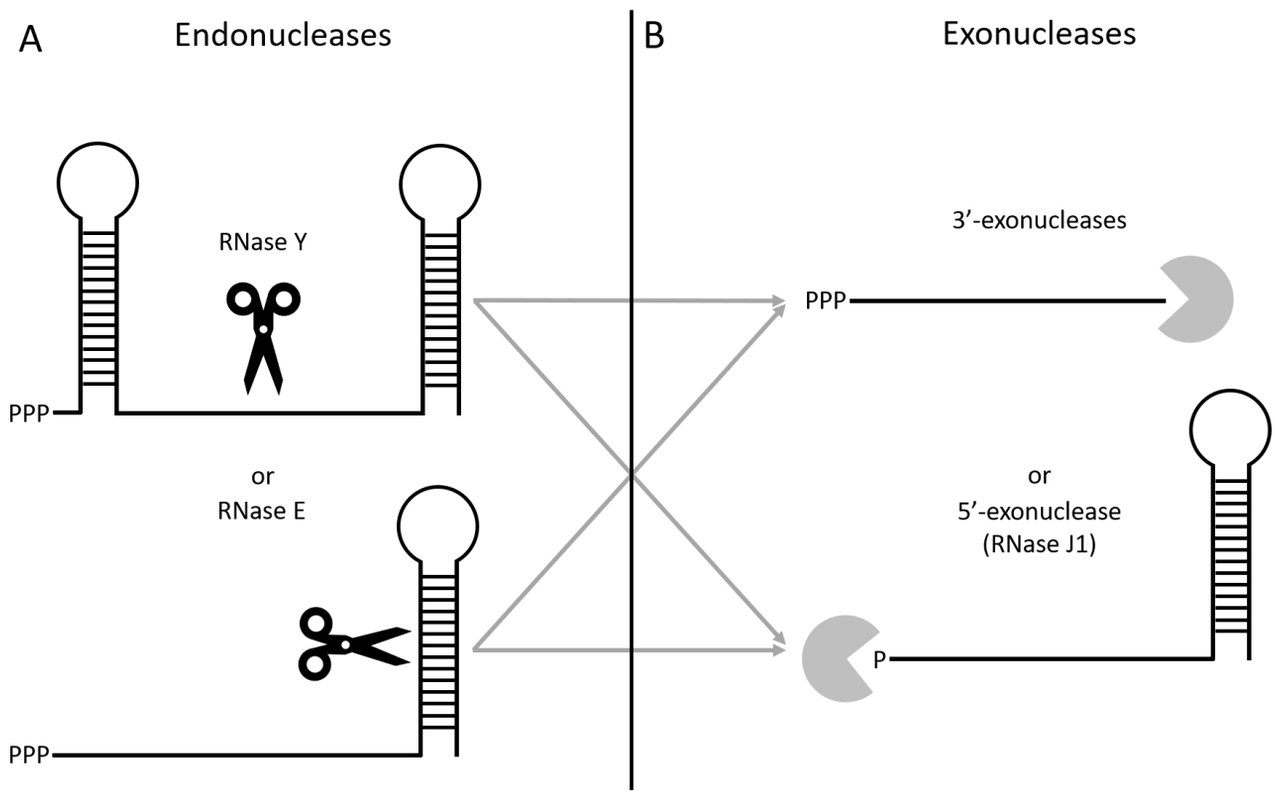

Figure 2: Schematic overview of various RNases and their function.
A) The rate limiting step for mRNA degradation in bacteria is the first endonucleolytic cleavage by endonucleases such as RNase Y or RNase III since the 5'-end is often protected by polyphosphorylation and/or secondary structures, while for the 3'-end only the latter applies. RNases recognize certain motives, a certain sequence of nucleotides, or a specific secondary structure to bind and cleave in their vicinity. There cleavage generates mRNAs without protected 5'-ends or 3'-ends and can dissolve secondary structures. B) The unprotected mRNA fragments can then be targeted by exonucleases. 3'-exonucleases degrade the mRNA from the 3'-end, while 5'-exonucleases degrade these from monophosphorylated 5'-ends (adapted from Trinquier *et al.*, 2020).

RNase Y primarily cleaves inside AU- rich regions with a G-residue directly upstream (Khemici *et al.*, 2015), causing a break in the mRNA and generating a 5'-end without a protective 3'-loop that is sensitive to 3'-exoribonucleases like PNPase or RNase R (Oussenko *et al.*, 2005). The old 3'-end can

undergo further degradation by RNase Y, exhibiting an additional 3’-exonuclease activity, or by 0oother 5’-exonucleases. (Trinquier *et al.*, 2020).

Monophosphorylated 5’-caps can also be generated through endoribonucleolytic cleavage by RNase III or RNase J2, riboswitches that cause self-cleavage, or dephosphorylation by RppH (Mathy *et al.*, 2007; Collins *et al.*, 2007; Richards *et al.*, 2011; Durand *et al.*, 2012). Once the mRNA with an accessible 5’-end is generated, a 5’-exoribonuclease may proceed with the mRNA degradation. *B. subtilis* encodes the 5’-exoribnuclease RNase J1, which can target monophosphorylated 5’-ends. RNase J1 has been speculated to form heterodimers with RNase J2, which could directly provide it with substrates (Commichau *et al.*, 2009; Lehnik-Habrink *et al.*, 2010; Newman *et al.*, 2011). Inactivation of RNase J1 or RNase Y cause severe phenotypes and often lead to loss of sporulation, genetic competence, and biofilm formation. Additionally, such mutants have an increased sensitivity to stresses such as heat or starvation (Lehnik-Habrink *et al.*, 2011; Durand *et al.*, 2012; Figaro *et al.*, 2013). These effects underline the importance of the regulation of mRNA degradation and processing.

An example of a type of regulation of the RNases are modifications by other proteins. Phosphorylation and acetylation are known to regulate the activity and stability of RNase II, RNase III and, RNase R in *E. coli* (Liang and Deutscher, 2012; Song *et al.*, 2016). An example of this is the *E. coli* protein YmdB, a 2’-O-acetyl-ADP-ribose deacetylase, which acts as a cofactor of RNase III by direct binding, modulating its activity. Although, nothing similar is known about RNase III in *B. subtilis* (Kim *et al.*, 2008; Zhang *et al.*, 2015). While phosphorylation and acetylation of RNases has been detected in *B. subtilis*, their purpose is yet unknown (Ravikumar *et al.*, 2018).

The activity of RNases can further be modified by modifications of the RNA itself, such as NAD-, Np4-caps or methylation, that are described in the following subchapter (Coste *et al.*, 1987; Kowtoniuk *et al.*, 2009; Deng *et al.*, 2015; Bird *et al.*, 2016; Luciano *et al.*, 2019). Another contributor to the regulation of mRNA are secondary structures within the mRNA. These can hinder degradation of mRNA by 3’- or 5’-exoribonucleases. These secondary structures can be resolved by specific endoribonucleases, degrading these parts (Trinquier *et al.*, 2020). If such structures are present in the 3’-end of the mRNA, degradation can still be initiated with the help of an RNA-helicase like CshA and subsequent degradation by PNPase (Liou *et al.*, 2002; Huen *et al.*, 2017; Ingle *et al.*, 2020). This is not exclusive for the 3’-tail as the 5’-head can also have secondary structures, making

monophosphorylated caps inaccessible for RNase J1 or polyphosphorylated caps inaccessible for RppH (Deana *et al.*, 2008; Dorléans *et al.*, 2011; Richards *et al.*, 2011). Nonetheless, secondary structures can serve as specificity markers and may be required for the activity of endoribonucleases such as RNase Y (Marincola and Wolz, 2017). RNase III is also able to cut within double stranded regions of RNA, implying secondary structures (Mari and Bechhofer, 1993; Oguro *et al.*, 1998; Huntzinger *et al.*, 2005; Durand *et al.*, 2015). Lastly, the translation process itself affects the activity of RNA degradation, as stalled ribosomes can either protect mRNAs in translation from degradation (Hue and Bechhofer, 1991; Agaisse and Lereclus, 1996) or cause degradation via Rae 1 (Leroy *et al.*, 2017).

1.1.2. mRNA modifications

An additional layer for post-transcriptional regulation of genes is the modification of the mRNA itself in various forms, as indicated above. While much is known about post-transcriptional modifications in tRNAs and rRNAs, the modifications of bacterial mRNAs have yet to be studied (Marbaniang and Vogel, 2016).

Bacterial mRNA can undergo multiple 5'-cap modifications, see Figure 3, like coenzyme nicotinamide adenine dinucleotide (NAD) caps, which is incorporated into the mRNA by non-canonical transcription initiation. The first nucleotide of the promoter plays a significant role for the incorporation of NAD, e.g. thymine is more prevalent than cytosine, however NAD- capping occurs only on a small portion of mRNAs. The NAD-capping protects mRNA from degradation the by 5'-riboexonucelase RNase J1, yet the implications and regulation of this process is not entirely understood. It was suggested that NAD-capping adds an additional layer of regulation for translation in changing environments (Bird *et al.*, 2016; Frindert *et al.*, 2018).

Another kind of cap modification supposed to increase the stability of mRNA are Np_4 caps (Figure 3). These are synthesized when dinucleosides tetraphosphates (Np_4N) are present in abundance, mostly under stress, produced by aminoacyl-tRNA synthetases. These can then be incorporated by the RNA polymerase or the lysyl-tRNA synthetase into mRNA in *E. coli* (Coste *et al.*, 1987; Luciano *et al.*, 2019).

A rare 5'-cap modification is the post-transcriptional introduction of Coenzyme A (CoA). This happens via post-transcriptional thioesterification and has various forms, such as 3'-dephospho-CoA or succinyl-dephospho-CoA, an example as shown in Figure 3. These modifications are quite rare, and

an exact function has not been ascribed though they might be involved in localization, stability, or translation regulation (Kowtoniuk *et al.*, 2009). Plenty of these 5'-cap modifications are observed during oxidative stress, suggesting an important role during the adaptation to this condition (Bochner *et al.*, 1984; Gout, 2019). Methylation is also present in *B. subtilis* mRNA (e.g. m^6A; Figure 1) however, less frequent than in other bacteria as only 0.08% of all mRNAs are methylated. The incidence is minor even though the modification can occur along the whole mRNA molecule, in addition, its effects are unknown (Deng *et al.*, 2015).

Polyadenylation of 3'-mRNA tails represent another form of mRNA modification. In Gram-positive bacteria the tails are shorter than in Gram-negative bacteria, and a dedicated enzyme such as PAP I (poly(A) polymerase I) is missing. Their role is yet to be identified, but it has been suggested that they are linked to the degradation specificity of mRNA (Li *et al.*, 1998; Campos-Guillén *et al.*, 2005).

All in all, these examples show that several regulating modifications are used by the cell, however their function and precise regulation is still speculative.

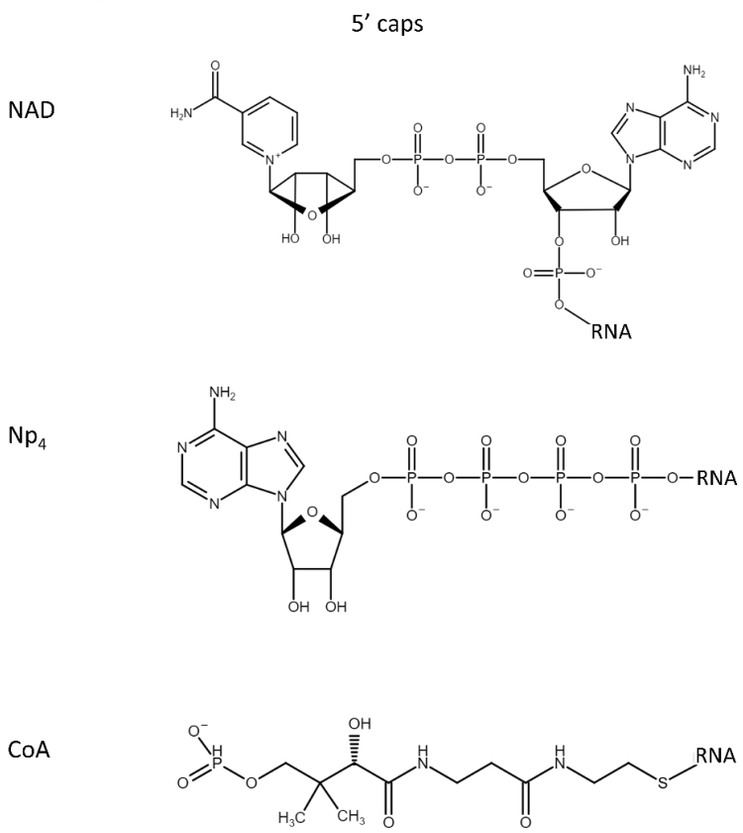

Figure 3: Schematic representations of 5'-cap modifications of bacterial mRNAs.
For NAD the exact structure is unknown, a possible conformation is represented (Bird *et al.*, 2016; Frindert *et al.*, 2018). For Np_4 an adenine was chosen as representation of a nucleotide, but T, G, and U are possible as well (Coste *et al.*, 1987; Luciano *et al.*, 2019). For CoA, the 3'-dephospho-CoA was chosen as representation (Kowtoniuk *et al.*, 2009).

1.2. The RicAFT complex

As aforementioned, the RicAFT complex is crucial for the regulation of mRNA maturation and stability in *B. subtilis* and its switch from a motile to a sessile biofilm forming lifestyle (DeLoughery *et al.*, 2016; DeLoughery *et al.*, 2018). During a screen for genes required for biofilm formation *ricA* (*ymcA*) and *ricF* (*ylbF*) were discovered, and either disruption caused major impairment (Tortosa *et al.*, 2000; Branda *et al.*, 2004). The third major player of the complex, *ricT* (*yaaT*) was later discovered by pull-down experiments and its disruption caused similar phenotypes: smooth unstructured biofilms, loss of genetic competence and a near stop in sporulation, yet less severe than a deletion of *ricA* or *ricF* (Carabetta *et al.*, 2013; DeLoughery *et al.*, 2016). In later analysis of the singular genes, it has been discovered that the three proteins form a complex with a 1:1:1 stoichiometry (Carabetta *et al.*, 2013; DeLoughery *et al.*, 2016). They were renamed to RicAFT, since the complex was found to regulate RNase Y and contain iron-sulfur clusters, hence Ric (regulatory iron-sulfur containing complex) (Carabetta *et al.*, 2013; DeLoughery *et al.*, 2016; Tanner *et al.*, 2017; DeLoughery *et al.*, 2018).
Since the deletion of these three genes independently affect biofilm formation and sporulation, the function of these proteins in both processes is of special interest.

1.2.1. RicAF: A subcomplex

RicF and RicA were first identified in the early 2000s (Tortosa *et al.*, 2000; Branda *et al.*, 2004). RicF has been initially discovered as a regulator for sporulation and competence, as it is involved in the post-transcriptional regulation of *comK* (Tortosa *et al.*, 2000). Later, *ricA* was discovered, together with *ricF*, during a screen for mutations that disrupt biofilm formation and sporulation. Mutants with deletions of *ricA* or *ricF* form inhomogeneous pellicles, and biofilms on solid medium are unstructured and smooth (Branda *et al.*, 2004). These phenotypes are overcome by mutations in *sinR*, that were most likely loss of function mutations (Branda et al., 2004, Kearns et al., 2004). SinR is the major repressor of biofilm formation and its activity is in turn countered by SinI (Kearns *et al.*, 2004). Since both deletions of *ricA* and *ricF* were overcome by the loss of activity of SinR, the conclusion was drawn that RicAF must act in one pathway (Branda *et al.*, 2004).
It has been proposed that the effect of the *ricF* deletion is simply caused by the increased instability of ComK due to decrease of ComS. ComK is responsible for the activation of competence in *B. subtilis*

and the regulation of over 100 genes (van Sinderen and Venema, 1994; Sinderen *et al.*, 1995; Berka *et al.*, 2002; Hamoen *et al.*, 2002). ComS increases the protein stability of ComK by binding to the protease ClpCP and the adaptor protein MecA, thereby inhibiting degradation of ComK (D'Souza *et al.*, 1994; Hamoen *et al.*, 1995; Turgay *et al.*, 1997; Turgay K *et al.*, 1998). While deletion of *comK* in the presence of RicF does not affect biofilm formation, biofilms are highly affected upon the deletion of *ricF*. This allows the conclusion that RicF must have further regulatory functions than the regulation of ComK (Tortosa *et al.*, 2000; Branda *et al.*, 2004). In *B. subtilis*, *ricA* is encoded in an operon with the tRNA methylthiotransferase *ymcB* (*miaB*) (Anton *et al.*, 2010). This organization is conserved in several species, such as *Staphylococcus aureus* or *Clostridioides difficile*. Like RicF (149 amino acids), RicA is a short protein with 143 amino acids whose exact function is unknown. The two proteins are not only similar in length, but they also share a high sequence similarity (19 % identity, 51% similarity) see Figure 4. Despite this, they do not seem to be homologous in function as they do not complement the deletion of one another (Branda *et al.*, 2004; DeLoughery *et al.*, 2016). Noteworthy differences between them include the C-terminal region of RicF, which is astonishingly cysteine- and glycine-rich. A structural comparison will be presented later.

RicA has been found to form homodimers that form a clamp-like structure (PDB: 6PRH, shown in Figure 5; Adusei-Danso *et al.*, 2019) yet the function of this complex remains unknown. *ricF* is encoded in a two gene operon with *ylbG* but still has its own terminator. *ylbG* has no assigned function and its dysregulation is not the cause of the phenotypes of a *ricF* disruption, as it is transcribed normally and its deletion does not phenocopy a *ricF* deletion (Branda *et al.*, 2004). However, this operon structure is not completely accurate, as revealed by the transcriptomic data, therefore, the operon could be extended to *ricF-ylbG-ylbH-ylbI* (Nicolas *et al.*, 2012). Despite *ricA* and *ricF* being located in different operons, they are upregulated by Spo0A~P during exponential growth (Tanner *et al.*, 2017). As described above, RicF shares similarities with RicA and is involved in the same pathway as RicA. Later studies have been able to discover that it forms a heterodimer with RicA. X-ray analysis resolved the crystal structure and revealed that RicA and RicF form heterotetramers in a 2:2 stoichiometry (Figure 5; PDB: 6PRK; Adusei-Danso *et al*., 2019).

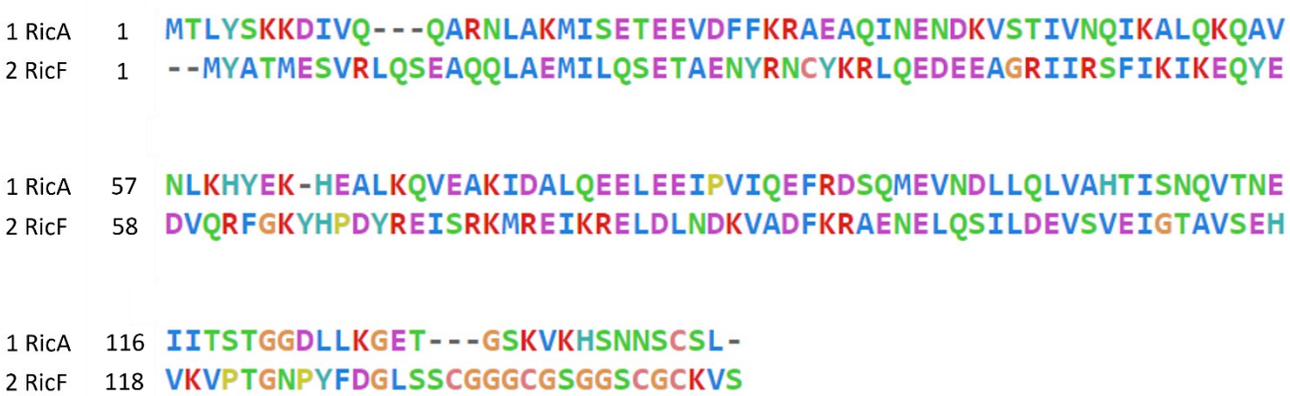

Figure 4: Protein sequence comparison of *B. subtilis* RicA and RicF.
The sequence comparison was done with BLAST. Positively charged amino acids are colored red, negatively charged purple, neutral polar green, non-polar blue, glycine is orange, cyclic polar are turquoise, proline is yellow, and cysteine is salmon colored.

This complex forms even when the C-termini of the proteins are truncated by about 20 amino acids. Contrarily, in solution the full-length complex behaved like a 1:1 heterodimer of RicA and RicF (Adusei-Danso *et al.*, 2019). It is worth mentioning that the crystal structures of the RicA homodimer and the RicAF heterodimer look remarkably similar (Figure 5) as both complexes are characteristic in the formation of a clamp-like structure. However, RicA alone cannot mimic the function of RicF and *vice versa* (Branda *et al.*, 2004). In addition, the N- and C-termini of both proteins are in close vicinity to each other and the clamp forms a large space in between of ~50 Å. The proteins interact via their N- and C-terminal regions by helices α1, α2, and α5 (see Figure 5; Adusei-Danso *et al.*, 2019). As shown in Figure 5 by the superimposition of the dimers of the RicA/RicF and RicA complexes, the structures are nearly identical. Even so, there are distinct differences. For one, the hinges in the RicAF heterodimer are not aligning with the hinges of the RicA dimer. Also noteworthy is the stronger distortion of the RicA N- and C-termini away from the axis of the RicAF complex in comparison to the RicA homodimer. Recently it has been found that RicA is acetylated at lysines K41, K64, and K133, and it was suggested that the acetylation at position 64 is crucial for biofilm formation (Reverdy *et al.*, 2018). This study also revealed that many proteins involved in biofilm formation are acetylated, such as Spo0A and TasA (Reverdy *et al.*, 2018). This post-translational modification possibly adds another layer of regulation to RicA and the RicAFT complex. In this context it is important to know that RicAF is concomitantly conserved in Bacilli and the genes are only found in this phylum. An exception is *Streptococcus salivarius* in which no RicA was found, but only RicF. However, this might be due to a large genetic variance in RicA (Table 1; Tanner *et al.*, 2017).

Table 1: RicAFT distribution in various organisms. X marks the organism in which the corresponding protein is present. In parenthesis the percentage of identity in comparison to the *B. subtilis* homologs is given.

Organism	RicA (% identity)	RicF (% identity)	RicT (% identity)
Bacillus subtilis	**X (100)**	**X (100)**	**X (100)**
Geobacillus thermodenitrificans	**X (61)**	**X (55)**	**X (78)**
Staphylococcus aureus	**X (35)**	**X (40)**	**X (62)**
Listeria monocytogenes	**X (47)**	**X (54)**	**X (66)**
Streptococcus pneumoniae	**X (66)**	**X (60)**	**X (67)**
Clostridioides difficile	**_**	**_**	**X (60)**
Thermotoga maritima	**_**	**_**	**X (49)**
Deinococcus radiodurans	**_**	**_**	**X (40)**
Crenarchaeota archaeon	**_**	**_**	**X (58)**
Schizosaccharomyces pombe	**_**	**_**	**X (29)**

In contrast to the variable N-terminus, the cysteine- and glycine-rich C-terminus of RicF is highly conserved among different species, except *Streptococcus salivarius*. The conserved region of RicA seems to be the central region of the protein rather than its termini. Unfortunately, the conserved C-terminus of RicF is not resolved as it was truncated by 20 amino acids in the study by Adusei-Danso *et al.*, 2019. This is possibly due to the flexibility of the C-terminus, which is detrimental for crystal packing. The gathered evidence exemplifies the importance of the heterocomplex and the interdependence of the proteins it is composed of. Nonetheless, RicAF only makes up two third of the regulating RicAFT complex. The far more widespread protein RicT is as an additional indispensable building block of the complex.

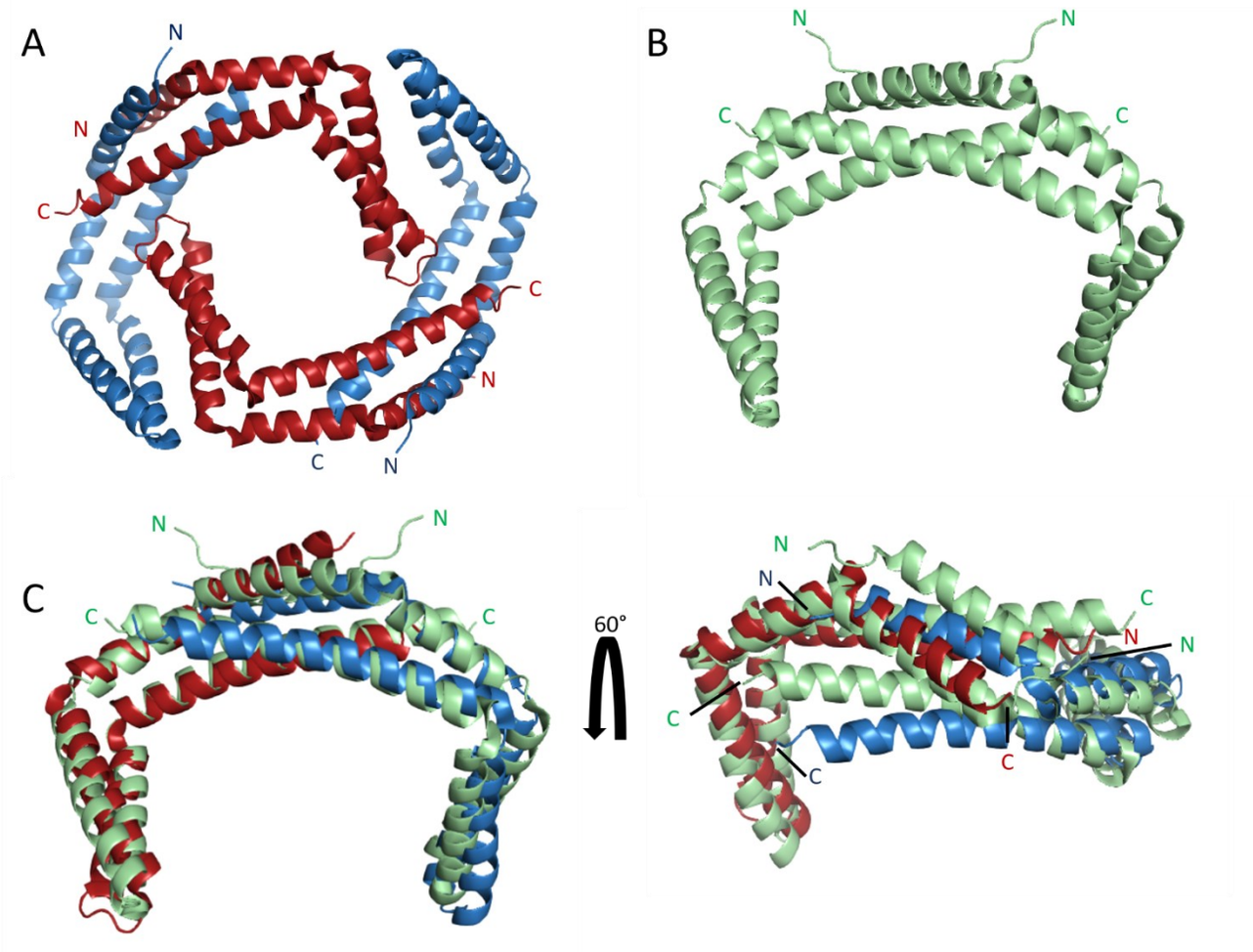

Figure 5: Crystal structure of RicA homodimer and RicAF heterodimer.
A) RicF is colored in red, RicA in blue. N- and C-termini are labeled in their respective color. Note that the structures are not complete, RicA is modeled from L5 to T121 and RicF is modeled from E6 to K120 (PDB: 6PRK, Adusei-Danso *et al*., 2019). B) RicA homodimer N- and C-termini are labeled (PDB:6PRH, Adusei-Danso *et al*., 2019). C) Superimposition of RicAF heterodimer and RicA dimer and, a 60° rotation of the superimposition. The color code has been maintained from the previous figures.

1.2.2. RicT: The missing center piece

ricT is encoded in a large operon with seven other genes, amongst which *darA*, *holB*, *yabA*, and *trmN6* have known functions. These proteins are involved in second messenger binding (DarA), tRNA methylation (TrmN6) or replication (HolB, YabA) (Noirot-Gros *et al.*, 2002). RicT was initially identified as a stage 0 sporulation protein, stopping sporulation before it is initiated (Piggot and Coote, 1976; Hosoya *et al.*, 2002). Sporulation and biofilm formation in *B. subtilis* are regulated by a phosphorelay in which Spo0A plays a major role (Burbulys *et al.*, 1991; Fujita *et al.*, 2005; Chai *et al.*, 2010). In Figure 6 a simplified scheme of this regulation is shown.

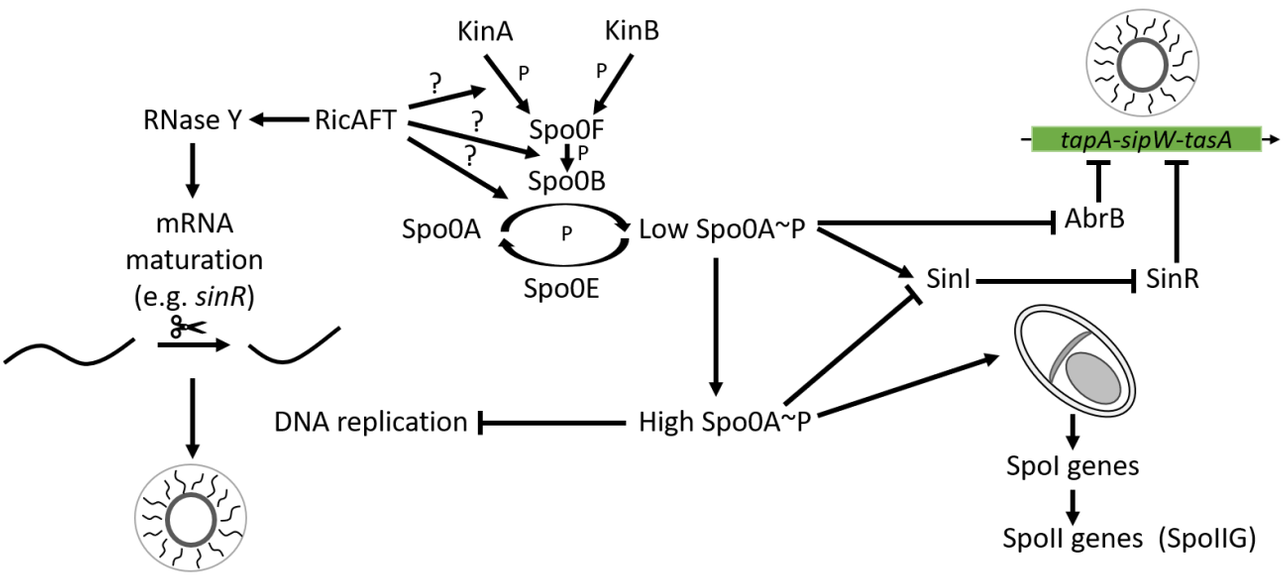

Figure 6: Phosphorelay network of Spo0A.
Signals detected by the kinases KinA or KinB cause phosphorylation of Spo0F and subsequently Spo0B. Spo0B then phosphorylates Spo0A continuously, while the phosphatase Spo0E dephosphorylates Spo0A constantly. When enough Spo0A molecules are phosphorylated, biofilm formation is activated by expression of SinI and repression AbrB. However, if more Spo0A is phosphorylated, biofilm formation is repressed and sporulation is initiated.

The stage 0 sporulation phenotype can be bypassed by a Spo0A mutation that causes autophosphorylation, thereby alleviating the need for the phosphorelay and disproving the necessity of RicT for spore formation. RicT has no influence on the stability of Spo0A, though it acts on the mRNA stability of *spo0A* and is located to the membrane during sporulation and cell division. Hence, it was implied that RicT is involved in the phosphorelay of Spo0A (Hosoya *et al.*, 2002; DeLoughery *et al.*, 2018). For localization of RicT to the membrane RNase Y is necessary, otherwise RicT is distributed in the cytoplasm (DeLoughery *et al.*, 2018). Moreover, in a proteomic screen RicT was identified to form a stable complex with RicAF, most likely occupying the ~50 Å gap between the hinges of the

RicAF complex. This screen was conducted to study the effects of RicAF mutations on biofilm formation, sporulation, and competence (Carabetta *et al.*, 2013). This effect is suggested to be linked to the regulation of RNase Y by the RicAFT complex, possibly in addition to its role in the phosphorelay (Carabetta *et al.*, 2013; DeLoughery *et al.*, 2016; Dubnau *et al.*, 2016; DeLoughery *et al.*, 2018). This adds further complexity to the regulation of the RicAFT complex and its function, which will be discussed in the next section (see 1.2.3).

In contrast to RicAF, RicT is conserved beyond Bacilli (Table 1). Especially the central region of RicT, is conserved, foremost cysteines such as C160, C165, C166, C198, C203, and C204 (Tanner *et al.*, 2017; Figure 44). This region is not limited to prokaryotes (see Table 1) and parts of it can be found in eukaryotes such as *Schizosaccharomyces pombe (*a fission yeast) or Archaea. In *S. pombe*, the central region is found in a PSP1 protein, which is associated to heat-stress protection (Jang *et al.*, 1997). However, it should be mentioned that the PSP1 protein is three times the size of a regular RicT protein and has a much longer N-terminal region. Moreover, RicT is able to bind a single [4Fe-4S] cluster that is oxygen sensitive, and RicT in solution is present as a monomer (Tanner *et al.*, 2017; Adusei-Danso *et al.*, 2019). However, no structure of any RicT protein has been resolved so far. As all the subunits of the complex have been introduced and their singular functions presented, the functions and regulation of the complete RicAFT complex will be demonstrated in the subsequent chapter.

1.2.3. The RicAFT complex(ity)

The role of the RicAFT complex is still disputed, as it is assumed to be involved in the regulation of various mRNAs by RNase Y and in the phosphorelay of Spo0A. Both assumptions are made on account of various phenotypes caused by the disruption of any subunit (Carabetta *et al.*, 2013; DeLoughery *et al.*, 2016; Dubnau *et al.*, 2016; DeLoughery *et al.*, 2018). First, observations are presented that demonstrate that the RicAFT complex is likely involved in the phosphorelay of Spo0A, which is required for phosphorylation of Spo0A, which in turn is necessary for the formation of biofilms, genetic competence, and sporulation, see Figure 6 (Burbulys *et al.*, 1991; Hosoya *et al.*, 2002; Fujita *et al.*, 2005; Chai *et al.*, 2010; Carabetta *et al.*, 2013; Dubnau *et al.*, 2016). The phosphorelay is a complex machinery that is part of the bet-hedging strategy of *B. subtilis* that allows for a preadaptation in case of a changing environment. Some individuals are primed for a certain lifestyle, for example biofilm formation by constituent chaining, or active competence in stationary phase

(Dubnau and Losick, 2006; Lopez *et al.*, 2009). The extent of Spo0A phosphorylation is a determining factor for which lifestyle is adapted by the cell (Figure 6; Branda *et al.*, 2001; Molle *et al.*, 2003; Mirouze *et al.*, 2011). Yet, a *ricT* deletion has a less severe impact on the developmental characteristics of biofilm formation than *ricAF* deletions (Carabetta *et al.*, 2013). Deletions of any component of the RicAFT complex can be bypassed by a *spo0E* knockout, the phosphatase that dephosphorylates Spo0A, reconstituting the ability of sporulation and biofilm formation (Perego and Hoch, 1991; Ohlsen *et al.*, 1994; Carabetta *et al.*, 2013). In line with this, the RicAFT complex accelerates the phosphorelay from KinA to Spo0A, increasing the phosphorylation of Spo0A. This observation would explain the resulting deletion phenotypes, although, RicF alone slows down this reaction *in vitro* (Carabetta *et al.*, 2013). In the same study it was found that RicA interacts with Spo0F and Spo0B, which are integral parts of the phosphorelay (Carabetta *et al.*, 2013). KinA and KinB are histidine kinases that respond to different nutritional conditions and accordingly phosphorylate the phosphotransferase Spo0F which then phosphorylates Spo0B, which in turn transfers the phosphate group to Spo0A as shown in Figure 6 (Burbulys *et al.*, 1991; LeDeaux *et al.*, 1995). These effects are elicited in the undomesticated *B. subtilis* strain NCIB3610, apparently by a mutation in *sigH* causing a faster accumulation of Spo0A~P (Healy *et al.*, 1991; Bramucci *et al.*, 1995; Dubnau *et al.*, 2016). *sigH* encodes the sporulation dependent sigma factor σ^H, which regulates the expression of many sporulation genes like *spo0A* or *kinA* (Healy *et al.*, 1991; Britton *et al.*, 2002). This complex regulation is also important for the development of genetic competence. A deletion of *ricA* causes an increased transcription of *comK* without increasing the chance of genetic competence. This hints towards additional functions of RicA in competence regulation (Dubnau *et al.*, 2016). Furthermore, all RicAFT proteins were shown to interact with Spo0B, Spo0F, and with KinA, all of which are kinases in the phosphorelay for Spo0A (Figure 6; Burbulys *et al.*, 1991; LeDeaux *et al.*, 1995; Dubnau *et al.*, 2016).

As mentioned above, the RicAFT complex is suggested to be involved in the regulation of mRNA maturation via RNase Y by direct interaction with RNase Y (DeLoughery *et al.*, 2016; DeLoughery *et al.*, 2018). The *sinR* mRNA is correctly maturated only in the presence of the RicAFT complex due to cleavage by RNase Y (DeLoughery *et al.*, 2016). As SinR is a major repressor of biofilm formation and is associated with swimming motility (Kearns *et al.*, 2004) the impact of the RicAFT complex on the *sinR* mRNA explains the biofilm-related phenotype of the single mutants (Carabetta *et al.*, 2013; DeLoughery *et al.*, 2016; DeLoughery *et al.*, 2018). In a differing study, the stabilizing activity of RicAFT

on the *sinR* mRNA could not be observed (Dubnau *et al.*, 2016). Additionally, gene expression of Spo0A~P regulated genes, like *abrB*, is not obstructed in a RicAFT deletion mutant, yet growth defects at the onset of stationary phase are observed in rich medium (DeLoughery *et al.*, 2016; Dubnau *et al.*, 2016). AbrB is a repressor for genes required for biofilm formation as for example *tasA* (Hamon *et al.*, 2004). This opposes the proposition that RicAFT is regulating biofilm formation by the phosphorylation state of Spo0A. Similarly, sporulation and expression of *spoIIG*, encoding a protease involved in the maturation of the sporulation sigma factor σ^E (Jonas *et al.*, 1988; Stragier *et al.*, 1988; Imamura *et al.*, 2008) is not affected upon *ricT* or *ricA* deletion. Although, the contrary for a *ricT* deletion has been observed as well (Hosoya *et al.*, 2002; Dubnau *et al.*, 2016; DeLoughery *et al.*, 2018).

However, it has been reported that SinI, the antagonist of SinR, is partially dependent on Spo0A~P. Hence, a defect in the phosphorelay might be the cause for dysfunctional biofilm formation (Bai *et al.*, 1993; Dubnau *et al.*, 2016). It has been suggested that this is caused by the transcription of *tasA*, encoding a major protein of the extra-cellular matrix needed for biofilms, that might be regulated by RicT (Romero *et al.*, 2010; Romero *et al.*, 2011; Dubnau *et al.*, 2016; DeLoughery *et al.*, 2018). Nonetheless, the regulating effect of RicAFT on mRNA has not only been observed for *sinR*, but for the majority of RNase Y maturated mRNA and even riboswitches, amongst them S-box riboswitches (Shahbabian *et al.*, 2009). The deletion of the RicAFT complex often results in longer transcripts, altered translation starts, and more stable riboswitches. This supports the idea that RicAFT is a specificity transmitting factor for RNase Y, as deletions mutants do not completely phenocopy the RNase Y deletion mutant (DeLoughery *et al.*, 2018).

The localization of the RicAFT complex is not completely known either. The complex has been implicated to be membrane-associated via RNase Y. RicT, however, has been found to be at least partially cytoplasmic which might be dependent on the presence RicF (Dubnau *et al.*, 2016; DeLoughery *et al.*, 2018). Moreover, the phenotypes of *ricA* or *ricF* deletion mutants are nearly identical in their transcriptome, while deletion of *ricT* leads to an increase of prophage genes, increasing the evidence of different functions of the single components. Furthermore, deletion of *ricF* leads to an increase in *ricT* transcript, and *vice versa*, hinting towards a complex internal autoregulation. The localization phenotype as well as the mRNA maturation phenotype has been also

observed in *Staphylococcus aureus*, emphasizing the conserved function of the complex in Firmicutes (DeLoughery *et al.*, 2018).

The RicAFT complex has also been found to bind FAD or $FADH_2$ and two $[4Fe\text{-}4S]^{2+}$ clusters. However, the presence or absence of FAD or $FADH_2$ had no influence on the acceleration phosphorelay from KinA to Spo0F, while exposure to O_2 did (Tanner *et al.*, 2017). This gives rise to the question whether the processes catalyzed by RicAFT are dependent on the redox state of the cell (Tanner *et al.*, 2017). Yet, the connection between this and the mRNA maturation phenotype of the single mutants remains elusive (DeLoughery *et al.*, 2018).

As noted above, the RicAFT heterotrimer has a stoichiometry of 1:1:1. Although, *in vivo* the amounts of RicT, RicF and RicA were found to be not stoichiometric. RicT is the most abundant, followed by RicA and then RicF (100:5:1), which is in opposition to earlier observations (Adusei-Danso *et al.*, 2019). Nevertheless, this supports the idea that the individual proteins have additional functions aside from the RicAFT complex (Dubnau *et al.*, 2016; DeLoughery *et al.*, 2018). Recently, a structure of a RicAF heterotetramer has been solved and the locations of the [4Fe-4S] cluster coordinating cysteines were assigned by mutation studies, despite not being present in the crystal structure (Adusei-Dans *et al.*, 2019; PDB: 6PRK). For RicT, these residues are C161, C166, C198, and C203, and the absence of any of those residues prevents the binding of the iron-sulfur cluster. This coordination of the [4Fe-4S] with Cys-X_4-Cys-X_{31}-Cys-X_4-Cys is not in line with the usual observed binding motif for four cysteine ligands. Ordinarily the configuration is Cys-X_2-Cys-X_2-Cys and a more remote cysteine, or Cys-X_2-Cys-$X_{8\text{-}16}$-Cys-$X_{11\text{-}15}$-Cys. Yet the observed configuration is more in line with a [2Fe-2S] cluster fold Cys-X_4-Cys-$X_{30\text{-}35}$-Cys-X_3-Cys (Johnson and Smith, 2011; Adusei-Danso *et al.*, 2019). Even more remarkably, the second cluster of the RicAFT complex is located at the interface of all three proteins, requiring C167 of RicT, C134 and C146 of RicF, and probably C141 of RicA of *B. subtilis*. The importance of the C-termini is highlighted by the fact that deletion of the last 25 residues of either RicA or RicF prevents interaction via the second [4Fe-4S] cluster with RicT (see Figure 5; Adusei-Danso *et al.*, 2019).

Mutations in the cysteine residues that coordinate the first [4Fe-4S] cluster in RicT in the wild type strain NCIB3610 mimic a *ricT* deletion regarding the mRNA maturation phenotype (DeLoughery *et al.*, 2018; Adusei-Danso *et al.*, 2019). In addition, such mutants are also affected in biofilm formation and sporulation like a *ricT* deletion mutant and they exhibit increased stability of *ricF* mRNA (Adusei-

Danso *et al.*, 2019). However, the mutant proteins are still able to form the complete RicAFT complex. Additionally, a probable assembly of RicAF and RicT in combination with the [4Fe-4S] clusters was proposed. Nonetheless, the C-termini of neither RicA nor RicF with the coordinating cysteine residues are resolved therefore making it impossible to judge the proposition (DeLoughery *et al.*, 2018; Adusei-Danso *et al.*, 2019).

The RicAFT complex is involved in various pathways that regulate cell fate. However, extraordinarily little is known about the exact function. The presence of [4Fe-4S] cluster could help to formulate the possible function. An overview of different functions and mechanisms in which [4Fe-4S] cluster are involved is given in the following chapter.

1.2.4. [4Fe-4S] cluster proteins

RicAFT is a protein complex that constitutes two $[4Fe\text{-}4S]^{2+}$ clusters, yet the reaction catalyzed by it remains elusive. Hence, a comparison with other [4Fe-4S] cluster-containing proteins and their catalyzed reactions is adequate in order to narrow down the potential function of these clusters.

Iron-sulfur clusters (ISCs) are an ancient prosthetic group found in every organism. The reactions requiring iron-sulfur clusters are often essential and with a broad functional diversity ranging from respiration and photosynthesis to DNA repair and regulation of gene expression (Beinert *et al.*, 1997). This is exemplified by the range of forms of these clusters, from simple [2Fe-2S] clusters to large [8Fe-7S] clusters. The primary role of ISCs is electron transport, in which they can donate and receive electrons, as both the iron and sulfur can switch between different oxidation states (Beinert *et al.*, 1997; Beinert, 2000; Lill, 2009; Balk and Pilon, 2011; Johnson and Smith, 2011; Mettert and Kiley, 2015).

As [4Fe-4S] clusters are the most common ISCs in nature, they will be discussed in detail. Most commonly they are present as pairs in proteins and protein complexes, as is the case in the RicAFT complex. Nonetheless, as shown in Table 1, there are organisms that encode only RicT, hence in these there might not be a second [4Fe-4S] cluster or these could have other interaction partners providing another [4Fe-4S] cluster. The common [4Fe-4S] cluster is in a cubic formation and is involved in a plethora of reactions and proteins, an overview of some ISCs is given in Figure 7 (Beinert, 2000; Johnson and Smith, 2011; Broderick *et al.*, 2014). The information regarding the [4Fe-4S] clusters of the RicAFT complex is rather limited. The detected [4Fe-4S] cluster is in an oxidation state of 2+ and

the binding of the [4Fe-4S] cluster by RicT requires four cysteines with the motif Cys-X_4-Cys-X_{31}-Cys-X_4-Cys (Tanner *et al.*, 2017; Adusei-Danso *et al.*, 2019). As most ISCs, the [4Fe-4S] cluster is involved in electron transfer, which requires an electron donor like NADPH or $FADH_2$ (Hubbard *et al.*, 2003; van den Heuvel *et al.*, 2004; Johnson and Smith, 2011) as has been discovered in the RicAFT complex (Tanner *et al.*, 2017).

A class of this electron transfer ISC proteins are the ferredoxins, which can function as electron donors or acceptors. Ferredoxins are ubiquitous, a famous example are the ferredoxins in the respiratory chain of mitochondria, incorporated in the membrane (Yankovskaya *et al.*, 2003; Friedrich and Böttcher, 2004). Yet, ferredoxins are not limited to the membrane, many small ferredoxins are

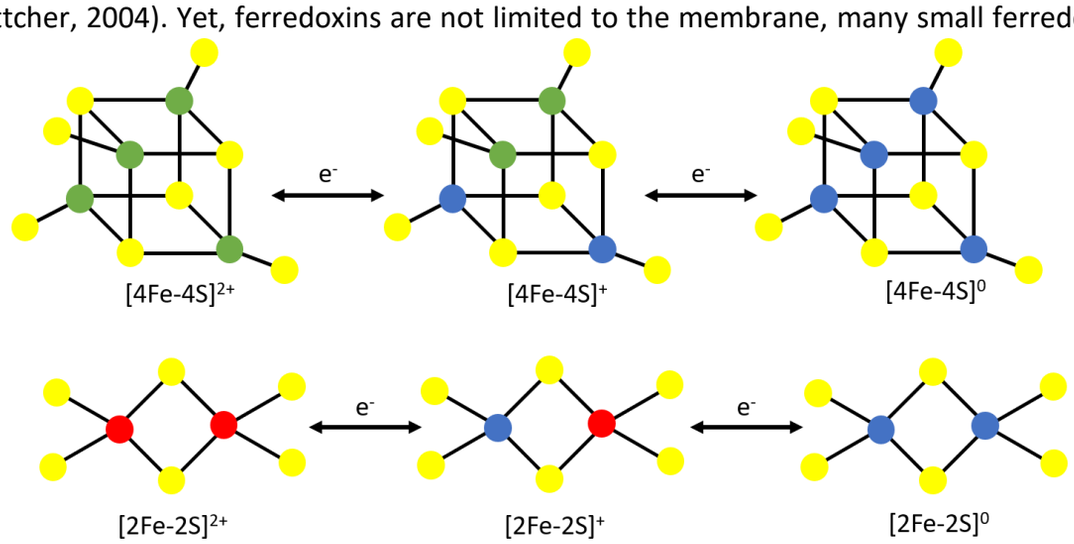

Figure 7: Schematic overview of the oxidation state and form of [4Fe-4S] and [2Fe-2S] clusters.
[4Fe-4S] clusters are most often in a cubic conformation. However, these can be distorted by their coordinating ligands. [2Fe-2S] clusters are planar. Yellow globes represent sulfur, blue represent Fe^{2+}, green $Fe^{2.5+}$, and red Fe^{3+}.

water soluble with a wide variety of interaction partners. Often these incorporate one or multiple [4Fe-4S] clusters, regardless of their localization. The incorporation of multiple [4Fe-4S] clusters allows further specificity to the reaction catalyzed, as these determine the number of transferred electrons or the electron potential resulting from it (Lamotte and Mouesca, 1997; Sticht and Rösch, 1998; Beinert, 2000; Johnson and Smith, 2011). The so called polyferredoxins contain multiple [4Fe-4S] clusters and might serve as electron or ISC storages (Reeve *et al.*, 1989; Hedderich *et al.*, 1992; Mansy and Cowan, 2004; Johnson *et al.*, 2005). The ability of electron transfer is also used directly for enzymes and catalyzes various reactions, which might be the potential role of the RicAFT complex.

An example for such direct use would be the reduction of disulfides to form dithiols. The ferredoxin-thioredoxin reductase uses a [4Fe-4S] cluster and NADPH as a two-electron donor for the FAD-mediated disulfide reduction (Dai *et al.*, 2000; Walters and Johnson, 2004). Another example for the utilization of $[4Fe\text{-}4S]^{2+}$ clusters in enzymes is the sulfite and nitrite reduction in which siroheme is used for the electron transfer to SO_3^{2-} or NO_2^- to split the S-O or N-O bond, respectively (Crane *et al.*, 1995; Crane *et al.*, 1997; Johnson and Smith, 2011). Yet, neither siroheme nor NADPH has been found in the RicAFT complex, making it unlikely that such reactions are catalyzed by the complex, however, there are plenty of other reactions catalyzed by [4Fe-4S] clusters (Tanner *et al.*, 2017). To this group belong the radical SAM (S-adenosyl methionine) enzymes, which are the most common biological radical generators. They catalyze reactions like methylation, sulfur insertion, isomerization, ring formation, anaerobic oxidation, and protein radical formation. Additionally, they can function as DNA precursors, cofactors, vitamin cofactors, and antibiotics. The $[4Fe\text{-}4S]^{2+}$ cluster is coordinated via the motif C-X_3-C-X_2-C. The SAM is bound by a unique Fe site that is not coordinated by a cysteine (see Figure 7) and then reductively cleaved to form a 5'-deoxyadenosyl radical (Cheek and Broderick, 2001; Sofia, 2001; Jarrett, 2003; Layer, 2003; Berkovitch, 2004; Hanzelmann and Schindelin, 2004; Landgraf *et al.*, 2013; Broderick *et al.*, 2014). MiaB is an example for this reaction, it modifies the adenosine 37 in the $tRNA^{Phe}$ to 2-methylthio-*N*-6-isopentyl adenosine (ms^2i^6 A-37) providing the transferred Ado radical and the methyl group, see Figure 1 (Anton *et al.*, 2010). However, it has been demonstrated that RicT requires four cysteines to coordinate the [4Fe-4S] cluster and the coordination of the second [4Fe-4S] cluster is unknown, therefore it appears unlikely that RicAFT is a protein using SAM for catalysis.

[4Fe-4S] clusters are also involved in the regulation of enzyme activity, as it is the case in phosphoribosylpyrophosphate amidotransferase in *B. subtilis* which catalyzes the first step in purine nucleotide synthesis. This reaction is catalyzed with a [4Fe-4S] cluster that is not involved in substrate activation or electron transfer, but plays a crucial role for the reaction, possibly by sensing the O_2 concentration (Grandoni *et al.*, 1989; Smith *et al.*, 1994). Even though this could possibly be a function of the RicAFT complex, evidence for it is missing. Related to this, $[4Fe\text{-}4S]^{2+}$ can have a structural role in proteins like in the endonuclease III or in various helix-hairpin-helix DNA repair enzymes, involved in base lesions. In these enzymes, the ISC is inert and is structurally relevant at sites where DNA binding is occurring to stabilize the structure (Kuo *et al.*, 1992; Hoseki *et al.*, 2003; Balueva *et al.*,

2008). Furthermore, [4Fe-4S] clusters can be deciding for the regulation of gene expression as it is the case in FNR (fumarate and nitrate reduction) in *E. coli*. FNR controls more than 200 genes and is essential for the transition from anaerobic to aerobic respiration. It contains a $[4Fe\text{-}4S]^{2+}$ cluster and acts as a helix-turn-helix transcription factor. In O_2 rich medium the cluster rapidly degrades to $[2Fe\text{-}2S]^{2+}$ and destroys the homodimer, hence reducing the transcription of the regulated genes (Khoroshilova *et al.*, 1997; Popescu *et al.*, 1998; Kiley and Beinert, 1998; Mettert and Kiley, 2015). The protein is conserved in *B. subtilis*, however the ISC seems not to be responsible for the dimerization (Reents *et al.*, 2006; Gruner *et al.*, 2011; Mettert and Kiley, 2015). A similar role for the [4Fe-4S] cluster of the RicAFT complex might explain the change in mRNA maturation and the differences in gene expression in *B. subtilis* (DeLoughery *et al.*, 2016; Dubnau *et al.*, 2016; DeLoughery *et al.*, 2018). However, the clusters are oxygen-labile and upon removal of the ISC the complex forms regardless, opposing these suggestions (Tanner *et al.*, 2017).

Lastly, [4Fe-4S] clusters are used for different reactions in a single enzyme such as in aconitase. Aconitase in eukaryotes regulates mRNA, by binding to iron responsive elements (IREs) often located in mRNAs coding for proteins involved in the iron import. Aconitase binds these elements in the 5'- or 3'-UTR, thereby increasing its stability and their translation, leading to an enhanced iron import. This can only occur upon degradation of the [4Fe-4S] cluster (Haile *et al.*, 1992; Hentze and Kuhn, 1996). A similar regulation is known in *B. subtilis* in which it is known as a moonlighting enzyme (Alen and Sonenshein, 1999; Serio *et al.*, 2006; Pechter *et al.*, 2013). Additionally, aconitase uses the ISC (Beinert *et al.*, 1996; Kiley and Beinert, 2003) for substrate binding and activation: a unique non-cysteine ligated iron atom of the $[4Fe\text{-}4S]^{2+}$ cluster is used as a Lewis acid to abstract the hydroxyl group of citrate and a proton from a carbon (Doukov, 2002; Darnault *et al.*, 2003; Svetlitchnyi *et al.*, 2004). Since in the RicAFT complex all irons are coordinated by cysteines, such a reaction appears highly unlikely.

The above-mentioned examples demonstrate that the reactions catalyzed by ISCs are wide-ranging. The precise function of the [4Fe-4S] clusters in RicAFT can only be roughly estimated without a clearer understanding of the coordination and structure of the complex and its ISCs.

2. AIM OF THE STUDY

The RicAFT is an elusive yet crucial regulator for specificity of the major endoribonuclease of *B. subtilis*, RNase Y, and possibly has an influence of the phosphorelay of Spo0A. Singular deletions of its components lead to the impairment of biofilm formation (Branda *et al.*, 2001; Carabetta *et al.*, 2013; Dubnau *et al.*, 2016) probably due to the obstruction of maturation of several mRNAs via RNase Y (DeLoughery *et al.*, 2016; DeLoughery *et al.*, 2018) and/or stimulation of the phosphorelay of Spo0A (Carabetta *et al.*, 2013; Dubnau *et al.*, 2016; Tanner *et al.*, 2017). As these different observations highlight, the exact function of the RicAFT complex is a matter of dispute. The exact reaction catalyzed by the complex is unknown and whether its influence on the phosphorelay causes the change in mRNA regulation or *vice versa*. Possibly these are two independent results of the complete function of the complex. Hence, the aim of this study is to shed light on the function and structure of the RicAFT complex. Since to date only the structure of RicA and the heterodimer RicAF is known, it will be of special interest to obtain further information about the entire complex. In addition, the presence of two iron-sulfur clusters in the complex gives rise to many speculations about potential functions. The elucidation of the function of the complex might also shed light onto the fact that deletions of some subunits of the complex are more severe than others, hinting to possible additional functions of the single subunits of the complex. This is further elicited by the fact that RicT is present in organisms lacking RicAF and hence only one [4Fe-4S] cluster is present, which gives rise to the question if there are more interaction partners of the complex. RNase Y has been shown via indirect methods to interact with the complex *in vivo*, and the cause and presence of this possible interaction will be further investigated as well (DeLoughery *et al.*, 2018).

It is obvious that the RicAFT complex has a plethora of important functions in *B. subtilis*, especially in the determination of cell fate, however, the route of this regulation is highly disputed. Structural insights into the complex would allow a better estimation of its possible function and were therefore a main focus for this work.

3. MATERIAL AND METHODS

3.1. Material

Chemicals, utilities, equipment, commercially available systems, antibodies, enzymes, and oligonucleotides are listed in the Appendix 10.1 and 10.4. Oligonucleotides were diluted to 100 µM final concentration with deionized water.

3.1.1. Bacterial strains and plasmids

The bacterial strains and plasmids used in preparation of this work are listed in the Appendix 10.2 and 10.3.

3.1.2. Media and buffers

Solutions, buffers, and growth media were prepared with deionized water and autoclaved for 20 min at 121 °C and 2 bar. Thermolabile substances were dissolved and sterilized by filtration with membrane filters with a nominal pore diameter of 0.22 µm. For agar plates, 18 g/l agar was supplemented to the respective growth media. Antibiotics and other thermolabile substances were added after the media cooled down to approximately 50 °C before pouring the plates.

3.1.3. Complex media and facultative supplements

LB-Medium (1 l)	10 g	Tryptone
Lysogeny Broth medium	5 g	Yeast extract
	10 g	NaCl
	ad 1 l	dH_2O

IPTG	Stock solution 1 M (0.238 g/ml) in dH_2O Working concentration for protein production: 1 mM or 500 µM
Bacitracin	Stock solution 20 mg/ml in diluted HCl (0.75 %) Working concentration for protein production: 30 µg/ml

Antibiotics were prepared in 1000-fold concentrated stock solutions, filter-sterilized, and stored at -20 °C. Ampicillin and kanamycin were dissolved in deionized water, lincomycin was dissolved in 50 % (v/v) ethanol, and erythromycin in 100 % (v/v). The antibiotics were added to the medium when it had a temperature of 50 °C or less. The used concentrations were:

Selection concentration	100 µg/ml	Ampicillin
Escherichia coli	50 µg/ml	Kanamycin
Selection concentration	25 µg/ml	Lincomycin
Bacillus subtilis	4 µg/ml	Erythromycin
	5 µg/ml	Chloramphenicol

3.2. Methods

3.2.1. Standard methods

Standard methods that were used to prepare this work were previously described in literature are listed in Table 2.

Table 2: Standard methods

Method	Reference
Measurement of optical density	Eschbach *et al.*, 1990
DNA gel electrophoresis	Eschbach *et al.*, 1990
Ligation of DNA fragments	Eschbach *et al.*, 1990
Plasmid isolation from *E. coli*	Green and Sambrook, 2016
Chain terminator sequencing	Sanger *et al*., 1977
Gel electrophoresis of proteins	Laemmli, 1970
Determination of protein amounts	Bradford, 1976

3.2.2. Cultivation and storage of bacteria

Unless stated otherwise, *E. coli* and *B. subtilis* were grown in LB-Medium at 37 °C and 200-220 rpm in test tubes or 100 ml flasks. Inoculation was done using single colonies from fresh plates or from cryo-cultures.

Strains of *E. coli* were stored on LB agar plates for several days at 4 °C. *B. subtilis* strains were stored at RT protected from light. For long-term storage, glycerol cryo-cultures were prepared in 2 ml screw-cap tubes. For this, 600 µl of glycerol (60 % (v/v)) were added to 400 µl of a fresh culture at OD_{600} = 0.8-1.0 from a single colony and stored at -80 °C. To monitor contamination, a sterile control without antibiotics and bacteria was incubated alongside the other cultures.

3.2.3. Preparation of competent cells

***E. coli* long-term storage:**

A single colony was used to inoculate 20 ml LB medium in a test tube and incubated overnight. The next morning this culture was used to inoculate 250 ml LB medium to OD_{600} = 0.05 in a baffled 1 l Erlenmeyer flask. The culture was incubated until an OD_{600} = 0.4-0.6 was reached at 37 °C with agitation (220 rpm). The culture was cooled for 10 min on ice and harvested by centrifugation

(10 min; 4000 rpm; 4 °C). The supernatant was discarded, the cell pellet resuspended in 20 ml TFB 1 buffer and incubated in ice for 15 min, and the centrifugation step repeated. The supernatant was discarded again; the cell pellet resuspended in 1 ml TFB 2. After a short incubation on ice, the suspension was divided into 30 µl aliquots in 1.5 ml micro tubes, which were then rapidly frozen in liquid nitrogen. The competent cells were stored at -80 °C until further use (Hanahan, 1983; Hanahan *et al.*, 1991).

TFB 1	30 mM	Potassium acetate
	100 mM	$RbCl_2$
	10 mM	$CaCl_2$
	50 mM	$MnCl_2$
	15 % (v/v)	Glycerol
	→adjusted pH to 5.8 with acetic acid	
	→sterile filtered, stored at 4 °C	

TFB 2	10 mM	MOPS
	10 mM	$RbCl_2$
	75 mM	$CaCl_2$
	15 % (v/v)	Glycerol
	→adjusted pH to 6.5 with NaOH	
	→sterile filtered, stored at 4 °C	

Transformation of competent *E. coli*

10 to 100 ng of DNA were added to an aliquot of 30-50 µl of competent *E. coli* cells and incubated together for 15 min on ice. After a heat shock at 42 °C for 60 s without agitation, the cells were incubated 5 min on ice, and, after the addition of 400 µl of LB medium, shaken for 1 h at 37 °C with agitation (220 rpm). Of each sample, 100 µl were directly plated on LB selective medium with the respective antibiotics, while the remaining cell solution was harvested by centrifugation (1 min; 12000 rpm; room temperature (RT)). The supernatant was discarded except of 50 µl of LB medium. The cell pellet was resuspended in it and plated on selective LB plates with the respective antibiotics. The plates were incubated overnight at 37 °C (Inoue *et al.*, 1990).

3.3. Preparation and analysis of DNA

3.3.1. Isolation of plasmid DNA

Plasmid DNA was isolated from *E. coli* cells grown overnight in 4 or 10 ml LB. The isolation was done using the GeneJET Plasmid Miniprep Kit (Thermo Scientific™) according to the manufacturer's instructions. This isolation procedure is based on alkaline lysis followed by chromatographic purification.

3.3.2. Sequencing of DNA

Sequencing was performed based on the chain termination method with fluorescence labeled nucleotides at SeqLab (Göttingen, Germany). Sequences were analyzed with SnapGene (V 5.08).

3.3.3. Polymerase chain reaction (PCR)

Polymerase chain reactions were performed using either chromosomal DNA or plasmid DNA as templates. The samples were mixed according to the set-up shown in Table 3 and prepared in a PCR thermocycler using the respective programs. Phusion™-based PCRs were done to amplify DNA for cloning purposes, either from plasmids or chromosomal DNA. The melting temperature for the primers was calculated by SnapGene (V 5.08).

Table 3: Reaction set-up for Phusion PCR

Reaction set-up for Phusion™ polymerase (50 µl) and standard reaction program				
1 µl Template DNA (~50 ng)	**Reaction**	**Temp.**	**Duration**	**Cycles**
2 µl Primer (Fwd.; 20 pmol)	Initial Denaturation	98 °C	5 min	1
2 µl Primer (Rev.; 20 pmol)	Denaturation	98 °C	45 s	
dNTPs (12.5 µmol/ml)	Annealing	55 °C	45 s	34
10 µl 5 x Phusion HF buffer	Elongation	72 °C	1 min / kb	
1 µl Phusion™ polymerase (2 U/µl)	Final Elongation	72 °C	10 min	1
32 µl Deionized H_2O	Hold	8 °C	∞	1

Purification of PCR products

PCR products were purified for further use, e.g. restriction, by using the GeneJET Gel Extraction Kit (Thermo Scientific™). The purification was done according to the manufacturer's manual.

3.3.4. Gel electrophoresis

Gel electrophoresis was performed to analyze the DNA by separation. Therefore, gels were prepared with 2.5 to 1 % (w/v) agarose in 1 x TTE by heating, so the agarose is completely dissolved. Then the solution is cooled down to 50 °C. 30 ml of the solution was taken and 3 µl 1 % ethidium bromide was added to stain the DNA. The DNA samples were mixed with 6 x Purple Loading Dye (New England Biolabs) and loaded onto the gel, as well as the size standard (1 kb GeneRuler™ 1kb Plus DNA Ladder; Thermo Scientific) for later determination of the DNA fragment sizes. The gel was run at 120 V for 20 to 45 min, depending on the expected size of the DNA fragments. The gel was photographed under UV-light (λ = 254 nm). To dissect the DNA from a preparative gel, the fragments were detected at λ = 365 nm and cut out using a scalpel. Subsequent purification from the gel was done by the GeneJET Gel Extraction Kit (Thermo Scientific™) according to the manufacturer's manual.

20 x TTE buffer	109 g	Tris
	75 g	Taurine
	10 ml	0.5 M EDTA pH 8.0
	ad 1 l	dH_2O

3.3.5. Restriction and ligation of DNA

Restriction of DNA was performed using the respective CutSmart™ endonucleases and the CutSmart™ buffer as recommended by the manufacturer (New England Biolabs). The amount of enzyme was adjusted to the DNA concentration and volume of the reaction mixture. The samples were incubated at 37 °C for 30 min to 2 h. For controlling the restriction, 6 x Purple Loading Dye (New England Biolabs) was used. Afterwards, the reaction mixture was purified using the GeneJET Gel Extraction Kit according to the manufacturer's instructions (Thermo Scientific™). The size of the vector and insert DNA was checked prior ligation by SnapGene (V 5.08), gel electrophoresis and NanoDrop™ Lite. Ligation of the DNA fragments was performed using the T4 DNA ligase and buffer,

as recommended by the manufacturer (New England Biolabs). 10 to 100 ng of digested vector DNA and a 3- to 7-fold excess of insert DNA was used for ligation. The mixture was incubated for at least 1 h at room temperature, or overnight at 16 °C.

3.4. Analysis of proteins

3.4.1. Protein alignment and protein topology prediction

For the protein alignment MUSCLE (Madeira *et al.*, 2019) was used. Identity and similarity of proteins were determined with this tool as well.

3.4.2. Protein overproduction

For test expressions the *E. coli* strains were grown to OD_{600} = 0.3-0.5 in their respective growth medium. Then, the expression was induced with 1 mM or 500 µM IPTG. The strains were grown in 10 ml medium and samples were taken before the induction, 1 h after induction, and 2 h after induction. In addition, test expression cultures of 100 ml with appropriate antibiotics were grown overnight at 30 °C with 1 % lactose using a single colony as inoculant. The strain used for overexpression was *E. coli* BL21 (DE3).

For large scale protein overproduction *E. coli* strains were grown overnight in growth medium supplemented with 1 % (w/v) D(+)-lactose-monohydrate at 30 °C. For IPTG induction 100 ml cultures with appropriate antibiotics were grown overnight at 37 °C. The next day 1 l cultures were inoculated to OD_{600} = 0.1 and grown to OD_{600} = 0.4-0.7, then 1 mM or 500 µM IPTG was added. The cultures then either grew for 1 to 3 h or overnight at 20 °C with agitation. The cultures were harvested by centrifugation (12 min; 4000 rpm; 4 °C) and could be stored at -20 °C until further use.

For *B. subtilis* test expression a 5 ml culture was inoculated and grown overnight at 37 °C with agitation. Then a 100 ml culture with appropriate antibiotics was started with an OD_{600} = 0.08 and grown at 37 °C to OD_{600} = 0.5. Then the culture was induced by adding 30 µg/ml bacitracin. The induction was done for 2 to 3 h at 30 °C. For large scale overproduction the method used is the same, with upscaled culture sizes. For overexpression of genes in *B. subtilis*, the LIKE system was used. This plasmid system can be integrative (pLIKEint) or non-integrative (pLIKErep) and the translation of the gene of interest is under the regulation of a bacitracin-inducible promoter (liaI) (Toymentseva *et al.*, 2012).

3.4.3. Cell disruption via Microfluidizer

For disruption of the cells, cell pellets of a 1 l culture were resuspended in 15 ml 1 x Buffer A, SEC buffer, or Lysis buffer AFT (the same that was used later for purification). Disruption was performed with a M-110L Microfluidizer® Materials Processor (Microfluidics) at 10000 psi at least three times per sample. The cell lysate was centrifuged (20 min; 20000 rpm; 4 °C) to clear the lysate. The supernatant was used for protein purification.

10 x Buffer A	200 mM	HEPES
	2 M	NaCl
	200 mM	$MgCl_2$
	200 mM	KCl
	400 mM	Imidazole
	adjust pH to 8.0 with HCl	
	ad 1 l	dH_2O
10 x SEC buffer	200 mM	HEPES
	2 M	NaCl
	200 mM	$MgCl_2$
	200 mM	KCl
	adjust pH to 7.5 with HCl	
	ad 1 l	dH_2O
1 x Lysis buffer AFT	20 mM	HEPES
	250 mM	NaCl
	20 mM	$MgCl_2$
	40 mM	Imidazole
	10 % (v/v)	Glycerol
	adjust pH to 8.0 with HCl	
	ad 1 l	dH_2O

3.4.4. Co-immunoprecipitation (CoIP)

For CoIP experiments the cells with the overproduced proteins were harvested and resuspended in a small volume of LB medium. The cells were then freeze-dried with liquid nitrogen. The resulting pellets were disrupted using a precooled mixer mill. Proteins were then extracted using the supplemented HNN buffer.

HNN	50 mM	HEPES, pH = 7.5
	150 mM	NaCl

	50 mM	NaF
	→ sterile filtered, storable at -20 °C	

Supplemented prior use:	0.1 %	NP-40
	1 %	Polyvinylpolypyrrolidone
	0.5 %	Sodium choleate
	1 mM	PMSF
	1 µl/100 ml	cOmplete™ Protease Inhibitor Cocktail (Roche) (1/100 µl)

The cell powder was dissolved and afterwards centrifuged for 20 min at 20000 rpm at 4 °C. 4 ml of the supernatant was taken and 40 µl of magnetic Strep-beads (MagStrep "type3" XT beads; IBA) were added and incubated on a roller shaker for 1 h at 4 °C. These were pelleted using a magnetic rack, and the supernatant was discarded. The beads were washed four times with 100 mM ammonium bicarbonate. The beads were then frozen in liquid nitrogen. The precipitated proteins were digested on the beads and analyzed by mass spectroscopy with the help of Dr. Timo Glatter of the Max-Planck-Institute for Terrestrial Microbiology. The evaluation of the resulting data was done by using Perseus (v1.6.14.0). The low expression rows were removed. For control, cross references were used with a multiple-sample test, with 250 randomizations and a false discovery rate of 5 %. Further confidence was gained by a volcano plot of a sample against the other samples with 100 permutations. The selection was based on the multiple-sample test, the volcano plot, and direct comparison.

3.4.5. Affinity protein purification

To further purify the proteins, an artificial His_6-tag (HHHHHH), here abbreviated H_6, Strep-tag II (WSHQFEK), here abbreviated Strep, or GST (glutathione S-transferase)-tag were added. If an His-tag was added, the protein was purified with a 1 ml or a 5 ml HisTrap™ Fast Flow (GE Healthcare Life Sciences). The columns were equilibrated with 10 CV of lysis buffer and the cleared lysate was applied onto the columns with a peristaltic pump. The columns were then washed with at least 10 CV of lysis buffer to remove unspecific interactions. The protein was eluted by using 5 CV of Buffer B.

10 x Buffer B	200 mM	HEPES
	2 M	NaCl
	200 mM	$MgCl_2$
	200 mM	KCl

	2.5 M	Imidazole
	adjust pH to 8.0 with HCl	
	ad 1 l	dH_2O

If the protein had an added Strep-tag II, the purification was then done using a 1 ml StrepTrap™ HP (GE Healthcare Life Sciences). The cells were resuspended in 1 x SEC buffer and then continued as described above. 5 CV of SEC-buffer supplemented with 2 mM D-desthiobiotin was used for elution. If the proteins were tagged with GST, 5 ml GSTrap™ FF (GE Healthcare Life Sciences) columns were used. The cells were resuspended in 1 x SEC buffer, then it was proceeded as described above. For the elution, SEC-buffer supplemented with 20 mM reduced glutathione was used.

The RicAFT proteins were treated separately. After the proteins were applied to the columns, these were washed with 5 CV of Low-salt buffer, then 5 CV High-salt buffer, and then again 5 CV Low-salt buffer. The proteins were eluted by Elution buffer AFT or Low-salt elution buffer for the ion-exchange purification.

1 x Low-salt buffer	20 mM	HEPES
	40 mM	NaCl
	20 mM	$MgCl_2$
	40 mM	Imidazole
	10 % (v/v)	Glycerol
	adjust pH to 8.0 with HCl	
	ad 1 l	dH_2O
1 x High-salt buffer	20 mM	HEPES
	500 mM	NaCl
	20 mM	$MgCl_2$
	40 mM	Imidazole
	10 % (v/v)	Glycerol
	adjust pH to 8.0 with HCl	
	ad 1 l	dH_2O
1 x Elution buffer AFT	20 mM	HEPES
	250 mM	NaCl
	20 mM	$MgCl_2$
	200 mM	Imidazole
	10 % (v/v)	Glycerol
	adjust pH to 8.0 with HCl	
	ad 1 l	dH_2O

1 x Low-salt elution buffer	20 mM	HEPES
	50 mM	NaCl
	20 mM	$MgCl_2$
	200 mM	Imidazole
	10 % (v/v)	Glycerol
	adjust pH to 8.0 with HCl	
	ad 1 l	dH_2O

3.4.6. Ion exchange purification

For ion exchange purification the proteins were prepared in a low-salt elution buffer with a maximum concentration of 50 mM NaCl, originating from their standard purification buffer. The column used was the anion-exchange column 5 ml Hi Trap Q FF (GE Healthcare Life Sciences). The proteins were eluted with a high-salt elution buffer (SEC buffer gradient from 50 mM NaCl to 1 M NaCl) over 32 CV.

3.4.7. Size exclusion purification

For higher protein purity the proteins were separated according to their size. Then the eluted proteins were further concentrated to 1-5 ml using Amicon Ultra-15 centrifugal filter units (Merck Millipore) with an appropriate molecular weight-cutoff (MWCO) at an appropriate temperature. Afterwards, the solubility of the proteins in SEC buffer was checked. If the protein was soluble it was applied onto a size exclusion column (HiLoad 16/600 Superdex 200, HiLoad 26/600 Superdex 200, HiLoad 26/600 Superdex 75; GE Healthcare Life Sciences). The size exclusion chromatography was performed with an ÄKTA Prime, ÄKTA Purifier 10, or ÄKTA pure (Cytiva). The column was equilibrated with 1 x SEC buffer. The fractions containing protein were pooled and then concentrated with an Amicon Ultra-15 centrifugal filter unit with the appropriate size to a desired concentration specified by experimental requirements. The protein concentration was measured using a NanoDrop™ Lite spectrophotometer (Thermo Scientific).

3.4.8. Analytical size exclusion

For the determination of the molecular size of a complex in solution, the purified proteins were applied onto an equilibrated analytical size exclusion column (Superdex 200 Increase 10/300 GL). For this a minimum of 2 nmol of the protein was applied onto the column, which was equilibrated in the same buffer the protein was purified in. For appropriate size determination specific proteins with a

known molecular weight were analyzed on the column and their retention time was plotted against their molecular weight. This resulted in the retention volumes shown in Table 4.

Table 4: Size standards for analytical size exclusion chromatography.

Size (in kDa)	Retention volume (in ml)
669 (Thyroglobulin)	**9.01**
440 (Ferritin)	**10.36**
158 (Aldolase)	**12.36**
75 (Conalbumin)	**13.95**
43 (Ovalbumin)	**15.07**
29 (Carbonic anhydrase)	**16.29**
13.7 (Ribonuclease)	**17.7**

This plotting resulted in two functions to determine the size in a specific size range. For lower retention volumes (below 14 ml) the term is:

$$m\,(\text{protein}) = -122.42 \cdot v\,(\text{retention}) + 1733.589\ \text{kDa}$$

Unfortunately, at lower molecular weights the previous term is quite inadequate to correctly estimate the protein size. Hence, a second term is formulated for higher retention volumes (above 14 ml). It is the following:

$$m\,(\text{protein}) = -11.10 \cdot v\,(\text{retention}) + 210.19\ \text{kDa}$$

3.4.9. Multi angle light scattering (MALS)

Multi angle light scattering was used in conjunction with analytical size exclusion to further analyze the protein and protein complexes. For detection, the PN3150 RI Detector (Postnova Analytics) was used according to the manufacturer's specifications. For data evaluation the NovaMALS software (Postnova Analytics) was used. The signal of the RI had to be consistent for at least six different detectors (angles) to be deemed veritable. Calculations for the size and weight were done by using the Zimm-plot individually for every peak.

3.4.10. Denaturing polyacrylamide gel electrophoresis (SDS-PAGE)

Gels (1 mm thick) were prepared according to Laemmli, 1970, containing a stacking gel on the top to accumulate proteins and a resolving gel below for separation depending on their size. Protein

samples were mixed with SDS-loading dye (10 µl 5 x SDS loading dye and 40 µl SEC) and boiled (10 min; 95 °C) for denaturation. Gels were immersed in 1 x PAGE buffer and run at 270 V until the bands were properly resolved. The Pierce™ Unstained Protein MW Marker (Thermo Scientific) served as a marker. For Western Blots the PageRuler™ Plus Prestained Protein Ladder 10 to 250 kDa (Thermo Scientific) was used.

Stacking gel (5 % (v/v)	1.3 ml	Rotiphorese® Gel 30
	0.87 ml	1.5 M Tris-HCl pH 6.8
	100 µl	SDS (10 % (w/v))
	100 µl	APS (10 % (w/v))
	10 µl	TEMED
	6.3 ml	dH_2O
Resolving gel (15 % (v/v))	4 ml	Rotiphorese® Gel 30
	2.6 ml	1.5 M Tris-HCl pH 8.8
	100 µl	SDS (10 % (w/v))
	8 µl	APS (10 % (w/v))
	10 µl	TEMED
	3.3 ml	dH_2O
5 x SDS loading dye	15.65 ml	1 M Tris-HCl pH 6.8
	12.5 ml	Glycerol
	5 g	SDS
	12.5 ml	β-Mercaptoethanol
	2.5 ml	bromophenol blue solution 1%
	ad 50 ml	dH_2O
10 x PAGE buffer	144 g	L-Glycine
	30.3 g	Tris-base
	10 g	SDS
	ad 1 l	dH_2O

Colloidal Coomassie staining of polyacrylamide gels

Prior to staining, denaturing gels were incubated in fixation solution for 20 min. Fixation solution was discarded and replaced by ROTI® Blue (Thermo Scientific) solution and stained until the protein bands were pronounced. Gels were destained in dH_2O to decrease background staining.

Fixation solution	300 ml	Acetic acid
	ad 1 l	dH_2O

3.4.11. Western Blots

For Western Blots, the proteins were separated on an SDS-PAGE described in 3.4.10. Afterwards, these were blotted onto a fitting Amershan™ Protran® 0.45 µM nitrocellulose membrane (GE Healthcare) using a PerfectBlue 'Semi-Dry'-Blotter (VWR) according to the manufacturer's instructions for the size of the protein of interest.

After the transfer, the membrane was blocked in PBS-blocking buffer (PBS + 3 % BSA + 0.05 % Tween-20) overnight at 4 °C. Then the membrane was washed three times with PBS-Tween (PBS + 0.1 % Tween-20) for 5 min. The Strep Tactin® HRP (IBA Lifesciences) was diluted in enzyme dilution buffer (PBS + 0.2 % BSA + 0.1 % Tween-20) 1:100 and then 10 µl of this solution was added to 10 ml PBS-Tween and incubated with the membrane for 1 h at RT. Afterwards, the membrane was washed twice with PBS-Tween. For the detection reaction the Pierce™ ECL Western Blotting Substrate kit (Thermo Scientific) was used according to its manual. The detection itself was done with a ChemiDoC™ MP Imaging System (170-8280) (Bio-RAD).

10 x PBS	40 mM	KH_2PO_4, pH = 7.4
	160 mM	Na_2HPO_4
	1.15 M	NaCl
	ad 1 l	dH_2O
	→autoclave	

3.5. Protein crystallization

For crystallization, protein solutions with appropriate concentrations (0.5 mM – 1 mM) were used. These were used with the Crystal Gryphon (Art Robbins) to set up sitting-drop experiments with SWISSSCI MRC 2-well and 3-well (Jena Bioscience) crystallization plates. For precipitation solution the JCSG Core Suits I-IV (Qiagen) were used. 300-500 nl of the protein solution were mixed in a 1:1, 1:2.5 or 1:3 ratio with the precipitation solution and a reservoir amount of 30 µl (3 Well) or 50 µl (2 Well) were used. These were done with a Crystal Gryphon (Art Robbins).

For fine screens, the hanging drop method was employed using the VDX™ Plate with sealant (Hampton Research). Here, the initial crystal condition is used and modified to allow for optimal crystallization. Specifically, a 1 ml mother liquor solution for each condition is prepared in a reservoir and the protein is mixed in a 1:1 – 1:5 ratio on a glass slide that is put upside down on the top of the reservoir. All the crystallization experiments were performed at room temperature.

3.6. Data collection and structure determination

For data collection the crystals could be soaked in a cryoprotectant solution containing 20 % (v/v) glycerol or MPD. The crystals were then collected using Adjustable Mounted Cryo Loops™ (Hampton Research) of different diameters and then flash-frozen in liquid nitrogen. The data was collected at the Deutsches Elektronen-Synchrotron, Berliner Elektronenspeicherring-Gesellschaft für Synchrotronstrahlung, or European Synchrotron Research Facility (DESY, Hamburg; BESSY, Berlin; ESRF, Grenoble).

For integration, processing, and scaling, XDS was used and merged using AIMLESS of the CCP4 suite (Kabsch, 2010; Evans and Murshudov, 2013). The resolution cut-off was determined using the CORRECT-file of the XDS program.

For molecular replacement (MR) the merged-MTZ file was used in the CCP4-integrated PhaserMR (Winn *et al.*, 2011). The following refinement was done by using PHENIX.refine (Adams *et al.*, 2010). The models were manually refined further using COOT (Emsley and Cowtan, 2004).

3.7. Mass photometry

Mass photometry was done in collaboration with Dr. Georg Hochberg and Niklas Steube from the Philipps-University Marburg. The proteins were diluted in their respective buffer to a concentration between 50 nM to 100 nM, so that the solution was not too saturated. The samples were then analyzed with a Refeyn One (Refeyn) and AcquireMP v2.3.0 (Refeyn). Evaluation and visualization of the data was done using DiscoverM v2.2.0 (Refeyn).

3.8. Electron microscopy

Negative stain pictures were obtained in cooperation with Dr. Thomas Heimerl, from the Philipps-University Marburg. Samples were diluted to 5 – 20 ng/ml of protein and then spotted onto formvar-coated copper-grids, stabilized with evaporated carbon film, and negatively stained by applying 5 µl of a 2 % (w/v) uranyl acetate solution. The grids were dried and analyzed with a 200 kV Transmission Electron Microscope JEM-2100 (JEOL). Dr. Florian Altegoer and Dr. Jan Schuller helped with the preparation and evaluation of the cryo-EM data and the analysis was done with a 300 kV Titan Krios (FEI company) company and cryoSPARC (Punjani *et al.*, 2017). The protein concentration was 87.5 µM

that was applied on CF 1.2/1.3 grids Cu-50 and blotted for 12s at 100 % humidity at 10°C. The resulting data was processed and analyzed using cryoSPARC.

Protein-Crosslinking

The protein crosslinking was done with the Pierce™ Crosslinking Magnetic IP/CoIP-Kit (Thermo Scientific). Hence, the protein of interest was concentrated to at least 10 mg/ml in SEC-buffer and the crosslinking reaction was started by adding BS^3 (Thermo Scientific) in 10-fold molar excess, a mild lysine crosslinker. The reaction was incubated for 30 min at RT. The reaction was quenched by adding TRIS pH = 7.0 to a final concentration of 30 mM and incubation for 15 min at RT. Success was monitored by SEC and SDS-PAGE analysis.

3.9. Hydrogen/deuterium-exchange mass-spectrometry

HDX experiments were performed in close collaboration with Dr. Wieland Steinchen of the Philipps-University Marburg.

Sample preparation and measurements were aided by a two-arm robotic autosampler (LEAP technologies) and essentially performed as described previously (Osorio-Valeriano *et al.*, 2019). In brief, 7.5 µl of the *Bs*RicA/*Bs*RicF complex, *Gt*RicT, or the ternary *Bs*RicA/*Bs*RicF/*Gt*RicT (each 50 µM) complex were mixed with 67.5 µl of D_2O-containing buffer (20 mM HEPES-Na, pH 7.5, 20 mM KCl 20 mM $MgCl_2$ and 200 mM NaCl) to start H/D exchange. After 10/30/95/1000/10000 s incubation at 25 °C, 55 µl of the reaction were mixed with an equal volume of quench buffer (400 mM KH_2PO_4/H_3PO_4, 2 M guanidine-HCl, pH 2.2) pre-chilled at 1 °C and 95 µl of the resulting mixture immediately injected into an ACQUITY UPLC M-Class System with HDX Technology (Waters) (Wales *et al.*, 2008). Undeuterated samples were prepared similarly by 10-fold dilution in H_2O-containing buffer. Proteins were digested online with immobilized porcine pepsin at 12 °C with a constant flow (100 µl/min) of water + 0.1 % (v/v) formic acid, and the resulting peptic peptides collected on a trap column (2 mm x 2 cm) filled with POROS 20 R2 material (Thermo Scientific) kept at 0.5 °C. After 3 min, the trap column was placed in line with an ACQUITY UPLC BEH C18 1.7 µm 1.0 x 100 mm column (Waters), and the peptides eluted at 0.5°C using a gradient of water + 0.1 % (v/v) formic acid (A) and acetonitrile + 0.1 % (v/v) formic acid (B) at 30 µl/min flow rate as follows: 0-7 min/95-65 % A, 7-8 min/65-15 % A, 8-10 min/15 % A. Peptides were ionized by electrospray ionization (capillary temperature 250 °C, spray voltage 3.0 kV) and mass

spectra acquired over a range of 50 to 2000 *m/z* on a Synapt G2-Si mass spectrometer with ion-mobility separation (Waters) in HDMS^E or HDMS mode for undeuterated and deuterated samples, respectively (Geromanos *et al.*, 2009; Li *et al.*, 2009). Lock mass correction was performed with [Glu1]-Fibrinopeptide B standard (Waters). During separation of the peptides, the pepsin column was washed three times with 80 µl of 4 % (v/v) acetonitrile and 0.5 M guanidine hydrochloride, additionally, blank injections were performed between each sample. All measurements were carried out in triplicate.

Peptides were identified and analyzed as described previously with minor modifications (Osorio-Valeriano *et al.*, 2019). ProteinLynx Global SERVER 3.0.1 (PLGS, Waters) was employed to identify peptides from the non-deuterated samples acquired with HDMS^E employing low energy, elevated energy, and intensity thresholds of 300, 100 and 1000 counts, respectively. Peptides were matched using a database containing the amino acid sequences of *Bs*RicA, *Bs*RicF, *Gt*RicT, pepsin, and their reversed sequences. The following search parameters were used: Peptide tolerance = automatic; fragment tolerance = automatic; min fragment ion matches per peptide = 1; min fragment ion matches per protein = 7; min peptide matches per protein = 3; maximum hits to return = 20; maximum protein mass = 250000; primary digest reagent = non-specific; missed cleavages = 0; false discovery rate = 100. Deuterium incorporation was quantified with DynamX 3.0 (Waters) during which peptides had to fulfil the following criteria: identification in 3 of 6 undeuterated samples; minimum intensity of 10000 counts; maximum length of 30 amino acids; minimum number of products per amino acid of 0.1; maximum mass error of 25 ppm; retention time tolerance of 0.5 minutes. After automated data processing by DynamX, all spectra were manually inspected and, if necessary, peptides omitted (e.g. in case of low signal-to-noise ratio or presence of overlapping peptides).

4. RESULTS

4.1. The components of RicAFT: A mRNA and phosphorelay regulating complex

As described above, the RicAFT complex regulates the maturation of mRNAs in conjunction with RNase Y in *B*. *subtilis* (DeLoughery *et al.*, 2016; DeLoughery *et al.*, 2018) and is possibly involved in the phosphorelay of *B. subtilis* (Carabetta *et al.*, 2013; Dubnau *et al.*, 2016; Figure 6). Both of these functions affect the formation of biofilms in *B. subtilis*, hence a deletion of either *ricA*, *ricF* or *ricT* leads to incomplete maturation of mRNAs and a slower phosphorelay, thereby impairing biofilm formation (Carabetta *et al.*, 2013; DeLoughery *et al.*, 2016; Dubnau *et al.*, 2016; DeLoughery *et al.*, 2018). Although the *in vivo* importance concerning mRNAs of RicA and RicF has been shown, the mechanism is not understood. Nonetheless, the structure of RicAF has been published (Adusei-Danso *et al.*, 2019). In the present study the RicAFT complex is biochemically analyzed and the structure resolution was attempted. As described above (1.2.1.), the corresponding coding sequences of the complex subunit RicA and the tRNA methyltransferase are located in one operon across several species, with RNaseY located only few kilobase pairs upstream (Anton *et al.*, 2010). Thus, RicA and YmcB might form a complex to regulate mRNA degradation, possibly by disruption of the RicAFT complex. The binding of RicA to YmcB could alter the specificity or function of YmcB, as these are located in an operon and both are involved in RNA maturation or modification (Anton *et al.*, 2010; DeLoughery *et al.*, 2016; DeLoughery *et al.*, 2018). Nonetheless, this possibly requires the disassembly of the RicAFT complex, as it only can form if all three subunits are present. This would add another layer of regulation to the RicAFT complex.

4.1.1. RicA and YmcB do not form a complex *in vitro*

For the proper resolution of the putative complex the single components have been purified and crystallizations experiments performed (see 3.5). *B. subtilis ricA* was cloned into pET24d tagged with an N-terminal His-tag and expressed in *E. coli* BL21(DE3). Purification of the protein was performed as described in section 3.4.5 (see Figure 8 A). Further purification was performed as described in 3.4.7 with a HiLoad 16/600 Superdex 200 column. The resulting chromatogram, as well as the

corresponding SDS-PAGE of the fractions is shown in Figures 8 B and 8 C. Most of the protein eluted in peak 1 (see Figure 8 B). The protein-containing fractions were pooled and concentrated to 0.5 mM. *B. subtilis ymcB* was tagged with a C-terminal His-tag and cloned into pET24d for expression in *E. coli* BL21(DE3) and purified (see 3.4.5 and Figure 9 A). Further purification was performed with a HiLoad 16/600 Superdex 200 column (see 3.4.7). The resulting chromatogram, and the corresponding SDS-PAGE of the fractions can be seen in Figures 9 B and 9 C. The purification quality is comparable to *Bs*RicA.

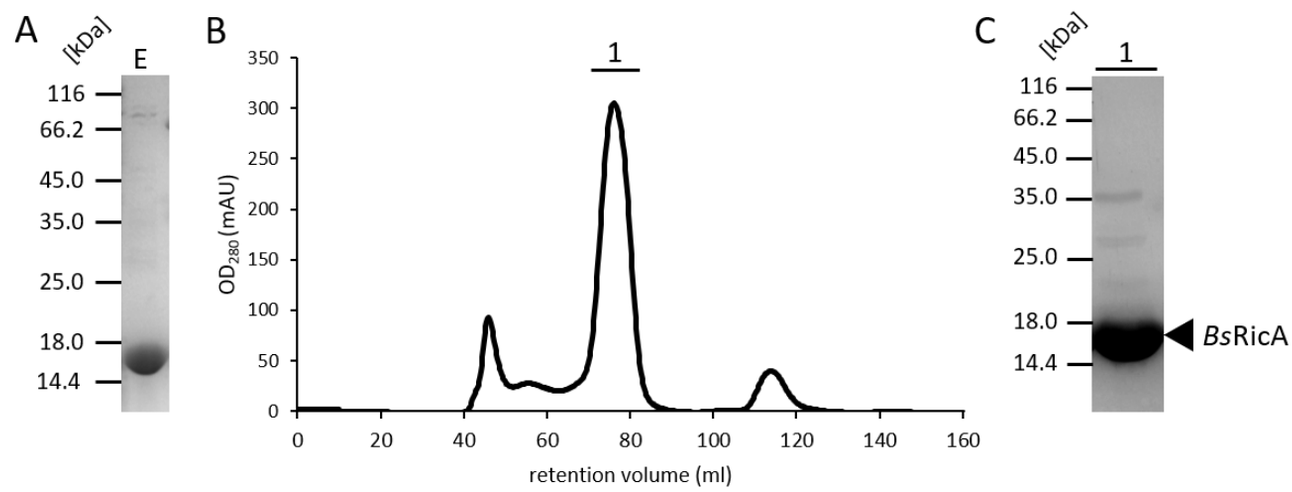

Figure 8: Ni-NTA purification and size exclusion chromatography purification of *Bs*RicA.
A) SDS-PAGE of Ni-purification elution of N-H_6-RicA. B) Size exclusion chromatography of *Bs*RicA. The peak containing most of the protein is labelled with 1. C) SDS-PAGE of peak 1 of *Bs*RicA, the protein band is marked with a calculated size of 16.7 kDa.

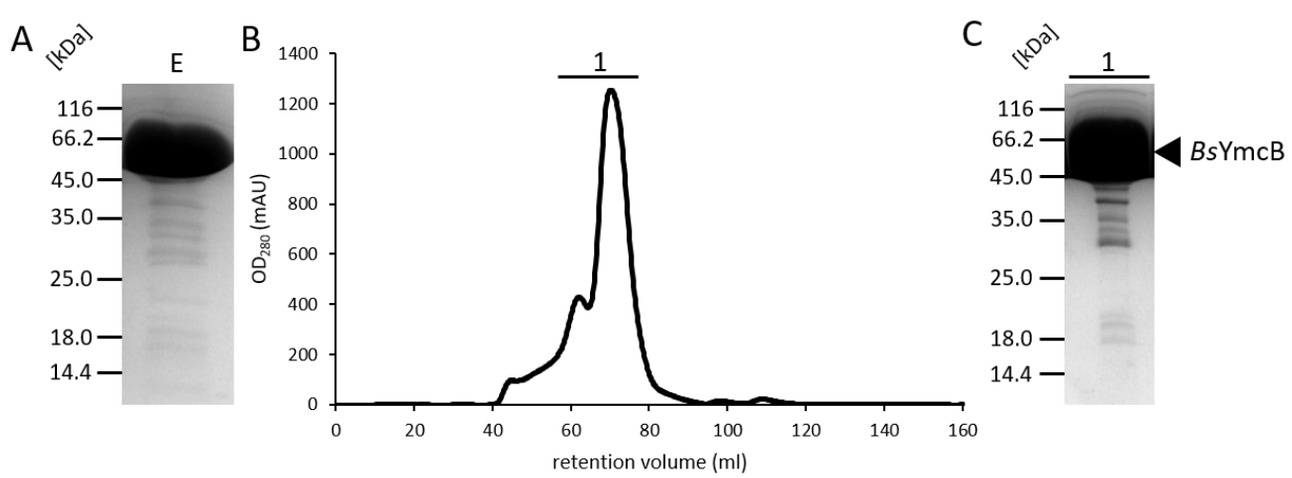

Figure 9: Ni-NTA purification and size exclusion chromatography purification of *Bs*YmcB.
A) SDS-PAGE of Ni-purification elution of C-H_6-YmcB. B) Size exclusion chromatography of *Bs*YmcB. The peak containing most of the protein is labelled with 1. C) SDS-PAGE of peak 1 of *Bs*YmcB, the protein band is marked with a calculated size of 58.8 kDa.

To test if *Bs*RicA and *Bs*YmcB interact *in vitro*, the purified proteins were mixed in stoichiometric amounts and incubated at room temperature for 5 min, then analyzed via size exclusion chromatography using a HiLoad 26/600 Superdex 200 column (see 3.4.7). The resulting chromatogram and the SDS-PAGE of the resulting fractions are shown in Figure 10. The presented SDS-PAGE shows the retention volumes of the proteins overlap, but they do not co-elute, hinting to no interaction between *Bs*RicA and *Bs*YmcB *in vitro*.

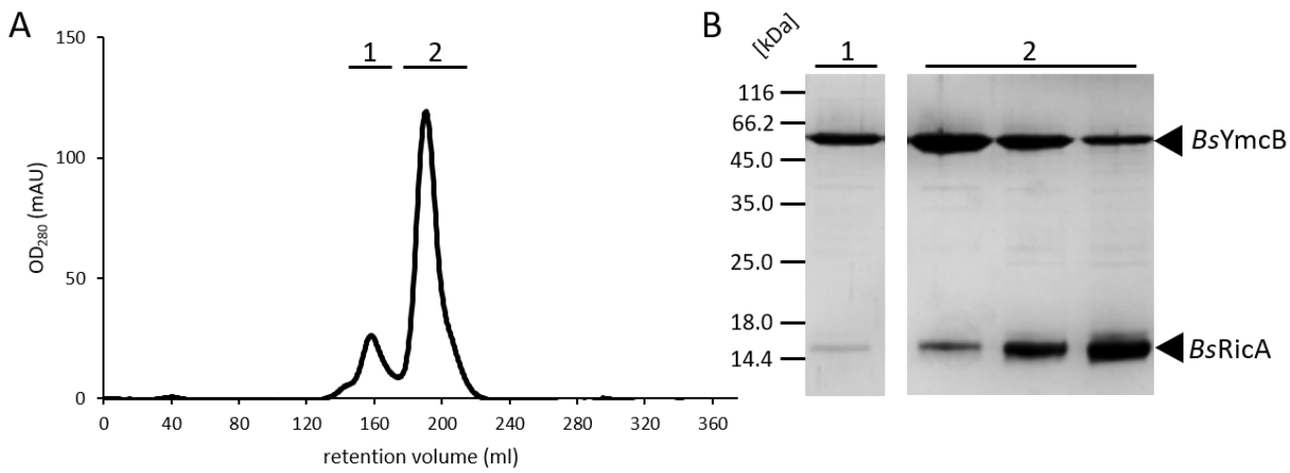

Figure 10: Size exclusion chromatography of *Bs*RicA and *Bs*YmcB mixed.
A) Size exclusion chromatography of *Bs*RicA and *Bs*YmcB mixed. The elution peaks are labeled with 1 and 2. B) SDS-PAGE of the protein peaks 1 and 2. The proteins bands are marked with their calculated molecular weight with *Bs*RicA at 16.7 kDa and *Bs*YmcB at 58.8 kDa.

Nonetheless, *Bs*RicA and *Bs*YmcB were used for crystallization experiments as described in 3.5, by mixing purified proteins in stoichiometric amounts. Crystals formed after 14 days in a sitting drop experiment. The crystals used for X-ray diffraction experiments can be seen in Figure 11. These formed in the following condition: 0.1 M calcium acetate, 0.1 M sodium cacodylate at pH= 4.5 and 40 % (v/v) PEG300. X-ray analysis of the crystals were performed at the DESY P14 beamline. In Figure 12 the final resolved crystal structure is shown. During molecular replacement it was realized that only *Bs*RicA is present in the asymmetric unit map and *Bs*YmcB is absent. The overall structure of *Bs*RicA is comparable to the published structure by Adusei-Danso *et al*., however, the use of the full-length construct allowed an improved resolution at the C-terminus and the structure was resolved until G131, compared to the G121 limit of the Adusei-Danso *et al*. structure. Yet, the C-terminus appears to be unstructured in absence of interaction partners and folds inwards, which according to previous suggestions would bind RicT (Tanner *et al.*, 2017; Adusei-Danso *et al.*, 2019; Figure 12). While similar to the general fold of the *Bs*RicAF dimer shown in Figure 5 (PDB: 6PRK), the

location and the angle of the arms of the *Bs*RicF subunit is narrower than in the *Bs*RicA dimer (marked by arrows). Additionally, in the *Bs*RicAF heterodimer the C- and N-termini are slightly distorted in comparison to the *Bs*RicA dimer (marked by arrows). The *Bs*RicF and *Bs*RicA C-termini point further outwards from the center than in the *Bs*RicA dimer. As a *Bs*RicA dimer is unable to bind *Bs*RicT, while a *Bs*RicAF heterodimer can (Figure 12).

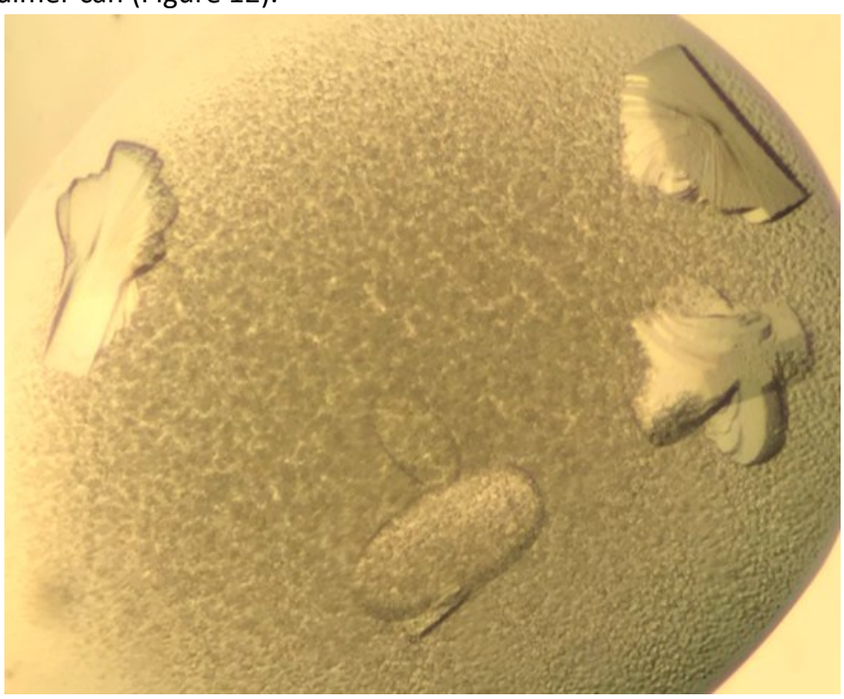

Figure 11: *Bs*RicA crystals in one crystallization condition.
The crystal form used in the X-ray diffraction experiment is shown. 0.1 M calcium acetate, 0.1 M sodium cacodylate, pH= 4.5 and 40 % (v/v) PEG300.

In Table 5 the crystallographic statistics for the data collection and the refinement are represented.

In addition, the protein was analyzed via analytical size exclusion (see 3.4.8). The resulting chromatogram can be seen in Figure 13. The retention volume of *Bs*RicA is around 15.07 ml which corresponds to a size of around 42 kDa hinting towards a dimer, which is in agreement with the observed crystal structure and previous published results (Tanner *et al.*, 2017; Adusei-Danso *et al.*, 2019). The expected size would be 34 kDa when calculating the theoretical weight of a *Bs*RicA dimer.

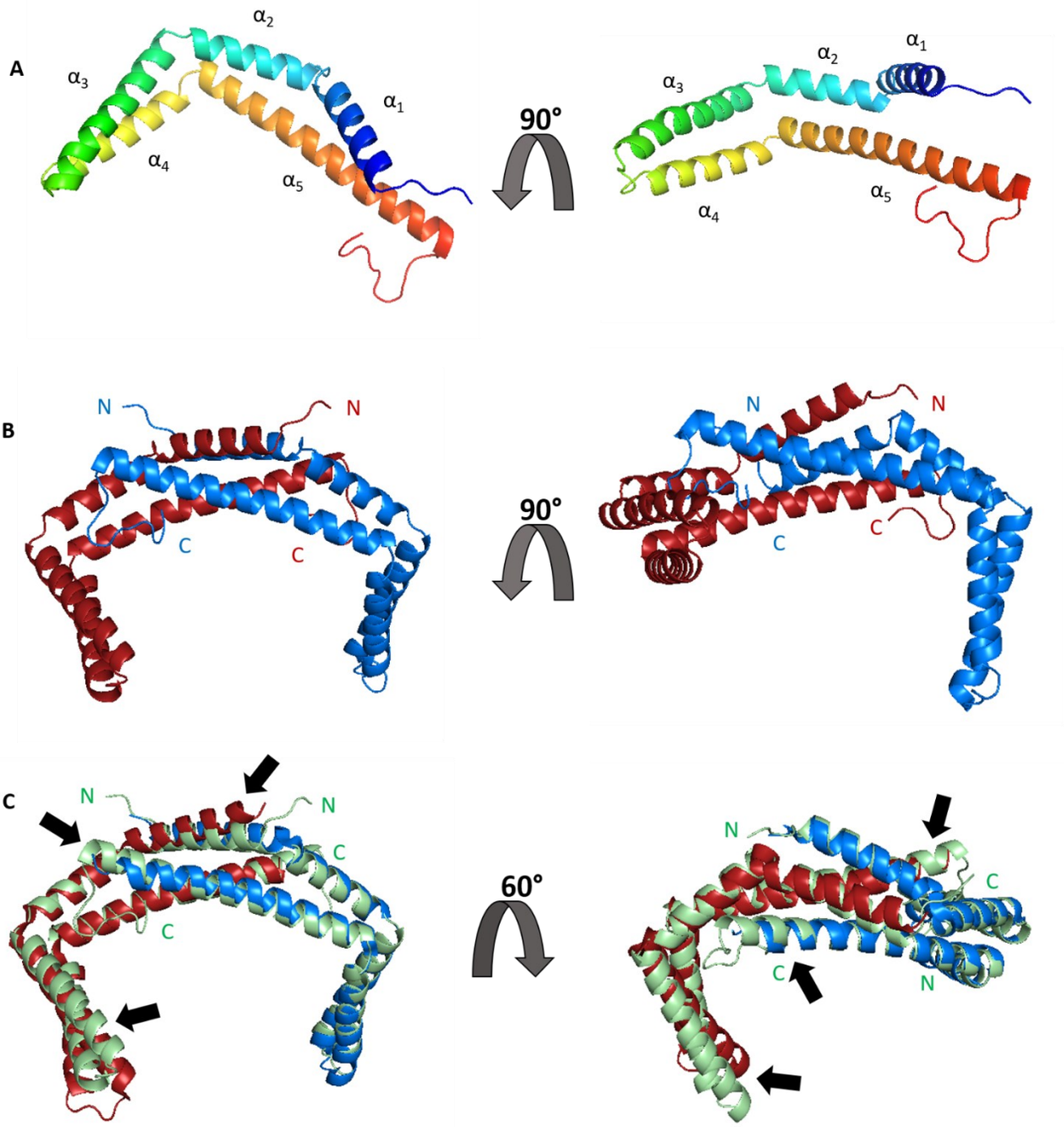

Figure 12: Crystal structure representation of *Bs*RicA monomer and dimer.
A) The *Bs*RicA monomer, resolved in this study, is shown until G131. The structure is colored from blue to red in an N- to C-terminus order. The helices are numbered according to their position in the structure. B) The *Bs*RicA dimer is shown. The monomers are colored either blue or red, their N-and C-termini are labeled accordingly. C) Overlay of *Bs*RicAF heterodimer (PDB: 6PRK), *Bs*RicF in red, and *Bs*RicA in blue, the *Bs*RicA dimer resolved in this study is in green.

Table 5: Data collection and refinement statistics for *Bs*RicA structure. The values in parenthesis refer to the highest resolution shell.

		***Bs*RicA**
Data collection	Resolution range	48.65 - 2.398 (2.484 - 2.398)
	Space group	P 22_1 2_1
	Unit cell (a, b, c) in Å	35.58
		105.33
		109.69
	α, β, γ (°)	90
		90
		90
	Unique reflections	16829 (1589)
	Multiplicity	6.6 (6.8)
	Completeness (%)	99.59 (97.78)
	Mean I/sigma(I)	11.62 (1.03)
	R-merge	0.09083 (1.24)
Refinement	CC1/2	0.999 (0.576)
	Reflections used in refinement	16816 (1588)
	R-work	0.2465 (0.3095)
	R-free	0.2986 (0.4109)
	RMS (bonds)	0.010
	RMS (angles)	1.12
	Ramachandran favored (%)	97.66
	Ramachandran allowed (%)	1.95
	Ramachandran outliers (%)	0.39
	Average B-factor	72.30
	macromolecules	72.23
	solvent	75.77

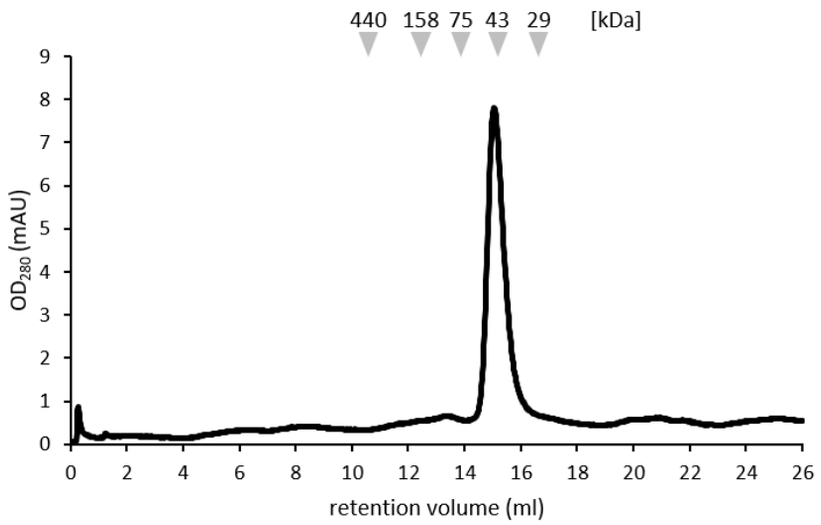

Figure 13: *Bs*RicA analytical size exclusion chromatography.
Chromatogram of the N-H_6-*Bs*RicA analytical size exclusion. The standard sizes are indicated with grey arrows, unit size is kDa (see 3.4.8).

In literature, no *in vitro* interaction of *Bs*RicA and *Bs*YmcB could be found, yet, this does not exclude a possible *in vivo* interaction. For this purpose, CoIP experiments were performed with N-terminal Strep-tagged *B. subtilis ymcB* and N-terminal Strep-tagged *B. subtilis ymcB* in combination with untagged *B. subtilis ricA*, amplified from *B. subtilis* NCIB3610 corresponding genes. The tagged constructs were cloned under the control of a bacitracin inducible promoter in a pLIKErep plasmid and transformed into *B. subtilis* NCIB3610. (3.4.2). The expression of the constructs was tested via Western Blots as described in 3.4.11. The expression was successful and can be seen in Figure 14.

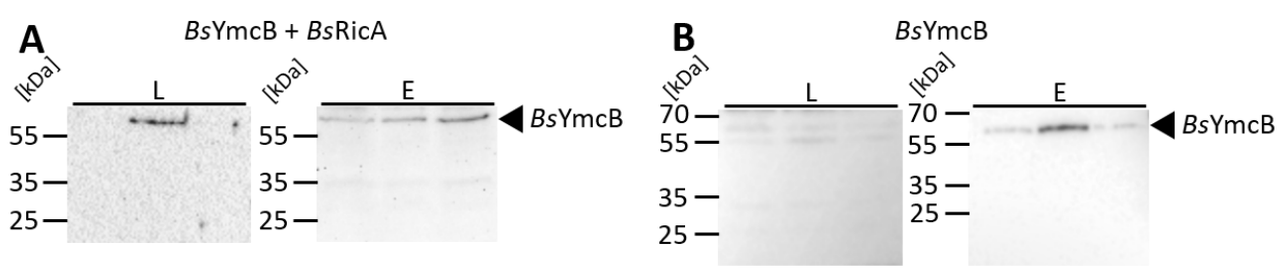

Figure 14: Western Blots of the CoIPs of *Bs*YmcB and *Bs*YmcB + *Bs*RicA overproduction in *B. subtilis* NCIB3610.
A) Western Blot of Strep-*Bs*YmcB overproduction. B) Western Blot of Strep-*Bs*YmcB and *Bs*RicA overproduction. The antibody used for detection was StrepTactin® HRP (IBA, Germany). L: lysate fraction; E: elution fraction. Protein size for *Bs*YmcB is indicated by arrows at around 58 kDa.

CoIP experiments were carried out as described in 3.4.4. To show that the proteins were successfully produced, were stable, and bound to the magnetic-Strep-beads, samples for Western Blots were prepared from the CoIP experiments. Results from CoIP experiments for *Bs*RicT and *Bs*YjbN, performed in this study, were used as comparative control (see 4.3). For the CoIP with *Bs*YmcB the proteins in Table 6 were found as potential interaction partners with the most confidence. DhbE is involved in the synthesis of bacillibactin, a siderophore responsible for iron acquisition. It activates

the 2,3-dihydroxy-benzoate by adenylation. The *dhbE* gene is encoded in a six gene operon (*dhbA-dhbC-dhbE-dhbB-dhbF-ybdZ*) that is repressed by Fur, AbrB, and Kre, and upregulated during biofilm formation (May *et al.*, 2001; May *et al.*, 2002; Baichoo *et al.*, 2002; Chumsakul *et al.*, 2011).

Phage-derived proteins were enriched as well, for example SunS and SunT. SunS/YolJ is a glycosyltransferase involved in the production of sublancin, an antimicrobial peptide derived from SunA. During the production process it transfers a sugar moiety on C22 (Oman *et al.*, 2011; Wang and van der Donk, 2011). SunT is the transporter and processor of sublancin and contains an ATP-binding cassette (Quentin *et al.*, 1999; Dorenbos *et al.*, 2002). Both are repressed by Rok, DnaA, and AbrA, and activated by Abh and YvrHB, as they are located in one operon: *sunA-sunT-bdbA-SunS-bdbB* (Chumsakul *et al.*, 2011; Seid *et al.*, 2017).

Soj is an ATPase that has a centromere-like function. It can stall DNA replication and is essential for correct partitioning of DNA, and ergo, chromosome integrity. It controls the activity of DnaA and is responsible for the repression of several sporulation genes (Quisel and Grossman, 2000; Murray and Errington, 2008; Scholefield *et al.*, 2012; Jindal and Emberly, 2019). The gene is located in an operon along with *parB,* repressed by Spo0A (Molle *et al.*, 2003).

GltT is the major Na^+/H^+ coupled glutamate/aspartate symporter. It has a high affinity for aspartate and glutamate (Holtmann *et al.*, 2003; Reyes *et al.*, 2013; Jensen *et al.*, 2013).

Table 6: Co-eluting proteins identified with most confidence for the *Bs*YmcB CoIP

Protein	Accession number	Function	Pathway/Essential
DhbE	P40871	2,3-dihydroxybenzoate-AMP ligase	Iron-acquisition/no
SunS/YolJ	O31986	Synthesis of sublancin	Defense/no
SunT	P68579	Transport and processing of sublancin	Defense/no
Soj/ParA	P37522	Negative regulator of sporulation initiation	Sporulation/no
GltT	O07605	Glutamate and aspartate uptake	Amino acid uptake/no

In the co-production of *Bs*YmcB and *Bs*RicA one additional protein was detected in the CoIP experiment with confidence, see Table 7.

SipS is signal peptidase I and is required for the secretion of several proteins. By cleaving the hydrophobic N-terminal signal peptide it processes the protein for secretion. Furthermore, it cleaves

the sigma factor RsiV, thereby degrading it and activating the sigma factor σ^V, a sigma factor required for defense against lysozyme (Bolhuis *et al.*, 1996; Tjalsma *et al.*, 1997; Tjalsma *et al.*, 1998; Hastie *et al.*, 2014; Zalucki and Jennings, 2017; Castro *et al.*, 2018).

In the CoIP experiment where only *Bs*YmcB was overproduced no *Bs*RicA was found, in contrast to the experiment in which *Bs*YmcB and *Bs*RicA were overproduced. Nevertheless, the amount was below the threshold to confidently conclude an *in vivo* interaction.

Table 7: Co-eluting proteins identified with most confidence for the *Bs*YmcB + *Bs*RicA CoIP

Protein	Accession number	Function	Pathway/Essential
SipS	P28628	Protein maturation	Protein secretion/no

4.1.2. Biochemical analysis of the RicAF complex

As shown in other studies, *Bs*RicA and *Bs*RicF form a complex (Carabetta *et al.*, 2013). In the crystal structure of Adusei-Danso *et al*. it forms a tetramer made from two heterodimers (Adusei-Danso *et al.*, 2019; PDB: 6PRK). The oligomerization of the *Bs*RicAF complex in solution is still unknown. Unfortunately, *Bs*RicF cannot be purified solely as it degrades during purification (Adusei-Danso *et al.*, 2019 and personal observation). Hence, N-H_6-*Bs*RicA and *Bs*RicF were overproduced in *E. coli* BL21(DE3) cells, encoded on a pETduet plasmid as it has been shown that *Bs*RicF is stable in presence of *Bs*RicA (Carabetta *et al.*, 2013; Adusei-Danso *et al.*, 2019). The proteins were purified with an N-terminally His-tagged *Bs*RicA and then further by size exclusion chromatography (see Figures 15 A and 15 B, and 3.4.5.). The contamination band in the elution fraction around 35 kDa could not be identified by mass spectrometry.

The elution of the affinity chromatography was concentrated to 2 ml and loaded onto a HiLoad 16/600 Superdex S200 column. The resulting chromatogram is shown in Figure 15 B with the respective SDS-PAGE in Figure 15 C. The protein eluted in an elongated peak with probably more N-H_6-*Bs*RicA than *Bs*RicF. The reoccurring contamination band at around 35 kDa can be observed again, for which no conclusive result via mass spectrometry could be obtained as the main detected components were *Bs*RicA and *Bs*RicF.

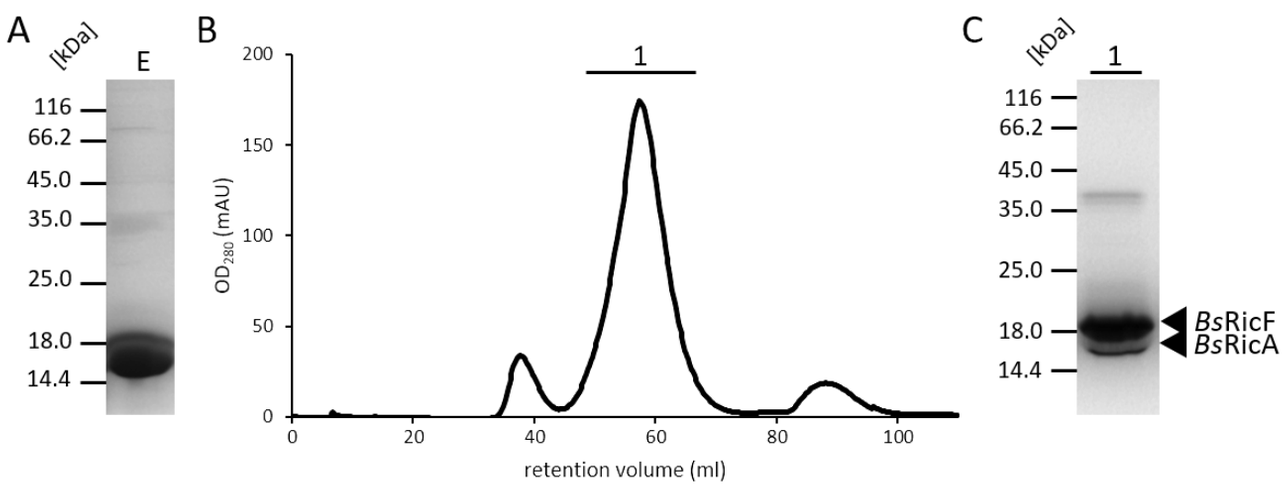

Figure 15: Ni-NTA purification and size exclusion chromatography purification of *Bs*RicAF.
A) SDS-PAGE of Ni-purification elution of N-H_6-*Bs*RicA and *Bs*RicF. B) Chromatogram of the N-H_6-*Bs*RicA and *Bs*RicF SEC purification. B) Respective Coomassie-stained SDS-PAGE of the N-H_6-*Bs*RicA and *Bs*RicF SEC-purification. The molecular weight of the marker is given in kDa. The protein bands are indicated with the calculated molecular weight of *Bs*RicA at 16.7 kDa and 16.9 kDa for *Bs*RicF.

The purified proteins were then analyzed for their molecular size in solution by analytical size exclusion (see 3.4.8 and Figure 16). The peak labeled with 1 has a retention volume of 13.69 ml, corresponding to a size of roughly 55 kDa, therefore this size is too small for the theoretical size of the *Bs*RicAF tetramer of 67.2 kDa. Nonetheless, a reference protein with a size of 75 kDa (Conalbumin; retention volume: 13.95 ml) elutes at 13.95 ml, hence the detected protein size is probably larger than the calculated. The peak labeled with 2 has its maxima at a retention volume of 15 ml, which corresponds to a calculated size of 42 kDa for the proteins in the peak. The estimated size of a *Bs*RicAF dimer is 33.6 kDa and is smaller than the calculated size of the peak.

The protein complex was analyzed by mass photometry as well (see 3.7 and Figure 17). Most of the protein sample is present around 68 kDa which would suggest most of the proteins are present as a heterotetramer, however, this is in direct contradiction to the results of the analytical size exclusion. It is worth noting that mass photometry has a detection limit of 50 kDa, so proteins and protein

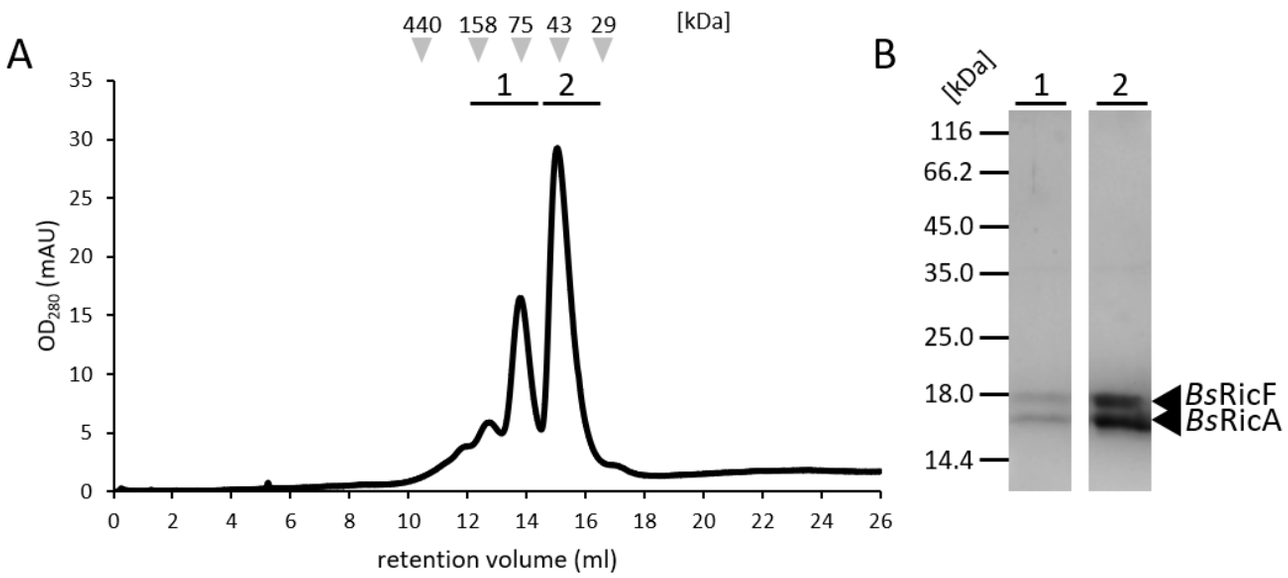

Figure 16: Analytical size exclusion chromatography of *Bs*RicA and *Bs*RicF.
A) Chromatogram of the analytical size exclusion of the N-H_6-*Bs*RicA and *Bs*RicF protein complex. The standard protein sizes are indicated with grey arrows, the unit size is kDa (see 3.4.8). B) Respective Coomassie-stained SDS-PAGE of the peaks of the *Bs*RicAF analytical SEC. The molecular weight of the marker is given in kDa. The protein bands are indicated with the calculated molecular weight of *Bs*RicA at 16.7 kDa and 16.9 kDa for *Bs*RicF.

complexes below that size are not detected, meaning a possible *Bs*RicAF dimer would not be observed. Nevertheless, as pure *Bs*RicA cannot form stable tetrameric complexes during size exclusion chromatography as opposed to the *Bs*RicAF protein complex, the detected tetramer could have some veracity.

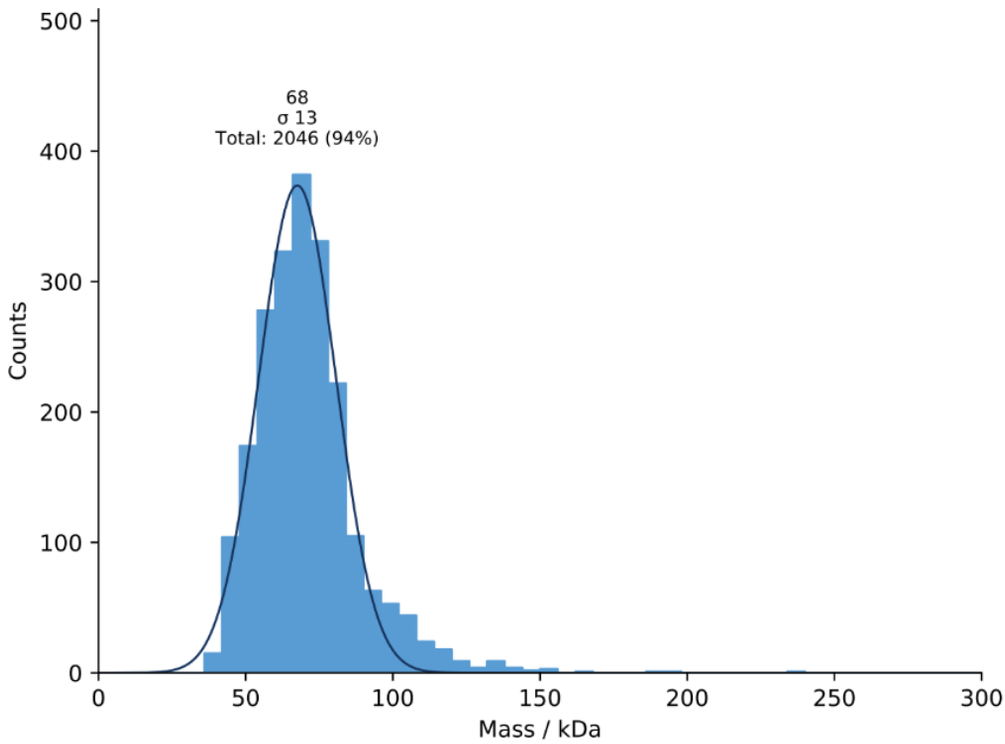

Figure 17: Mass photometry histogram of *Bs*RicAF.
The bars indicate the counts of the particles of the specific size. The curve is a function of the counts, its peak indicates the most likely size of the particle.

4.1.3. RicT: The unknown component

RicT is the possible, yet unknown structural centerpiece protein of the RicAFT complex. Deletion of its corresponding gene leads to a severely impaired biofilm formation in *B. subtilis* and obstructed RNA maturation (Carabetta *et al.*, 2013; DeLoughery *et al.*, 2016; Dubnau *et al.*, 2016; DeLoughery *et al.*, 2018). In addition, it was shown that it carries a [4Fe-4S] cluster and binds RicAF in a 1:1 stoichiometric ratio (Tanner *et al*., 2017; Adusei-Danso *et al*., 2019). To biochemically characterize RicT further in this study, N-H_6-*Bs*RicT was heterologously overproduced in *E. coli* BL21 (DE3) cells. Unfortunately, the protein was insoluble in the used buffer (data not shown) hence, an alternative approach was chosen. The genome of a close relative of *B. subtilis Geobacillus thermodenitrificans* encodes RicA, RicF, and RicT as well. Thus, the homologue of *B. subtilis ricT* (77.82 % identity, see Table 1) now called *GtricT* was chosen and cloned into pET24d with an N-terminal His-tag and produced in *E. coli* BL21 (DE3) cells. The protein was soluble, contrary to the B*. subtilis* homologue, yet several contaminating proteins were present (see 3.4.5; Figure 18 A). *Gt*RicT is the most abundant protein in the elution fraction. For further purification, the elution fraction was loaded onto a HiLoad 16/600 Superdex S200 column (see 3.4.7) the resulting chromatogram is shown in Figure 18 B. The protein could not be separated from all contaminations. Additionally, a large portion of the protein was not properly separated by size exclusion chromatography and eluted too quickly along with various contaminations. In the fractions in which the protein is present in abundance, contaminations or degradation bands are present, hinting towards a need for improvement of the buffer conditions to increase the stability of the protein. Nevertheless, the protein peak labeled with 1 was concentrated to a calculated concentration of 500 µM, and crystallization experiments were performed (see 3.5). Nonetheless, no crystals were obtained, which might be due to the impurity of the sample or to the time the crystals need to form.

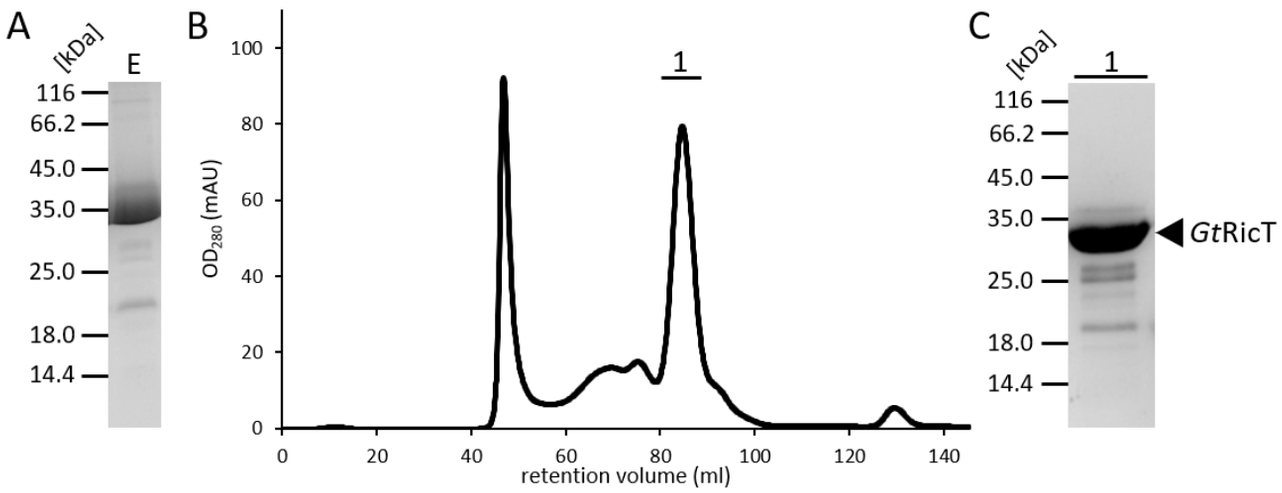

Figure 18: Ni-NTA purification and size exclusion purification of *Gt*RicT.
A) Elution fraction of Ni-affinity purification of N-H_6-*Gt*RicT. B) Chromatogram of the N-H_6-*Gt*RicT SEC purification. The major peak of N-H_6-*Gt*RicT is labeled with 1. C) The respective Coomassie-stained SDS-PAGE. The molecular weight of the marker is given in kDa. The highest peak contains primarily *Gt*RicT. The protein is marked with its calculated molecular weight of 32 kDa.

The oligomerization state of the protein was analyzed by analytical size exclusion chromatography (Figure 19; 3.4.8) and by mass photometry (Figure 20, 3.7). The analysis via analytical size exclusion chromatography reveals several not-well-separated small peaks and a larger peak. The large peak has a retention volume of 15.4 ml that corresponds to 39 kDa in size for the protein (3.4.8). This is in accordance with the predicted size of a *Gt*RicT monomer of 32 kDa. The smaller peaks eluting before the possible *Gt*RicT monomer are comprised of *Gt*RicT free of contaminations, which implies that a small fraction of the protein oligomerizes. This is confirmed by the results of the mass photometry, the counts of the detected proteins are low, yet the most significant peak is around 58 kDa and possibly corresponds to a *Gt*RicT dimer with an expected size of 64 kDa. In these results, there are also some large but more disperse peaks with even lower counts, making them negligible. Again, the resolution limit of this method is around 50 kDa, hence, the *Gt*RicT monomer could not be detected in this method. The oligomerization of *Gt*RicT might be explained by the oxidation of the bound [4Fe-4S] cluster. Therefore, it should be assumed that RicT exists mostly a monomer *in vivo*, as the amount of oxygen is limited and the chance for oxidation is low.

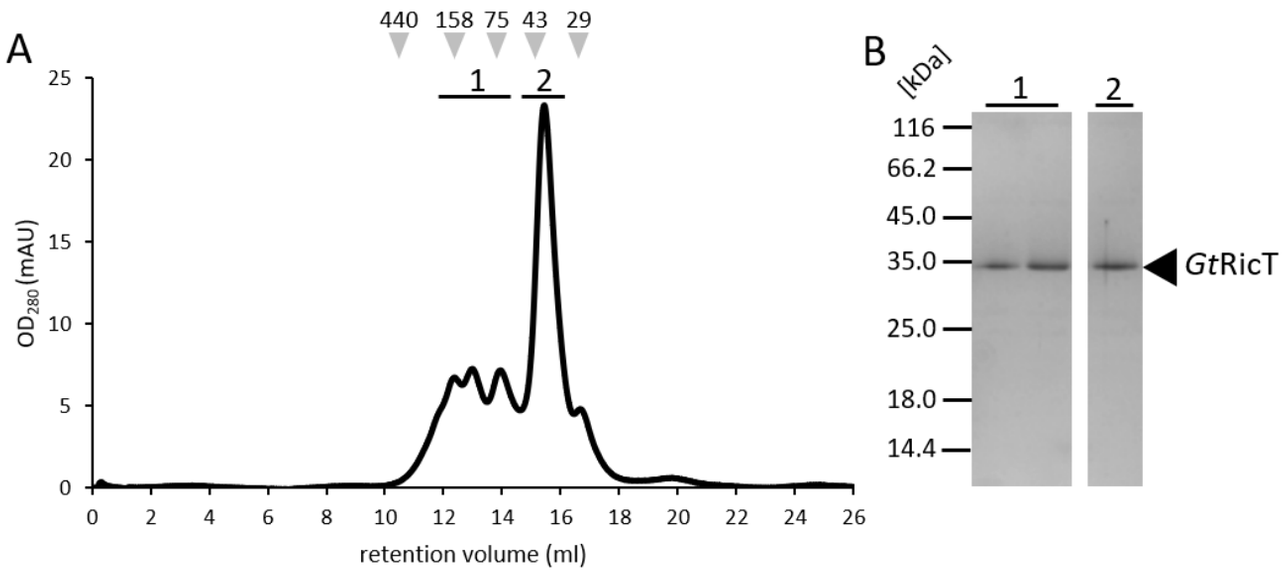

Figure 20: Analytical size exclusion chromatography of *Gt*RicT.
A) Chromatogram of the *Gt*RicT analytical SEC. B) The respective Coomassie-stained SDS-PAGE of the analytical size exclusion chromatography experiment. The molecular weight of the marker is given in kDa, protein size is indicated at its calculated molecular weight of 32 kDa. Peak 2 is solely *Gt*RicT. The peaks collectively labeled with 1 are most likely oligomers. The standard sizes are indicated with grey arrows, unit size is kDa (see 3.4.8).

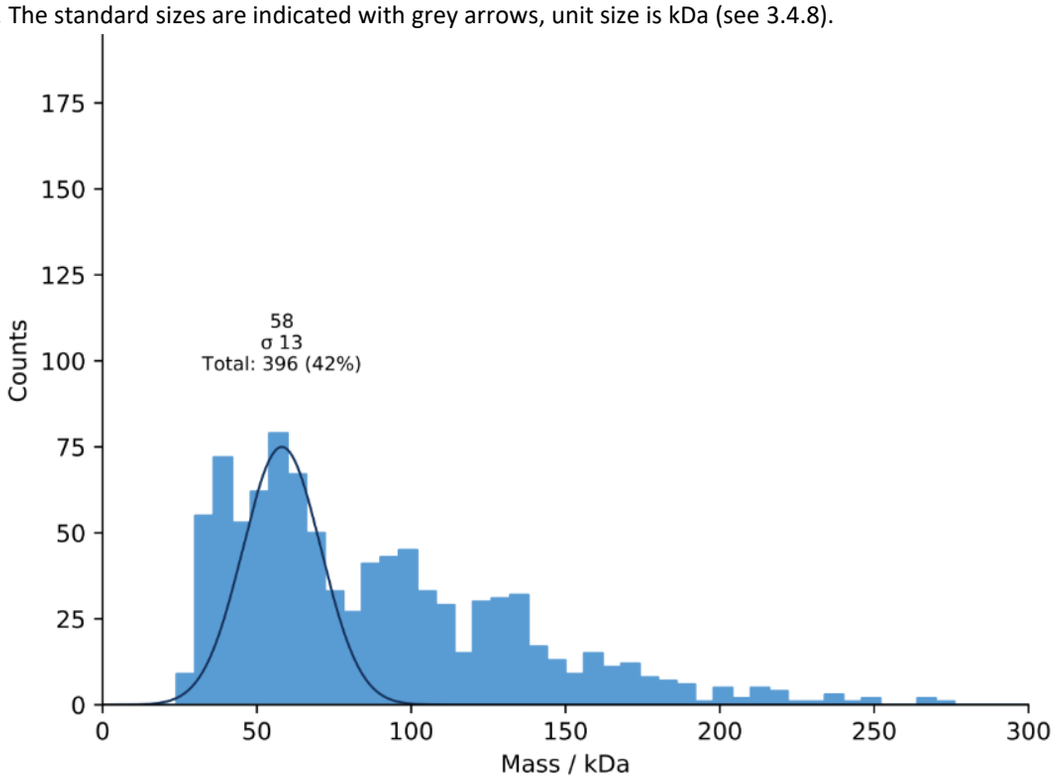

Figure 19: Mass photometry histogram of *Gt*RicT.
The bars indicate the counts of the particles of the specific size. The curve is a function of the counts, its peak indicates the most likely size of the particle.

4.2. The RicAFT complex

4.2.1. Biochemical analysis of the RicAFT complex

The RicAFT complex has been shown before to exist *in vivo* and *in vitro*, where it displayed a 1:1:1 stoichiometry (Carabetta *et al.*, 2013; DeLoughery *et al.*, 2016). Nonetheless, the complex has yet to be structurally and biochemically characterized, which therefore became an aim for this study. For this, the *Bs*RicAF construct from the previous section 4.1.2 was reused and in addition *ricT* from *B. subtilis* was cloned without an affinity-tag into pET24d to be co-transformed into *E. coli* BL21 (DE3) cells as it was shown that *Bs*RicT was soluble in the presence of *Bs*RicA and *Bs*RicF (see 4.2.1 and Carabetta *et al.*, 2013). The proteins were then expressed as described in 3.4.2 and purified by using the N-terminal His-tag on *Bs*RicA (see 3.4.5). The SDS-PAGE of the affinity purification elution is shown in Figure 21 A. Further purification was done by SEC using a HiLoad 16/600 Superdex S200 column (see 3.4.7, and Figures 21 B and 21 C). The chromatogram depicts three distinct peaks, *Bs*RicAFT is mainly present in peak 1 and 2. It was assumed that the protein concentration or oligomerizations differ from peak to peak, consequently, these were handled separately. To ensure this, fractions were collected individually. The concentrated protein peaks were used for crystallization experiments (see 3.5). No crystals formed in the performed experiments during the timeframe of this work.

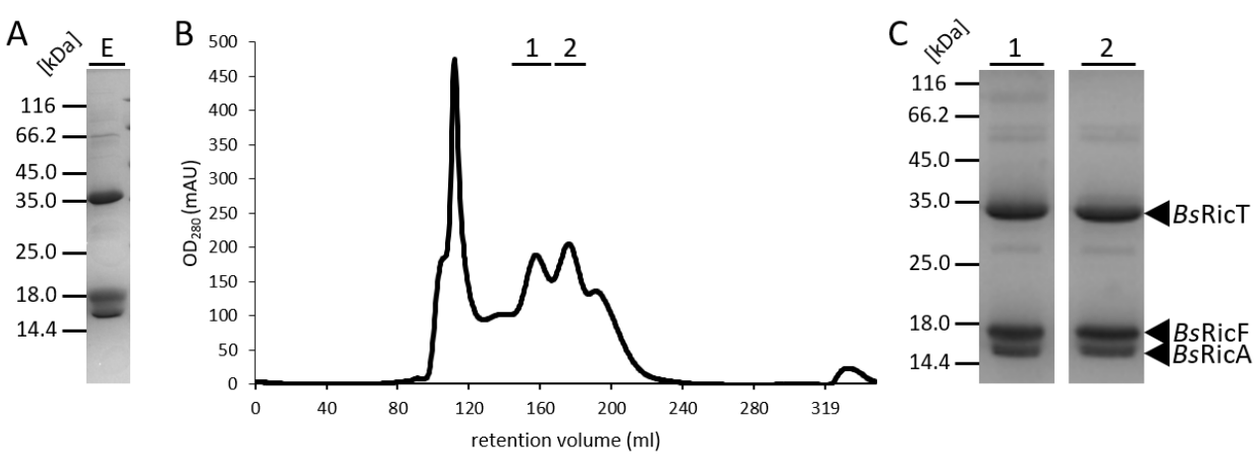

Figure 21: Ni-NTA purification and size exclusion purification of *Bs*RicAFT.
A) Elution fraction of the Ni-NTA purification of the *Bs*RicAFT complex. B) Chromatogram of the N-H_6-*Bs*RicA, *Bs*RicF and *Bs*RicT SEC purification. C) The respective Coomassie-stained SDS-PAGE. The molecular weight of the marker is given in kDa. In the peak 1 and 2 RicAFT seems to be the main components. Protein sizes are indicated with *Bs*RicA at 16.7 kDa, *Bs*RicF at 16.9 kDa, and *Bs*RicT at 32 kDa.

In addition, an analytical size exclusion experiment was performed to obtain biochemical insight of the different peaks (see 3.4.8). The result for the analytical size exclusion experiment for protein peak 1 is shown in Figure 22. The peak is still inhomogeneous, as three peaks form labeled from 1 to 3. Nevertheless, the most abundant proteins in the peaks remain *Bs*RicA, *Bs*RicF, and *Bs*RicT. The peak which contains the largest amount of the complex is peak 2. Its calculated size is around 255 kDa with a retention volume of 12.1 ml, however a reference protein (Aldolase, 158 kDa, retention volume: 12.36 ml) elutes very closely to the detected peak. Therefore, it is predicted that the protein complex is around 200 kDa of size (see Table 4). The respective SDS-PAGE of the analytical size exclusion revealed that the proteins are present in similar amounts, therefore a 1:1:1 stoichiometric ratio is assumed as presented before (Adusei-Danso *et al*., 2019). As a single tripartite complex would be roughly 68 kDa, and the calculated size of the complex by analytical size exclusion is around 200 kDa, the results hint towards an oligomerization of the *Bs*RicAFT complex into a trimer of trimers. Peak 3, which also contains RicAFT in a 1:1:1 stoichiometric ratio according to the SDS-PAGE (see Figure 22 B) elutes at 13.5 ml, resulting in a calculated size of around 59 kDa and therefore not entirely in agreement with the previous observed 1:1:1 heterotrimer corresponding to a 68 kDa size (Adusei-Danso *et al*., 2019). Yet, the reference protein Conalbumin (size: 75 kDa, retention volume: 13.95) is larger and elutes later, leading to the conclusion that the observed complex is larger as well.

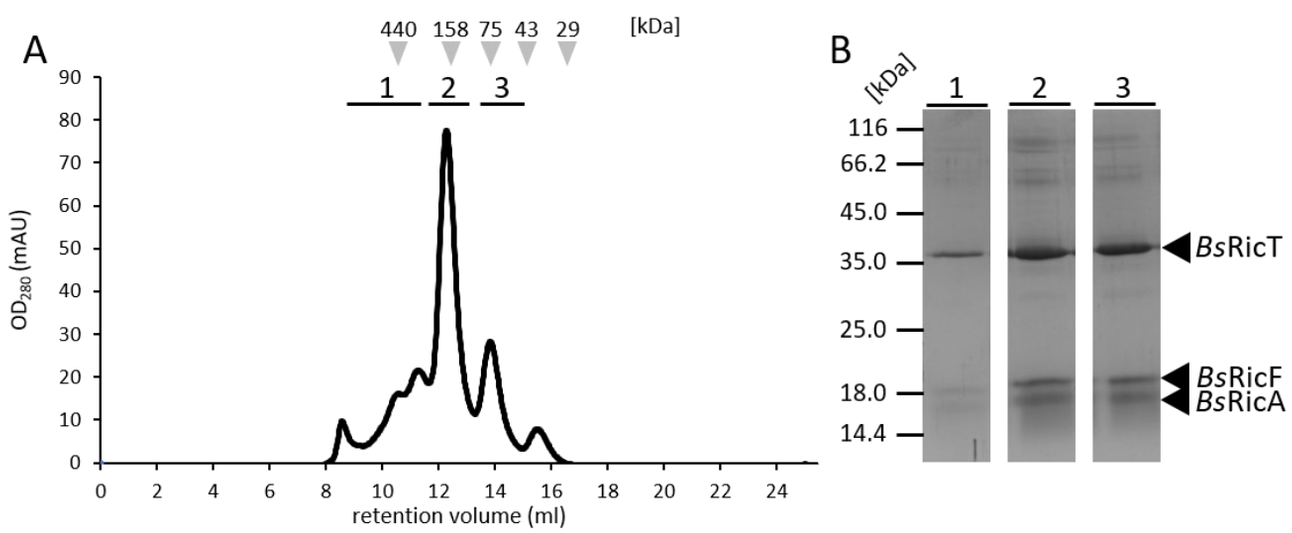

Figure 22: Analytical size exclusion chromatogram of *Bs*RicAFT peak 1.
A) Chromatogram of the N-H_6-*Bs*RicA, *Bs*RicF, and *Bs*RicT peak 1 analytical SEC. B) The respective Coomassie-stained SDS-PAGE of the analytical SEC. The molecular weight of the marker is given in kDa. Protein bands are indicated with *Bs*RicA at 16.7 kDa, *Bs*RicF at 16.9 kDa, and *Bs*RicT at 32 kDa. Peak 2 and 3 mainly contain *Bs*RicAFT complex, while peak 2 is significantly higher than peak 3. The standard sizes are indicated with grey arrows, unit size is kDa (see 3.4.8).

Peak 1 is probably comprised of larger aggregates due to the buffer conditions or instability of the proteins. The peak at around 15 ml is most likely an excess of *Bs*RicAF and might constitute the dimer. The same experiments were performed for peak 2 of the protein purification (see Figure 23). The observed results are nearly the same as for the peak 1 of the RicAFT complex. The absorption values are significantly higher and the high molecular weight aggregates of the complex in peak 1 are significantly lower, yet the observed retention volumes are the same. Thereby, both isoforms are detected in either peak. Henceforth, it is concluded that the RicAFT complex in solution can be present as a 1:1:1 trimer and oligomers of this trimer.

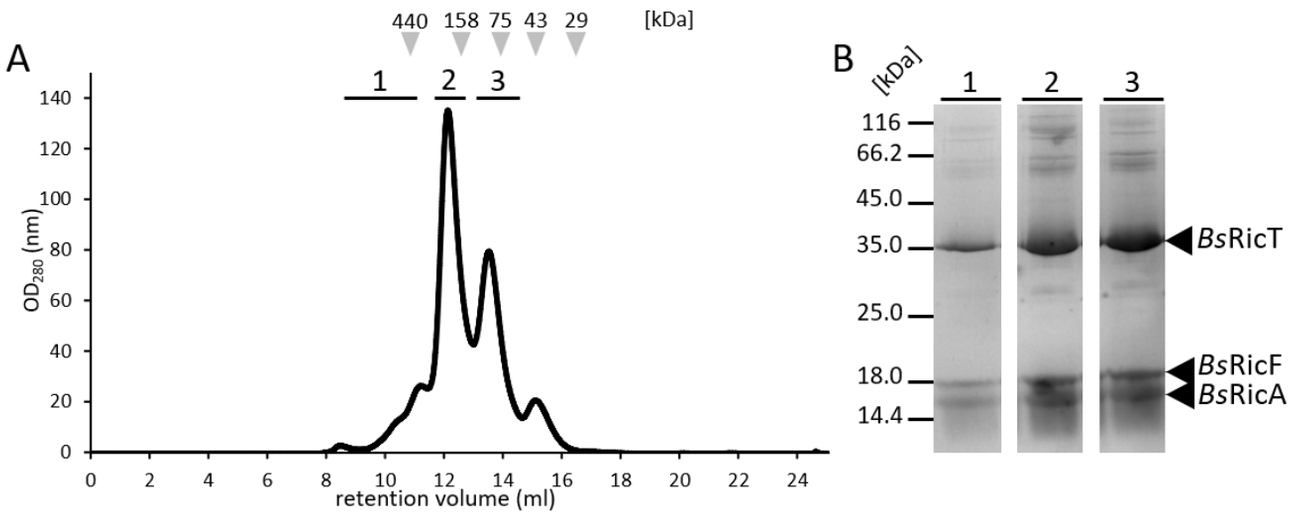

Figure 23: Analytical size exclusion chromatogram of *Bs*RicAFT peak 2.
A) Chromatogram of the N-H_6-*Bs*RicA, *Bs*RicF, and *Bs*RicT peak 2 analytical SEC. B) The respective Coomassie-stained SDS-PAGE. The molecular weight of the marker is given in kDa. Protein bands are indicated with *Bs*RicA at 16.7 kDa, *Bs*RicF at 16.9 kDa, and *Bs*RicT at 32 kDa. The peak 2 and 3 mainly contain *Bs*RicAFT complex, while peak 2 is significantly higher than peak 3. The standard sizes are indicated with grey arrows, unit size is kDa (see 3.4.8).

Since no crystals of the *Bs*RicAFT complex could be obtained, a second approach was chosen. The exact protocol employed to purify *Bs*RicAFT was used to reconstitute the whole complex from *G*. *thermodenitrificans* since proteins of thermophilic bacteria tend to be more readily crystallized, since they are usually less flexible (Vieille and Zeikus, 2001; Feller, 2010). Hence, the purification was repeated with *Gt*RicAFT. As shown in Figure 24 A, the purification was successful, although there are more contamination bands present in the lower molecular sections compared to *Bs*RicAFT. Mass spectroscopy verified that these are *Gt*RicF degradation products (results not shown).

Nonetheless, the complex was loaded onto a HiLoad 26/600 Superdex S200 column for further purification (see 3.4.7). The resulting chromatogram with the corresponding SDS-PAGE are shown in Figures 24 B and 24 C. The peaks are now distinct, yet the yields are low in comparison to the *B. subtilis* complex. Furthermore, the *Gt*RicF degradation products are persistent, which would reduce the chance for correct crystal packing. Additionally, *Gt*RicF migrates retardedly at around 22 kDa in comparison to its calculated molecular weight of 16.6 kDa, possibly because of its positive charge.

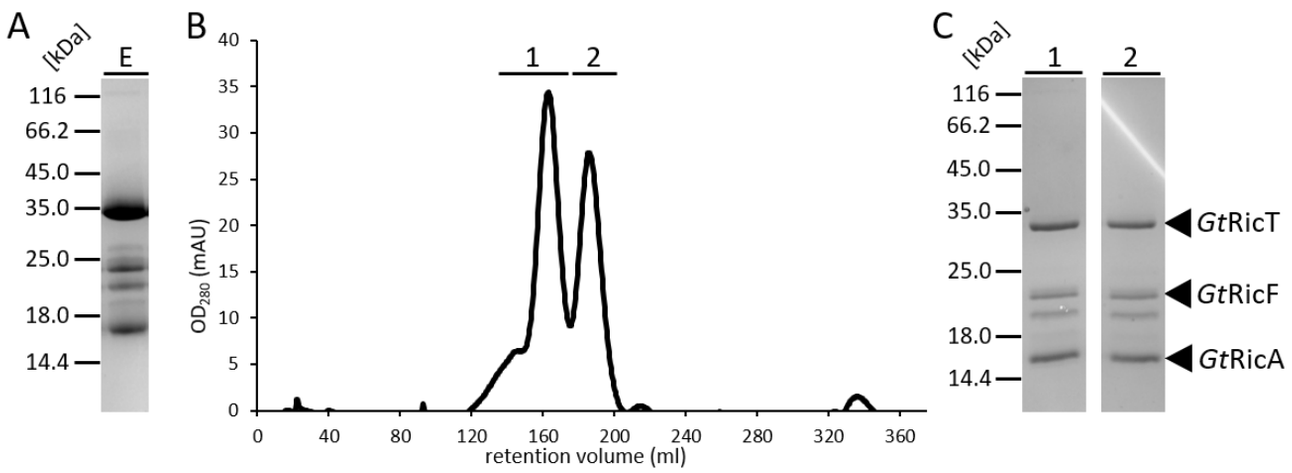

Figure 24: Ni-NTA purification and size exclusion purification of *Gt*RicAFT.
A) Elution fraction of the Ni-NTA of the *Gt*RicAFT purification. B) Chromatogram of the N-H_6-*Gt*RicA, *Gt*RicF, and *Gt*RicT SEC purification. C) The respective Coomassie-stained SDS-PAGE. The molecular weight of the marker is given in kDa. In peaks 1 and 2 *Gt*RicAFT seems to be the main components. Protein bands are indicated with *Gt*RicT at 32 kDa, *Gt*RicA at 16.1 kDa, and *Gt*RicF at around 22 kDa, even though its calculated size is 16.6 kDa.

As *Bs*RicT seemed to cause a lot of contaminations during the purification of the complex and *Gt*RicF seems instable, a combination approach was chosen in which *Gt*RicT replaced *Bs*RicT to increase the yield and purity. Therefore, the purification method is the same as for the *Bs*RicAFT complex. For this purpose, the proteins were produced in *E. coli* BL21 (DE3) cells and purified as described above (see 3.4.5 and Figure 25 A). It is proven that the complex can form with *Gt*RicT and *Bs*RicAF. This complex exhibits less contaminations than either the *Bs*RicAFT or the *Gt*RicAFT complex and the yields are increased. The purest fractions were pooled and further purified using a HiLoad 16/600 Superdex S200 column (see 3.4.7). The resulting chromatogram and the respective SDS-PAGE are shown in Figure 25 B and 25 C. Two distinct peaks of the complex form in both of which the complex is stoichiometrically present in a 1:1:1 ratio, as shown by the SDS-PAGE. Nevertheless, the peaks are more distinct in comparison to the *Bs*RicAFT complex and the first peak is purer. Still, there are several

contamination bands present in both peaks. The peaks were concentrated separately, and crystallization attempts made (see 3.5). From these no crystals could be obtained.

Nonetheless, the two separated peaks were further investigated by analytical size exclusion chromatography coupled to MALS, and by mass photometry. These experiments were performed to verify the results yielded from the *Bs*RicAFT complex and to confirm these for a *Bs*RicAF and *Gt*RicT complex (see Figure 22 and Figure 23). Thus, the peaks were concentrated separately, and the experiments executed under the same conditions as for the *Bs*RicAFT complex (see 3.4.8, 3.4.9, and 3.7).

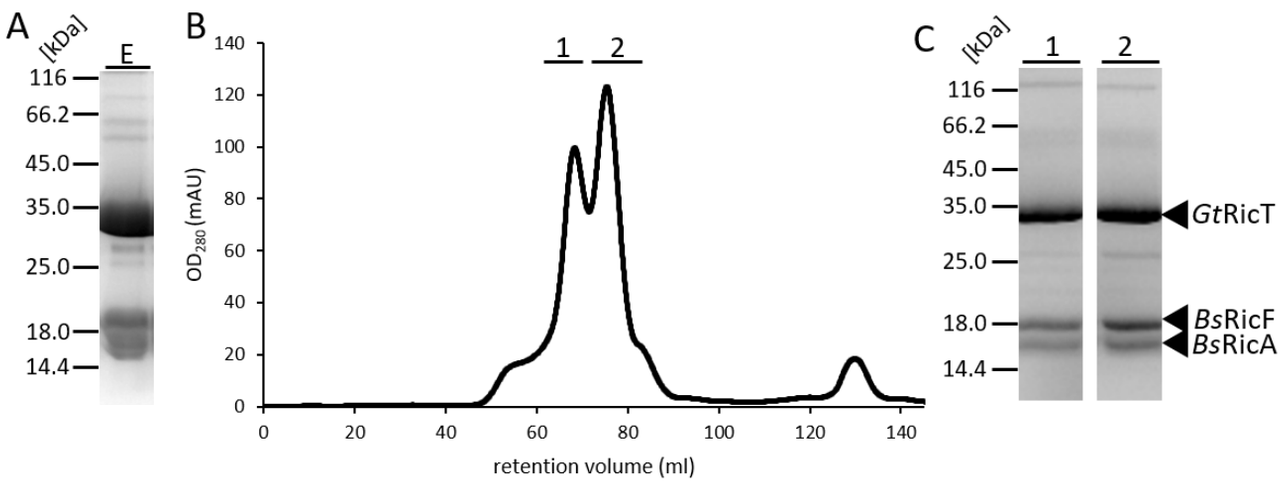

Figure 25: Size exclusion purification of *Bs*RicAF + *Gt*RicT.
A) Elution fraction of the Ni-NTA of the *Bs*RicAF + *Gt*RicT purification. B) Chromatogram of the N-H_6-*Bs*RicA, *Bs*RicF, and *Gt*RicT SEC purification. C) The respective Coomassie-stained SDS-PAGE. The molecular weight of the marker is given in kDa. There are two major distinct peaks, peak 1 and peak 2, where *Bs*RicAF and *Gt*RicT are the main components. The protein bands are indicated with *Gt*RicT at 32 kDa, *Bs*RicA at 16.7 kDa, and *Bs*RicF at 16.9 kDa.

The resulting chromatograms are displayed in Figure 26. The separately concentrated protein peaks are not constituted by one protein complex species, as in both peaks two separate peaks form. However, the species from which the peak was concentrated remained prevalent, hinting to a meta-stability of the complexes since there is no equilibrium between the two species, or it is only gradually achieved. The resulting retention volumes and the calculated protein sizes are in accordance with the previously observed complex for *Bs*RicAFT and *Gt*RicAFT.

Peak 1 elutes at around 12.3 ml, which results in a calculated size of around 227 kDa. However, in this system, the standard protein Aldolase with a size of 158 kDa has a retention volume of 12.36 ml, therefore this observed complex for *Bs*RicAF + *Gt*RicT in peak 1 is probably smaller than its calculated size, possibly 160 kDa (3.4.8). Peak 2 elutes at 13.9 ml which corresponds to a calculated size of

55 kDa, yet the standard protein Conalbumin elutes at 13.95 ml and has a size of 75 kDa, hence the protein complex detected in peak 2 is most likely around 76 kDa and larger than 55 kDa (see 3.4.8). The obtained MALS data are in agreement with the observed values from the size exclusion purification. Peak 2 would correspond again to a heterotrimer of *Bs*RicAF + *Gt*RicT with a calculated size of 63.7 kDa and peak 1 to a heterotrimer of heterotrimers with a calculated size of 191 kDa. These combined experiments show that the RicAFT complexes presumably have a 1:1:1 stoichiometry and can self-oligomerize when the proteins are derived from *B. subtilis* and *G. thermodentrificans* and in a combination of *Gt*RicT and *Bs*RicAF.

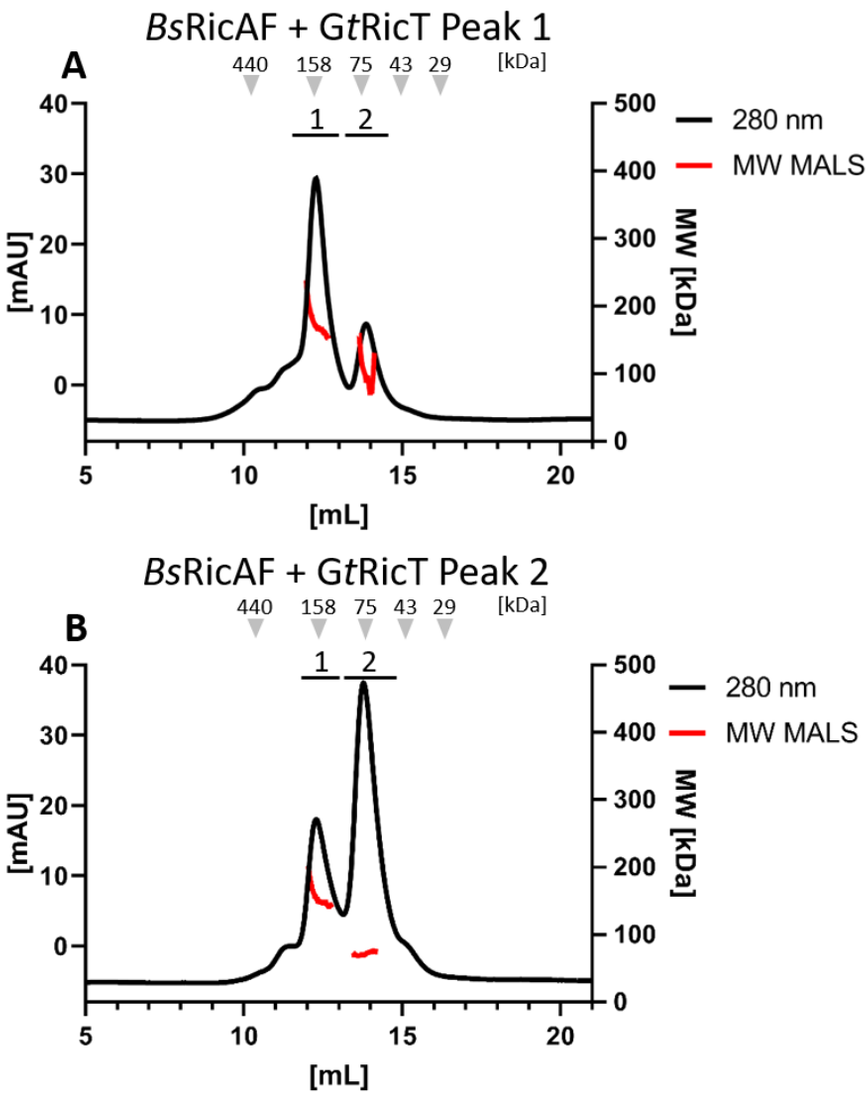

Figure 26: Analytical size exclusion of *Bs*RicAF and *Gt*RicT peak 1 and peak 2 with coupled MALS.
A) Chromatogram of *Bs*RicAF + *Gt*RicT peak 1. B) Chromatogram of *Bs*RicAF + *Gt*RicT peak 2.
The MALS results are plotted with red into the chromatogram at the corresponding peaks, the scale for them is on the right site. The scale for the size exclusion is on the left. The standard sizes are indicated with grey arrows, unit size is kDa (see 3.4.8).

These results were further reaffirmed by mass photometry (see Figure 27). Two peaks form regardless of the sample, yet in peak 1 the larger complex is more abundant (Figure 27 B) while in peak 2 the smaller complex is prevalent (Figure 27 A). The smaller complex is detected with a size of 73-75 kDa agreeing with the observed heterotrimer of *Bs*RicAF + *Gt*RicT in the analytical size exclusion experiments. However, the peak with a larger molecular size is detected with a size of 131-135 kDa, which is considerably smaller than observed in the analytical size exclusion and MALS. The detected particle size would be more in line with a dimer of heterotrimers in opposition to a trimer of

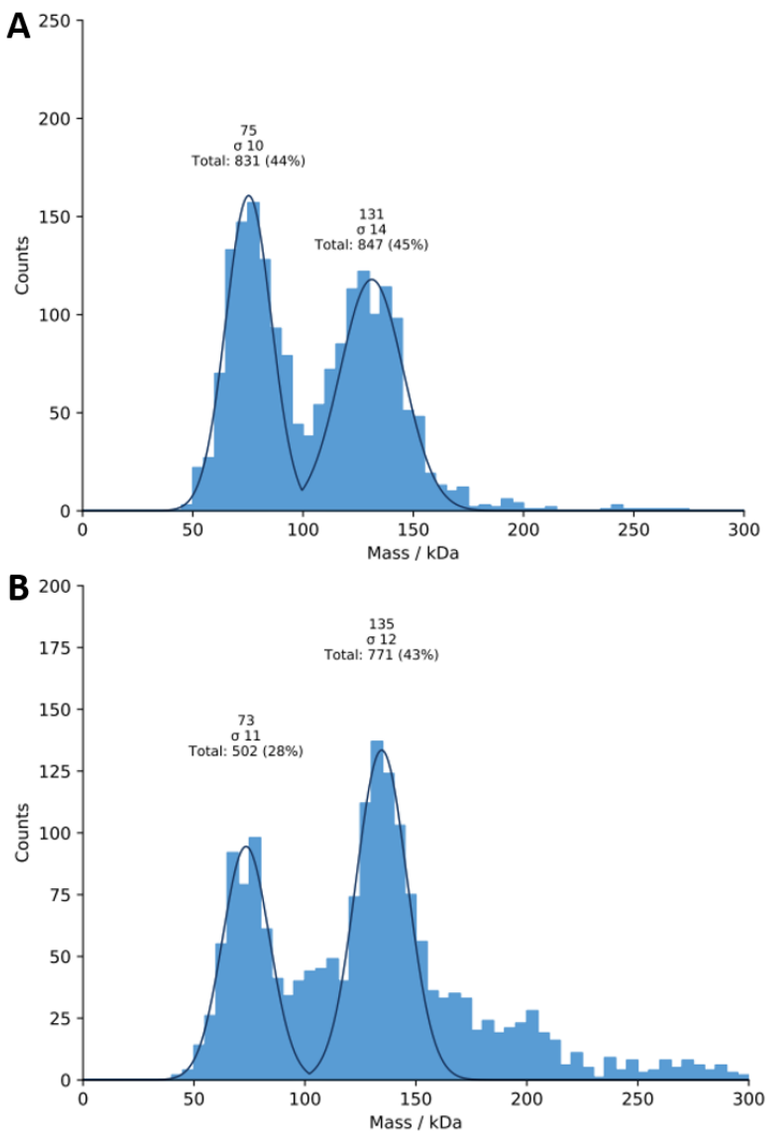

Figure 27: Mass photometry histogram of *Bs*RicAF + *Gt*RicT peak 1 and peak 2.
A) Mass photometry histogram of Peak 2. Two peaks are formed. B) Mass photometry histogram of peak 1. Two peaks are formed. The bars indicate the counts of the particles of the specific size. The curve is a function of the counts, its peak indicating the most likely size of the particle.

heterotrimers, suggested by the analytical size exclusion chromatography and MALS. As the complex was isolated from living cells and to exclude that one complex may be an artifact of the purification, the complex was reconstituted (see Figure 28). Therefore, individually purified *Bs*RicAF and *Gt*RicT were mixed in stoichiometric amounts and incubated for 5 min at room temperature before being evaluated by analytical size exclusion and mass photometry in the same manner as the coproduced *Bs*RicAF + *Gt*RicT complex was.

In Figure 28 the chromatogram of the analytical size exclusion of the reconstituted complex is displayed. The two peaks with the retention volumes of 12.3 ml and 13.9 ml are present again, these are the exact same retention volumes as observed for the coproduced *Bs*RicAF + *Gt*RicT complex. In both, the components of the complex are present in stoichiometric amounts judging from the SDS-PAGE (Figure 28 B). The third peak is excess *Bs*RicAF, as the retention volumes are the same with 15 ml (compare Figure 16) and mostly *Bs*RicAF is present in the SDS-PAGE.

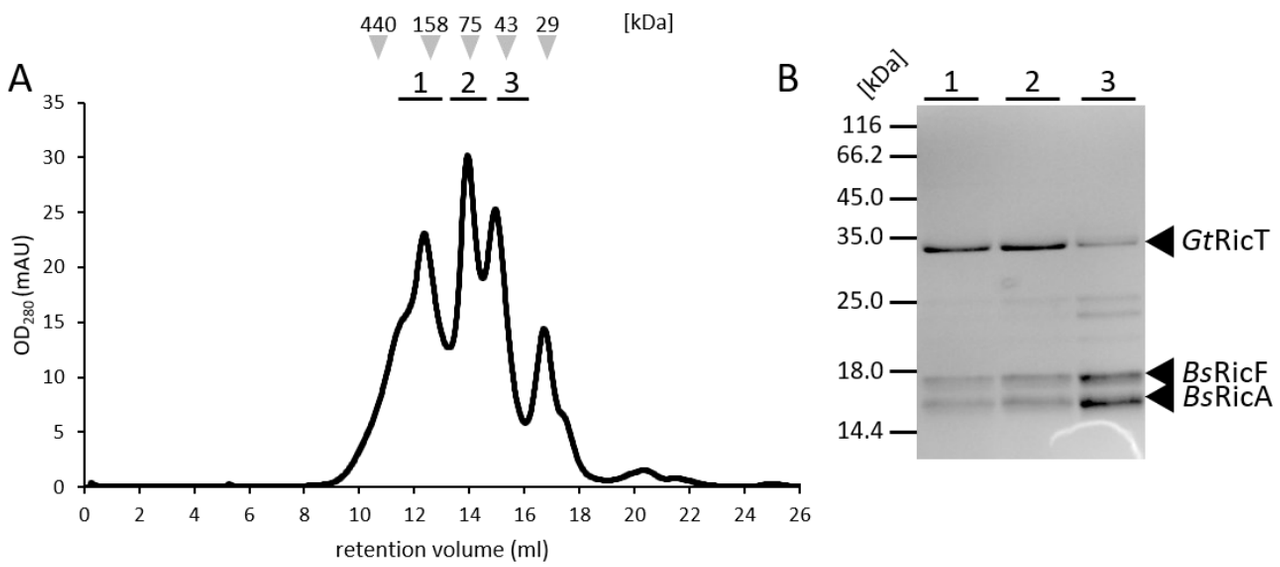

Figure 28: Analytical size exclusion chromatogram of the reconstituted *Bs*RicAF and *Gt*RicT complex.
A) Chromatogram of the analytical SEC of the reconstituted *Bs*RicAF and *Gt*RicT complex. B) The respective SDS-PAGE of the fractions. Peak 1 and 2 mainly contain RicAFT complex, peak 3 is excess *Bs*RicAF. The protein bands are indicated with *Gt*RicT at 32 kDa, *Bs*RicA at 16.7 kDa, and *Bs*RicF at 16.9 kDa. The standard sizes are indicated with grey arrows, unit size is kDa (see 3.4.8).

The mass photometry data, shown in Figure 29, replicates the results of the analytical size exclusion chromatography although the complexes are present in low amounts and the peaks are not as pronounced as from the coproduced complex. The observed particle sizes are still in order with the previously observed ones (see Figure 22, Figure 23, and Figure 26).

Collectively, these experiments showed that both complexes, the 1:1:1 trimer and probably a dimer of that complex, form naturally, without a preference for one or the other and that no additional proteins or cofactors are needed for the complex to assemble.

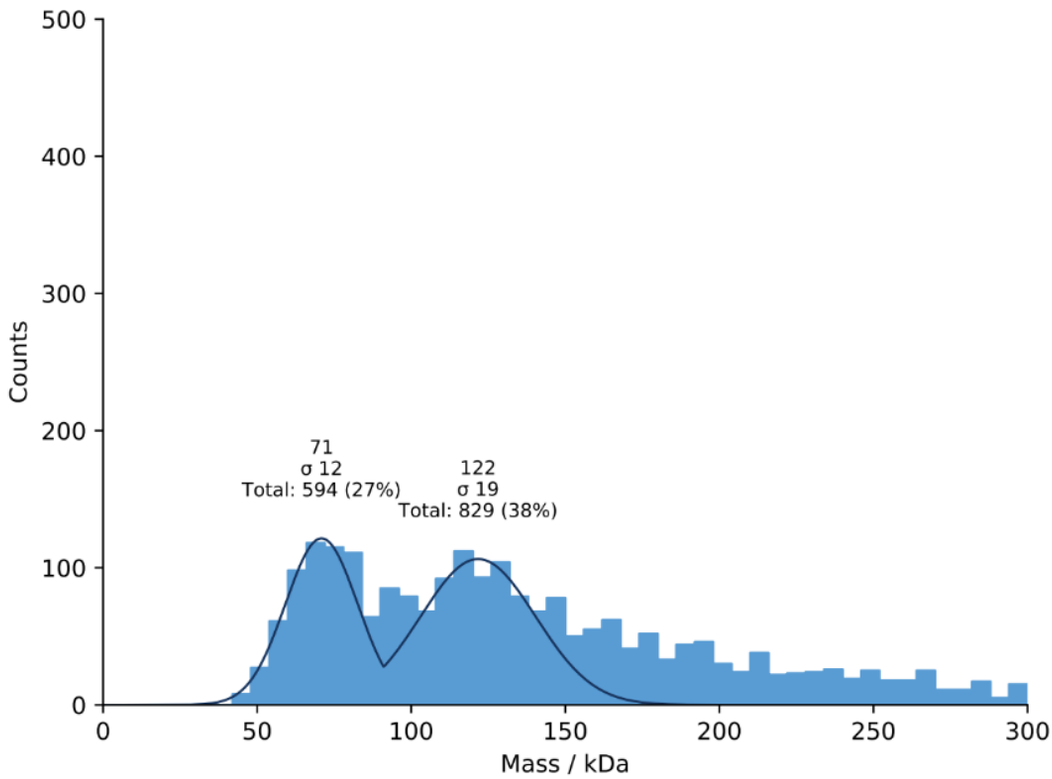

Figure 29: Mass photometry histogram of the reconstituted *Bs*RicAF and *Gt*RicT complex.
The bars indicate the counts of the particles of the specific size. The curve is a function of the counts, its peak indicates the most likely size of the particle.

4.2.2. The interaction sites of the RicAFT complex

No structure of the RicAFT complex is currently available, yet here it was observed that the complex can be present in two different oligomeric states *in vitro*. Consequently, the discovery of the interaction interface between the components of the complex should be studied. Potential differences in the interaction sites of the heterotrimer and the dimer-/trimer- of heterotrimers are of special interest. To this purpose, hydrogen-deuterium-exchange (HDX) was employed with the help of Dr. Wieland Steinchen. This method uses the trait of hydrogen to be exchanged by environmental hydrogen, especially in acidic conditions (Marolda *et al.*, 2010). This exchange occurs more easily on "accessible" hydrogens, where no interaction takes place. The deuterium is then used for the detection of the exchange (see 3.9).

Therefore, a comparison was made of HDX data from individual *Bs*RicAF and *Gt*RicT, with the two different oligomeric states of the *Bs*RicAF + *Gt*RicT complexes. For *Bs*RicAF no differences between the two oligomeric states of the *Bs*RicAF + *Gt*RicT complexes were detected (see Figure 46 and Figure 47). *Bs*RicA and *Bs*RicF were analyzed as a complex since *Bs*RicF is instable alone (Carabetta *et al.*, 2013, and personal observation). An illustration of the areas and their relative deuterium uptake as well as a structure of *Bs*RicAF with the plotted effects for peak 1 *Bs*RicAF + *Gt*RicT are displayed in Figure 30. For both proteins the majority of the peptides could be resolved in the HDX. For *Bs*RicA, the C-terminus showed no difference in deuteration pattern from I118 to L143. Nevertheless, the amino acids A13 to M19 displayed a 30 % decrease in deuterium uptake after prolonged exposure, suggesting an interaction at this site. The region from A16 to E116 also showed significant reduction in deuterium incorporation, missing area notwithstanding. This is indicative for an interaction that occurs along the whole protein. The areas in *Bs*RicA from K30 to T44 and E84 to E90 are particularly less incorporative, hinting towards a tight interaction with *Gt*RicT. For *Bs*RicF the C-terminus is mostly not affected by the deuterium exchange as none is incorporated from H118 to S133. From S7 to L17 in the N-terminus there is a strong decrease in deuterium incorporation, implying an interaction interface for *Gt*RicT. Similarly to *Bs*RicA, *Bs*RicF showed less deuterium incorporation along the central part of the protein (S7 to E117) although the changes are less severe compared to *Bs*RicA. These combined results are indicative for an interaction of *Gt*RicT with both proteins along the whole extent of the protein.

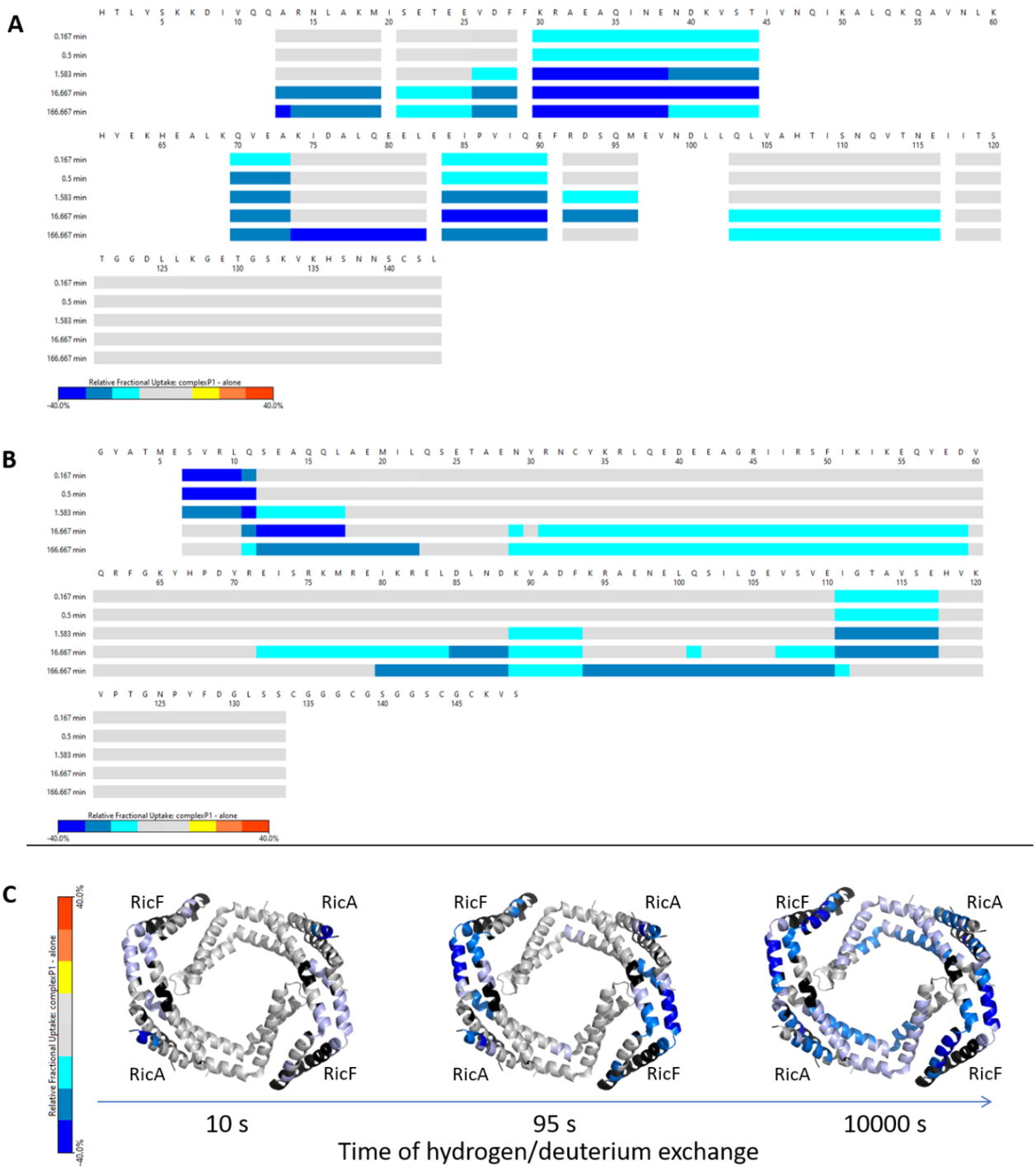

Figure 30: *Bs*RicA and *Bs*RicF peptides and structure with mapped deuterium exchange in comparison to *Bs*RicAF + *Gt*RicT peak 1.

A) Relative deuterium exchange of *Bs*RicA peptides from *Bs*RicAF in comparison to *Bs*RicAF + *Gt*RicT peak 1. The darker the areas, the fewer deuterium was incorporated in the *Bs*RicAF + *Gt*RicT complex. The N- and C-terminus are less effected by the formation of the complex. The interior parts of the protein basically α_1-α_4 are incorporating less deuterium. B) Relative deuterium exchange of *Bs*RicF peptides from *Bs*RicAF in comparison to *Bs*RicAF + *Gt*RicT peak 1. The darker the areas, the fewer deuterium was incorporated in the RicAFT complex. The C-terminus is less effected by the formation of the complex. The interior parts of the protein basically α_1-α_4 and half α_5 are incorporating less deuterium. C) *Bs*RicAF structure (PDB: 6PRK, Adusei-Danso *et al*., 2019) with the deuterium changes plotted on it.

For *Gt*RicT no differences in deuterium exchange between proteins isolated from peak 1 and peak 2 could be detected in comparison to the single protein (see Figure 25; Figure 31; Figure 48). The peptide coverage is nearly complete, yet the changes in the deuterium exchange are not as vast as in *Bs*RicAF where the changes stretched along nearly the whole protein. In addition, the exchange is not only hindered but also enhanced for *Gt*RicT. Regions with enhanced deuterium exchange are V75 to C89, and T218 to G223, which indicate structural changes and a more exposed conformation. Regions with reduced deuterium exchange are V51 to E69, E106 to F109, E128 to R144, T170 to A182, and K234 to Q246. The areas with the most pronounced decrease are T170 to A182 and E106 to F109 with a reduction of up to 40 %. Possibly these are interaction sites for *Bs*RicAF, that enable the binding. As stated above, there are also regions of increased exchange, which suggests that not only a binding event is occurring but also a larger conformational shift is happening. The changes plotted on the peptides of *Gt*RicT can be seen in Figure 31. Taken together, the data implies that the C-terminal and N-terminal regions are not involved in the binding and do not undergo large structural rearrangements.

The data from the HDX experiments provided valuable insight in the possible interaction surfaces of the RicAFT complex. From these results three amino acids of *Bs*RicA and *Bs*RicF have been selected for mutational analysis, as these showed severely reduced deuterium exchange upon *Gt*RicT binding. Hence, they are likely required for the interaction of the complex.

For *Bs*RicA the amino acid residues E80, E81, and E83 were selected for mutational analysis and converted into alanines. Additionally, double and triple mutants were constructed, which were performed with the constructs used in 4.2.1 for consistency reasons. For *Bs*RicF the residues K65, R71, and R78 were mutated to alanines. The mutated amino acids are displayed on the *Bs*RicAF structure in Figure 32 A. The pETduet constructs containing the mutated *Bs*RicA or *Bs*RicF and *Gt*RicT were handled as described before (3.4.2 and 3.4.5). The elution fractions were then analyzed on an SDS-PAGE to detect obstructed interaction. Surprisingly, only the *Bs*RicF mutation K65A displayed an inability to bind *Gt*RicT, while all other mutations had no influence, not even the *Bs*RicA triple mutant. The loss of binding in the *Bs*RicF K65A mutant was not due to direct effects, as mass spectroscopy analysis of the *Bs*RicAF band revealed that only *Bs*RicA was present (Figure 32 B). It is to be assumed that the mutation caused a disruption of the interaction between *Bs*RicA and *Bs*RicF, hence no dimer

could be formed to bind *Gt*RicT. This is especially interesting as the amino acid is not located at the direct interaction interface of the dimer as shown in Figure 32 A.

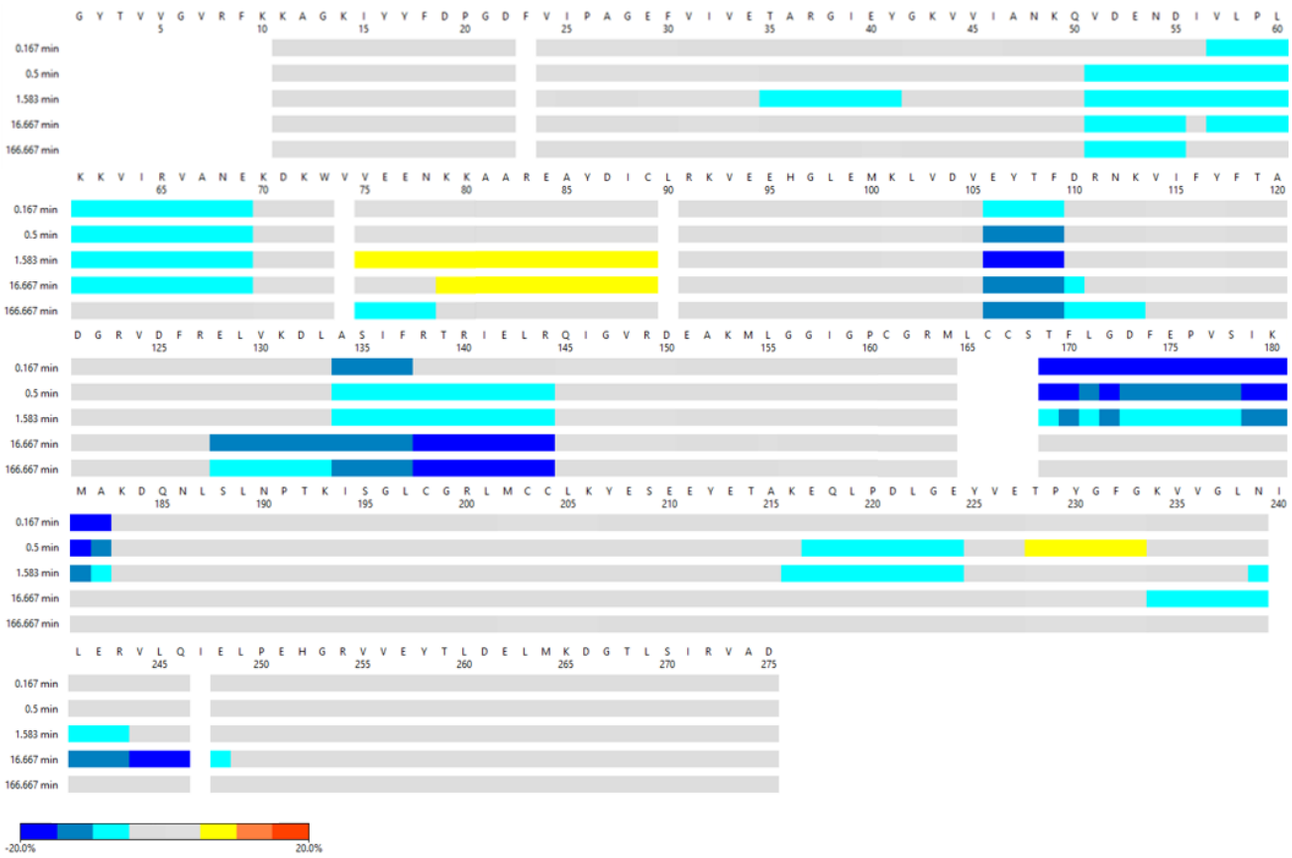

Figure 31: *Gt*RicT peptides mapped with relative deuterium exchange in comparison to *Bs*RicAF + *Gt*RicT peak 1.
The relative deuterium exchange of *Gt*RicT peptides in comparison to *Bs*RicAF + *Gt*RicT peak 1. The darker the areas, the fewer deuterium was incorporated in the *Bs*RicAF + *Gt*RicT complex, the brighter the areas the more the deuterium was incorporated. The N- and C-regions are less affected by the formation of the complex. The interior parts are locally affected by the binding of *Bs*RicAF.

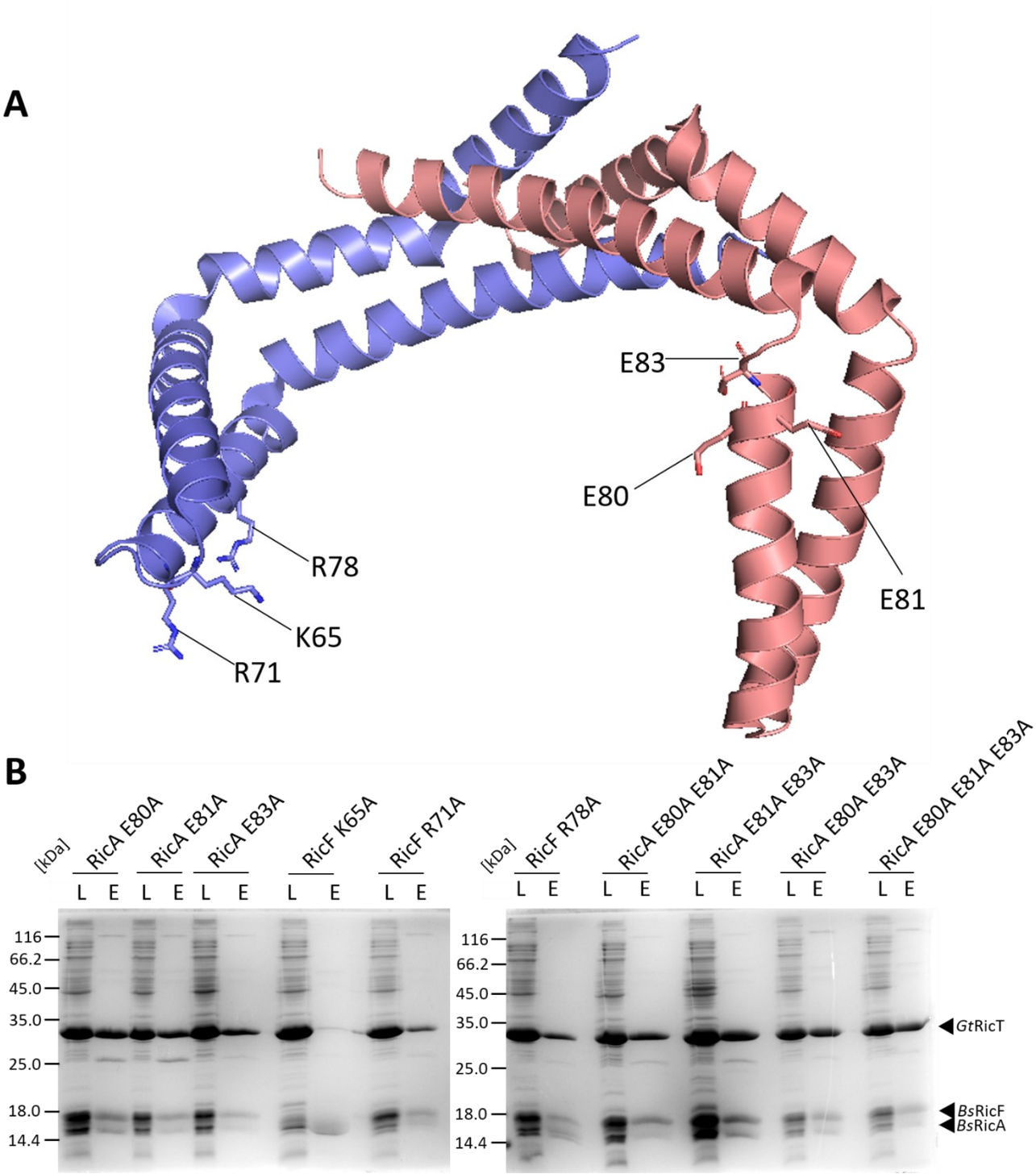

Figure 32: *Bs*RicAF structure and mutant interaction screen.
A) Crystal structure of *Bs*RicAF (PDB: 6PRK) with the mutated amino acids highlighted. *Bs*RicF is colored blue and *Bs*RicA red. B) SDS-PAGE of the lysate (L) for production of the proteins and the elution (E) fraction from the His-Trap columns. The proteins are indicated by their calculated sizes with *Gt*RicT at 32 kDa, *Bs*RicA at 16.7 kDa, and *Bs*RicF at 16.9 kDa.

4.2.3. *In vitro* interaction with RNase Y

Several groups made claims of an *in vivo* interaction of the RicAFT complex with RNase Y (Hosoya *et al.*, 2002; DeLoughery *et al.*, 2016; DeLoughery *et al.*, 2018) however, no publication to date directly proves this interaction. Therefore, a reconstitution of complexes of *Gt*RicT or *Bs*RicAF + *Gt*RicT with Δ1-22*Gt*RNase Y was attempted. As a direct interaction of RicT and RNase Y is expected (DeLoughery *et al.*, 2018) proteins originating from the same organism were chosen.

To this purpose, Δ1-22*Gt*RNaseY and *Gt*RicT, and Δ1-22*Gt*RNaseY and *Bs*RicAF + *Gt*RicT were co-purified (3.4.2 and 3.4.5). The purifications were handled as RNase Y purifications described before (Mora *et al.*, 2018) and the *Bs*RicAF and *Gt*RicT constructs from previous experiments were used (4.2.1). The deletion of the first 22 amino acids of *Gt*RNase Y is necessary, otherwise the protein integrates into the membrane and becomes insoluble in the buffers used (Mora *et al.*, 2018). The complex was then isolated by affinity-tag purification via C-Strep-tag on the Δ1-22*Gt*RNase Y protein. In Figure 33 A the SDS-PAGE of the *Gt*RicT and Δ1-22*Gt*RNase Y co-purification is depicted (see 3.4.5). Both proteins are well produced, though mainly Δ1-22*Gt*RNase Y is present in the elution.

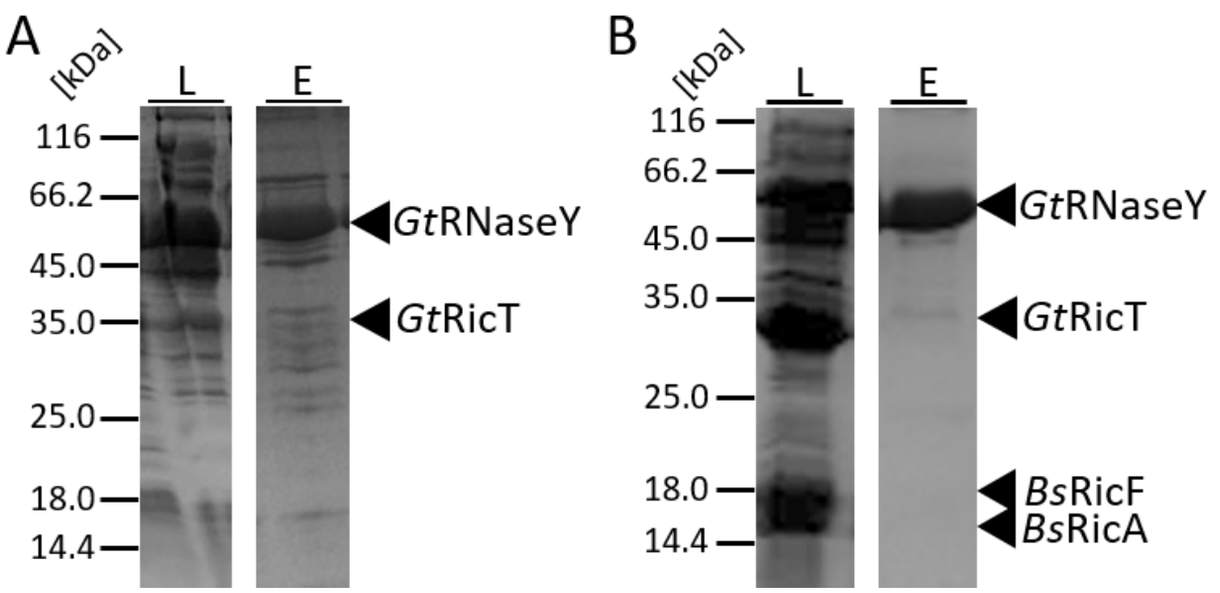

Figure 33: SDS-PAGE of affinity purification of *Gt*RicT and Δ1-22*Gt*RNase Y-Strep.
A) Strep-purification of Δ1-22*Gt*RNase Y and *Gt*RicT. Δ1-22*Gt*RNase Y can be clearly seen in the elution at around 65 kDa. *Gt*RicT is absent in stoichiometric amounts in the elution fractions. B) Strep-purification of Δ1-22*Gt*RNase Y and *Bs*RicAF + *Gt*RicT. Δ1-22*Gt*RNase Y can be clearly found in the elution at around 65 kDa. The proteins of the RicAFT complex are absent. Protein sizes are indicated at their calculated molecular weight, with *Gt*RicT at 32 kDa, *Bs*RicA at 16.7 kDa, and *Bs*RicF at 16.9 kDa. L= Lysate, E = elution fractions.

Nonetheless, some *Gt*RicT was visible in elution fractions, as determined by mass spectroscopy and its calculated molecular weight.

The same experiment was performed for *Bs*RicAF + *Gt*RicT + Δ1-22*Gt*RNase Y to investigate if the complete complex is needed for the interaction with RNase Y (3.4.2 and 3.4.5). Δ1-22*Gt*RNase Y was overproduced separately and the cells were merged with cells overproducing *Bs*RicAF + *Gt*RicT. The SDS-PAGE is shown in Figure 33 B, the four proteins are present in the lysate fraction. However, *Bs*RicAF and *Gt*RicT are absent from the elution fractions. These results hint towards a non-direct interaction of the RicAFT complex with RNase Y, or else, that cofactors are needed for the interaction. For verification of the obtained results, analytical size exclusion chromatography was performed (3.4.8 and Figure 34). Therefore, Δ1-22*Gt*RNase Y, *Gt*RicT, and *Bs*RicAF + *Gt*RicT are separately purified, then mixed in stoichiometric concentrations and incubated for 5 min at room temperature. Afterwards, the samples were injected onto a S200 analytical size exclusion column (3.4.2, 3.4.5, and 3.4.8). The resulting chromatograms are plotted in Figure 34. Δ1-22*Gt*RNase Y forms two peaks with retention volumes of 8.1 ml and 11 ml. These volumes are not changed upon addition of *Gt*RicT or *Bs*RicAF + *Gt*RicT, while the peaks previously observed for *Gt*RicT and *Bs*RicAF + *Gt*RicT at 15.4 ml (Figure 19) 12.3 ml and 13.9 ml (Figure 26) respectively, are still formed with the exact retention

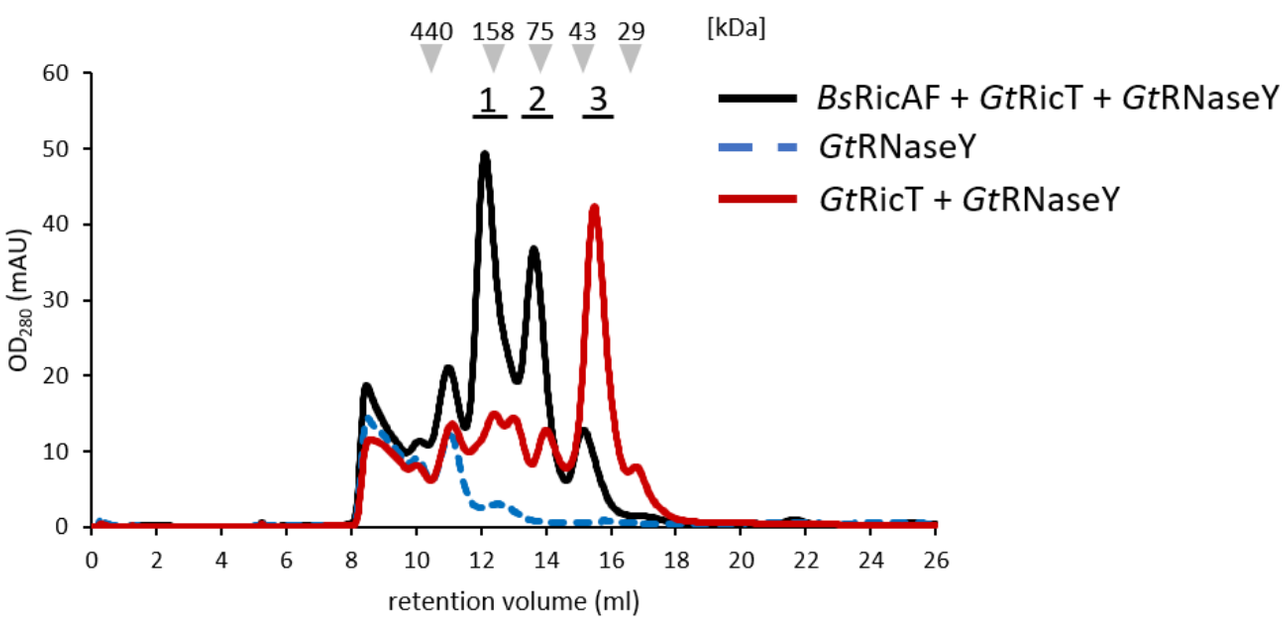

Figure 34: Analytical size exclusion chromatogram of *Gt*RNase Y, *Bs*RicAF + *Gt*RicT + *Gt*RNase Y, and *Gt*RicT + *Gt*RNase Y. The contents of each chromatogram are given in the legend. Peaks 1 and 2 mainly contain a RicAFT complex. Peak 3 is excess *Gt*RicT. The standard sizes are indicated with grey arrows, unit size is kDa (see 3.4.8).

volume as before. As no shift to lower retention volumes of the proteins is detected, the *in vitro* reconstitution of the RicAFT and RNase Y complex was not successful.

4.2.4. Single particle analysis of the RicAFT complex

So far crystallization of the RicAFT complex has not been successful. However, we could observe a larger complex corresponding to the dimer or trimer of the RicAFT complex heterotrimers (see 4.2.1) thus, we employed electron microscopy for complex characterization and structure determination. First, initial characterization was carried out by negative stain TEM (3.8). Here, the purified *Bs*RicAF + *Gt*RicT complex is embedded in a layer of uranyl acetate on carbon-coated grids. For the cryo-EM experiment the protein is vitrified on a carbon-coated grid by using a plunge freezer (FEI Vitrobot Mk. IV; 3.7) into liquid ethane, freezing the protein in a certain orientation within a thin layer of vitreous ice. The different forms of the complexes are frozen in their position and then imaged in the TEM 300 kV Titan Krios (FEI company) under cryogenic conditions.

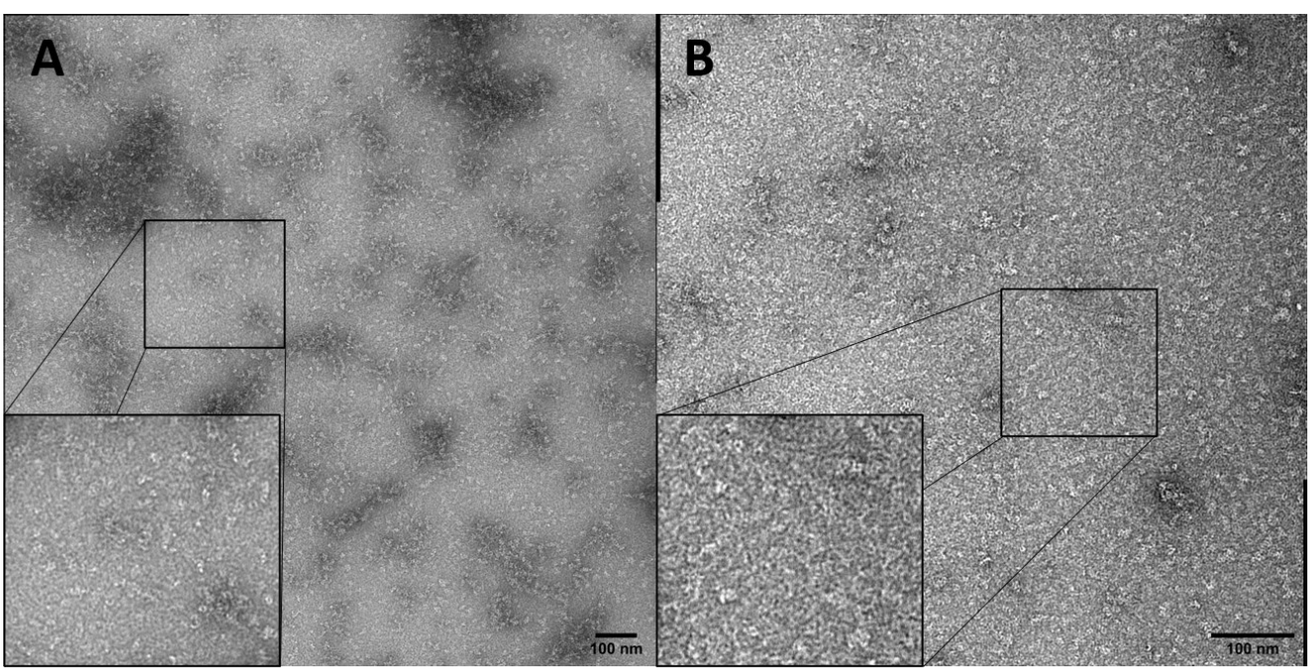

Figure 35: Negative stain images of the Ric*Bs*AF + *Gt*RicT complex.
A) Negative stain image of the *Bs*RicAF + *Gt*RicT complex at a 5 ng/ml concentration. B) Negative stain image of the *Bs*RicAF + *Gt*RicT complex at 10 ng/ml concentration. It is worth noting the ring-like structures in both images.

In the negative staining particles with an ample variation in size could be observed, as depicted in Figure 35. This variation is congruent with earlier observations that the purified *Bs*RicAF + *Gt*RicT complex is able to convert into other oligomeric isoforms (4.2.1). The reaffirmation of said results

underlines the inhomogeneousness and instability of the complex, hindering structure determination by single particle analysis. Hence, further improvement of the purification and separation of the complex was attempted by ion exchange purification with a 5 ml Hi-Trap Q FF column (see Figure 36 and 3.4.6). Initial trails of structure determination with improved purification methods and a purer complex, failed however, as the complex remained labile and the particles on the grid were too diverse. Therefore, an attempt was made to increase the stability of the complex by crosslinking the larger complex observed in the ion exchange (see Figure 36, peak 1). The applied crosslinker needs to be mild, as a too severe crosslinking may lead to disruption of the complex. Additionally, an increased air exposure might denature the complex or rapidly oxidize the [4Fe-4S] cluster and thereby disrupt the complex. Hence, the purification method was optimized by running an ion exchange column before crosslinking the complex with BS^3, a mild cross linker for water soluble proteins that is lysine specific (3.4.6 and 3.8). For the ensuing ion exchange, a HiTrap™ Q FF anion exchange column was used. The protein complex was purified as described above (3.4.5 and 3.4.6). In Figure 36 the corresponding chromatogram and the accompanying SDS-PAGE are shown. The first peak is slightly smaller, yet contains fewer contaminations than the second peak. Hence, the first peak was concentrated, BS^3 was added in a tenfold excess to the protein amount and incubated for 30 min at room temperature to achieve higher stability and therefore improve the cryo-EM data. The reaction was quenched by addition of 50 mM Tris for 15 min at room temperature. The resulting protein solution was subsequently applied onto a HiLoad XK 16/200 S200 for further purification (3.4.7). The resulting chromatogram is shown in Figure 37. All of the peaks in the chromatogram contain *Bs*RicAF + *Gt*RicT in stoichiometric amounts as concluded from the SDS-PAGE, however, peaks 2 and 3 are reminiscent of the peaks observed earlier in the size exclusion purification (Figure 25). The proteins of peak 1 are probably large unspecific aggregates linked by BS^3, therefore, ignored for future work. Peak 2 is most likely the peak of the dimer or trimer of *Bs*RicAF + *Gt*RicT heterotrimers. As this complex is sufficient in size for cryo-EM, it was chosen as the most suitable candidate. The protein solution was sprayed on grids for cryo-EM and vitrified by plunge freezing (3.8).

Moreover, to verify the stability of the isolated complex, the proteins from peak 2 were analyzed by analytical size exclusion and mass photometry (see 3.4.8 and 3.7).

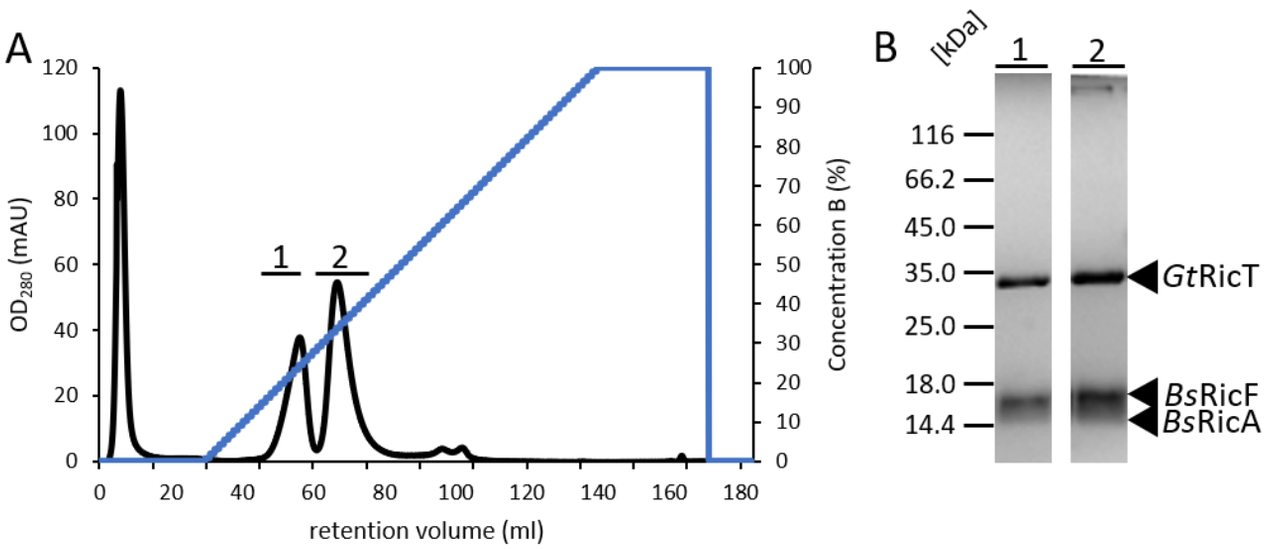

Figure 36: Ion exchange purification of *Bs*RicAF + *Gt*RicT.
A) Chromatogram of the ion exchange column. Two peaks are present, both elute between 30-40 % of the high-salt elution buffer, corresponding to about 300-400 mM NaCl (see 3.4.6). B) SDS-PAGE of the fractions of the two peaks in A). In peak 2 there is an additional contamination band visible above 116 kDa that is absent from peak 1. Protein sizes are indicated at their calculated molecular weight, with *Gt*RicT at 32 kDa, *Bs*RicA at 16.7 kDa, and *Bs*RicF at 16.9 kDa. The blue line indicates the concentration of the elution high-salt elution buffer.

The analytical size chromatogram is shown in Figure 38. The concentrated peak 2 displays one singular peak with a retention volume of 12.3 ml and does not disintegrate into two peaks again, as shown before (see Figure 22, Figure 23, and Figure 26). The same is shown by mass photometry in

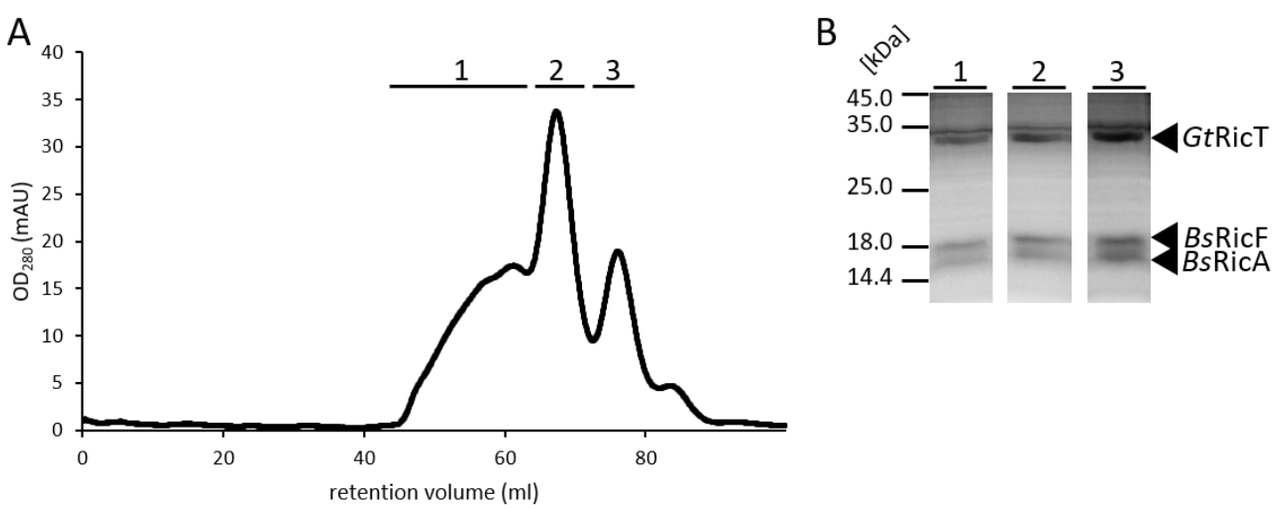

Figure 37: Size exclusion chromatogram of *Bs*RicAF + *Gt*RicT crosslinked with BS^3.
A) Chromatogram of the crosslinked *Bs*RicAF and *Gt*RicT proteins. The different peaks are indicated by the numerals above them. B) The respective Coomassie-stained SDS-PAGE. All three indicated areas contain *Bs*RicAF and *Gt*RicT, however area 1 is disperse. Protein sizes are indicated at their calculated molecular weight, with *Gt*RicT at 32 kDa, *Bs*RicA at 16.7 kDa and *Bs*RicF at 16.9 kDa.

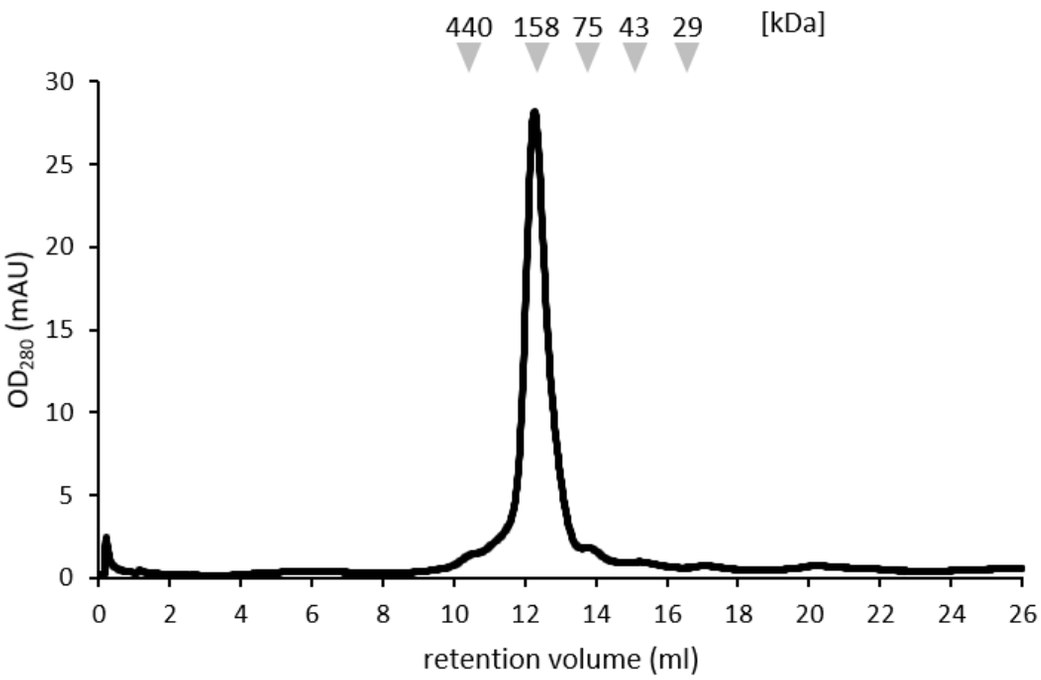

Figure 38: Analytical size exclusion of *Bs*RicAF + *Gt*RicT ion exchange peak 1 crosslinked with BS³.
Chromatogram of the analytical size exclusion of *Bs*RicAF+ *Gt*RicT crosslinked complex. The standard sizes are indicated with grey arrows, unit size is kDa (see 3.4.8).

Figure 39. The retention volume of the analytical size exclusion experiment is consistent with the results from the previous analytical size exclusion of the RicAFT complex (see Figure 26). The same holds true for the mass photometry result, which was handled as the mass photometry samples

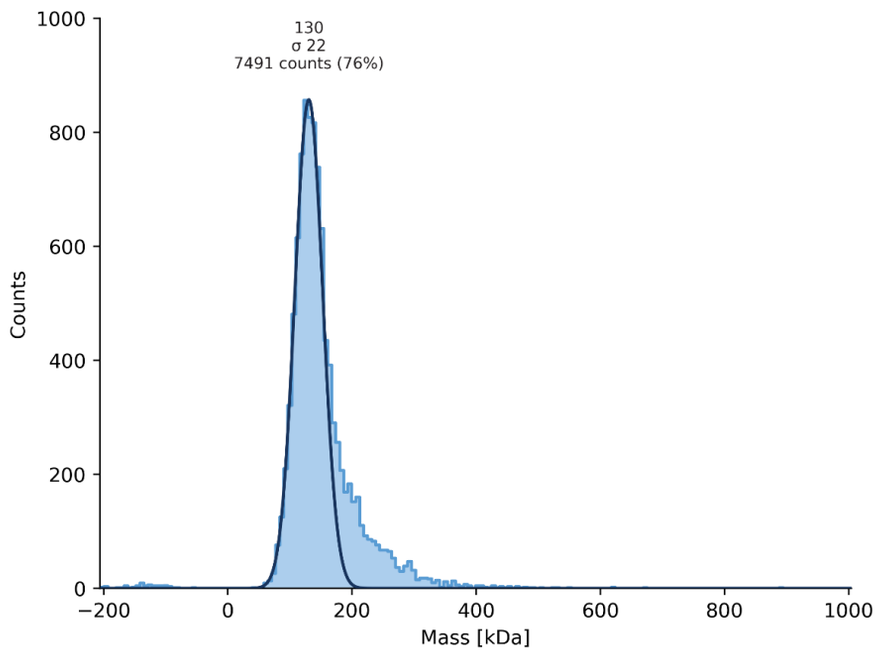

Figure 39: Mass photometry histogram of *Bs*RicAF + *Gt*RicT ion exchange peak 1 crosslinked with BS³.
The bars indicate the counts of the particles of the specific size. The curve is a function of the counts, its peak indicates the most likely size of the particle.

before (see 3.7 and Figure 27). The complex appears to be stable, as only a single peak forms with the same size as the previously observed dimers of *Bs*RicAF and *Gt*RicT heterotrimers (see Figure 27). The complex had a size of 130 kDa, and the heterotrimer with a size of around 74 kDa was absent. Hence, it can be concluded that the crosslinking worked and the complex is no longer labile, thereby, is now optimized for cryo-EM.

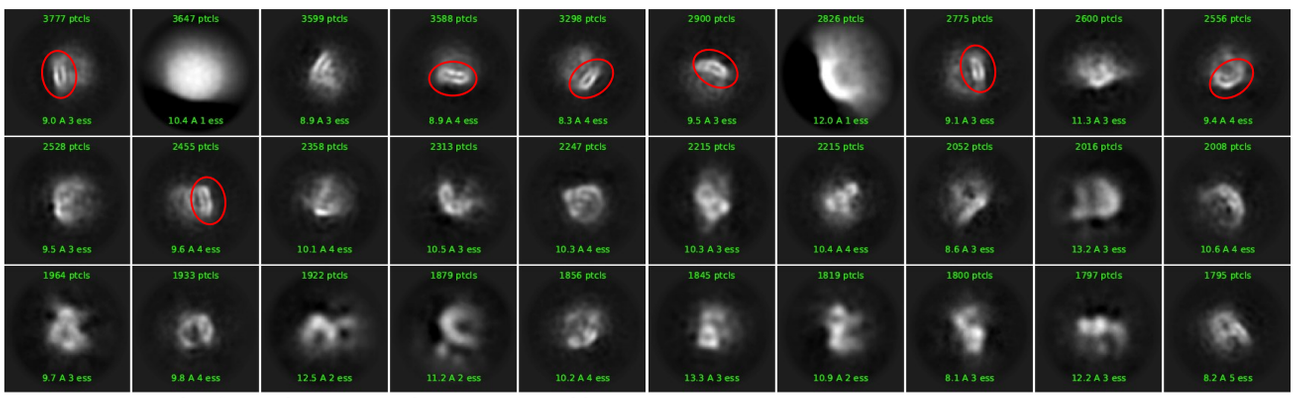

Figure 40: Samples from the 150 2D classes assigned by cryoSPARC.
The number of particles that were assigned to the respective group is written in the top part of the class. The value in the lower part gives the size of the particle in Å, the number after that indicates the poses in which the particle was found in. The red circles indicate a disk-like structure of high electron density, assumed to be the ring formed by *Bs*RicAF.

The crosslinked complex was then used for the creation of cryo-grids for cryo-EM. The resulting grids were then imaged on a 300 kV Titan Kris Cryo-Electron Microscope, Cs 2.7 mm (FEI company, Gatan imaging filter, K3 Camera (Gatan), 0.844Å/pixel, total dose: 40 $e^-/Å^2$, 40 frames, exposure time: 2.3 s, defocus: -1.5/-1.8/-2.1/-2.4). With the help of Dr. Jan Schuller, the resulting micrographs were subsequently evaluated by cryoSPARC. Particle picking was done by training the self-learning algorithm Topaz (Bepler *et al.*, 2019). The particles could then be classified into 150 reference-free 2D classes, an excerpt of 30 of these is shown in Figure 40.

The cryo-EM results show that the *Bs*RicAF complex is well-structured and is indicated in the images by red circles, see Figure 40. Thereby, 30 2D classes were picked and represented in Figure 41. *Gt*RicT is probably located on top of this complex, however, from the results it cannot be discerned if the density is of one or two molecules. The reason for this could be that it is too mobile and/or not as structured or it might be slightly degraded, or the [4Fe-4S] cluster oxidized, thus, the structure of the complex is disrupted. This may be prevented by purification of the complex in anaerobic conditions, as well as anaerobic application of the RicAFT complex on the grids. Furthermore, the addition of more crosslinker could stabilize the complex, as well as the addition of protease inhibitor and reducing agents to achieve an atomic resolution structure.

The resolution of the structures achieved here is too low to reconstruct an atomic model, nonetheless, the particles found imply that the complex stays intact upon application onto the grids.

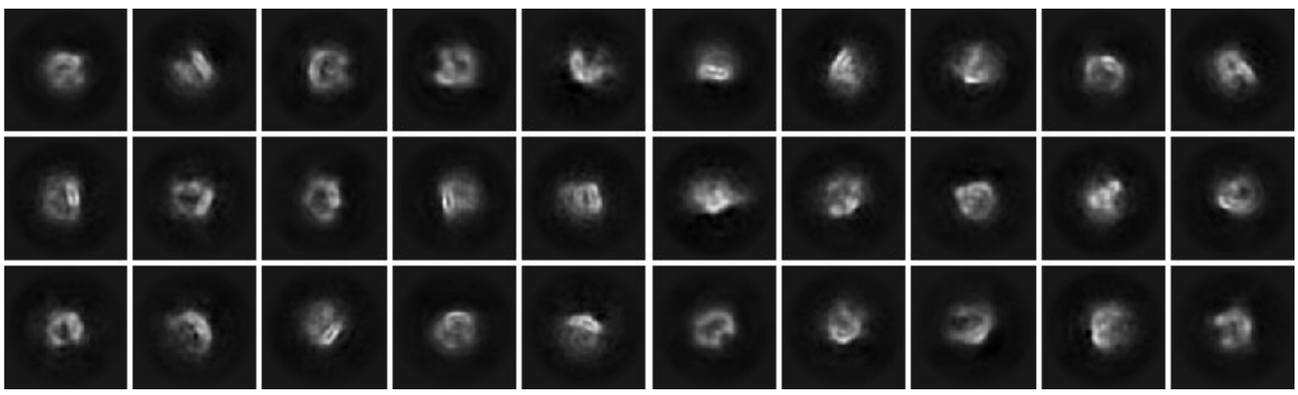

Figure 41: 30 2D classes with RicAF disk.
30 2D classes that were selected for their disk-like electron density of *Bs*RicAF. Atop of it is located a broader, more disperse electron density that is not as defined as the *Bs*RicAF disk and assumed to be *Gt*RicT.

4.3. CoIP experiments in *B. subtilis*

The RicAFT complex, in proposed conjunction with RNase Y, has major implications on mRNA maturation in *B. subtilis* (DeLoughery *et al.*, 2016; DeLoughery *et al.*, 2018) though proof of a direct interaction is still absent. Hence, it is of utmost importance to find possible interaction partners that might regulate the function or give further insight into the mechanism of the complex.

To find such interaction partners, CoIP experiments were performed. The genes of interest were cloned under the control of a bacitracin-inducible promoter with an N-terminal Strep-tag in a pLIKErep plasmid, a non-integrative replicating plasmid, and then transformed into *B. subtilis* NCIB3610 (3.4.4; Toymentseva *et al.*, 2012).

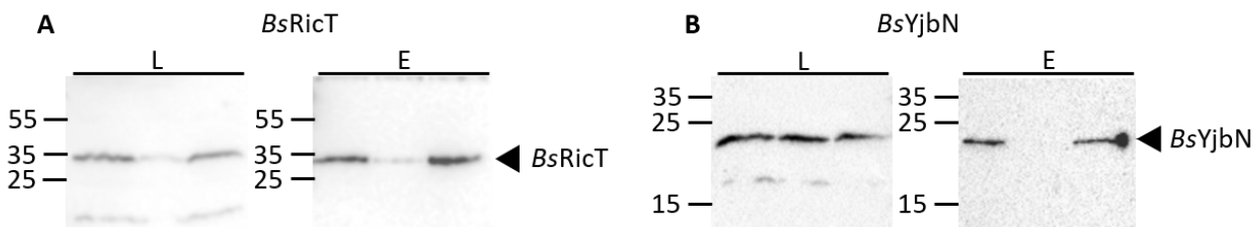

Figure 42: Western Blots of the CoIPs of *Bs*RicT and *Bs*YjbN overproduction in *B. subtilis* NCIB3610.
A) Western Blot of RicT overproduction. B) Western Blot of YjbN overproduction. L: lysate fraction; E: elution fraction. Protein sizes are indicated by arrows *Bs*RicT at 32 kDa and *Bs*YjbN at around 22 kDa.

The genes were amplified from *B. subtilis* NCIB3610. RicT was chosen to be the bait in the CoIP experiments as it is the component of the RicAFT complex that is widely conserved (DeLoughery *et*

al., 2018; see Table 1) it has a size of about 32 kDa. YjbN as an essential NAD-kinase, responsible for producing NADP from NAD and with a size of 30 kDa, was used as bait and as control since it is unlikely to interact with the RicAFT complex (Garavaglia *et al.*, 2003).

The CoIP experiments were carried out as described in 3.4.4. Samples were taken during the CoIP process and Western Blots performed to show that the proteins were successfully produced, remained stable, and bound to the magnetic-Strep-beads (see 3.4.11 and 4.1). As shown in the Western Blots in Figure 42, both fusion proteins are produced and visible in the lysate and the elution fractions. *Bs*RicT migrates according to its size, however, YjbN migrates at around 22 kDa instead of the expected 30 kDa but without signs of degradation. With this it was determined that the proteins were functional, and the resulting samples were analyzed by LC-MS. The data acquired from the CoIP experiments were first analyzed by simple comparison of the raw counts and afterwards by Perseus (see 3.4.4 and Figure 49) to achieve a high confidence in the found hits and rule out false positives. This was achieved by comparing the identified peptides of one sample with the peptides found in *Bs*YmcB, *Bs*YmcB + *Bs*RicA, and *Bs*YjbN or *Bs*RicT. Since the chance that all these proteins have the same interaction partners is highly improbable, this comparison serves as a control. Nonetheless, if some proteins have common interaction partners, these would be detected anyway since the hits are also individually analyzed (3.4.4). With Strep-RicT as bait in the CoIP experiments, the proteins shown in Table 8 were found with most confidence. Since the known interaction partners RicA and RicF were the proteins found with the highest abundance, this can be regarded as a proof of concept. These three proteins form a complex *in vitro* and *in vivo* (Carabetta *et al*., 2013; Adusei-Danso *et al*., 2019; this work). RNase Y was found with a similar abundance as RicA and RicF, yet neither the RicAFT complex nor RicT individually interacted with RNase Y *in vitro*, as shown in this work (see 4.2.3). Nonetheless, additional proteins were co-purified as well but with lower confidence, these included SufA, YmfH, and YuaB. YmfH is a non-essential, uncharacterized zinc-protease (Miethke *et al.*, 2008). This protein is encoded in a Mta-regulated operon together with *ymfD* and *ymfF*. YmfF is a protein of unknown function and YmfD is the exporter for bacillibactin, a siderophore responsible for Fe^{3+} binding and subsequent uptake (Miethke *et al.*, 2008).

SufA is a Fe-S carrier protein and belongs to the IscA group. This group of proteins is involved in the assembly and transfer of iron-sulfur clusters to certain iron-sulfur-cluster-utilizing proteins (Lu *et al.*, 2008; Albrecht *et al.*, 2010). SufA is not located in any operon.

YuaB is a bacterial hydrophobin that forms the water-repellent surface of *B*. *subtilis* biofilms. It is self-assembling and forms a membrane-like monolayer on top of the cells (Kobayashi and Iwano, 2012; Hobley *et al.*, 2013; Arnaouteli *et al.*, 2016). In addition, the protein inhibits the kinase activity of KinA and thereby sporulation (Garti-Levi *et al.*, 2013).

Table 8: Co-eluting proteins identified with most confidence for the *Bs*RicT CoIP

Protein	Accession number	Function	Pathway/Essential
RicF	O34412	mRNA maturation regulation	RNA maturation/no
RicA	O31779	mRNA maturation regulation	RNA maturation/no
Rny	O31774	mRNA degradation	RNA regulation/ +/-
YmfH	O31766	Possible zinc-protease	Protein degradation/no
SufA	O32113	Fe-S cluster transfer and assembly	Iron-sulfur cluster biosynthesis /no
YuaB	P71014	Biofilm formation, inhibitor for sporulation	Biofilm/no

For the YjbN CoIP experiment the proteins found with the most confidence are listed in Table 9. These are most likely direct interactors of YjbN under the conditions the cultures were grown in. From top to bottom the confidence of a significant interaction decreases. The protein found with

Table 9: Co-eluting proteins identified with most confidence for the *Bs*YjbN CoIP

Protein	Accession number	Function	Pathway/Essential
YhdR	O07587	Unknown (Annotated aspartate aminotransferase)	Unknown/no
HutU	P25503	Urocanase	Histidine utilization (L-glutamate)/no (NAD as cofactor)
Fbp	Q45597	Fructose-1,6-bisphosphatase	Gluconeogenesis/no
Mfd	P37474	Transcription-repair-coupling factor	NER/no
Buk	P54532	Butyrate kinase	Utilization of branched keto acids/no
YerA	O34909	Putative adenine deaminase	Adenine catabolism/no
AcsA	P39062	Acetyl-coenzyme A synthetase	Fatty acid utilization/no
YqfE	P46343	Unknown	Unknown/no

the most confidence is YhdR, a putative aspartate aminotransferase, as such it would catalyze the reaction of L-aspartate and 2-oxoglutarate to L-glutamate, and oxaloacetate with Vitamin B_6 as a cofactor. This would place this enzyme at the start of the TCA cycle by providing oxaloacetate. Hence, this protein is at the starting point of the major catabolic reactions in a prokaryotic cell, possibly showing a connection between the TCA and the switch between NAD and NADP homeostasis (Nakai *et al.*, 1999). It is localized in the cytoplasm, but any regulation is unknown.

The second most confidently found protein is the urocanase HutU. This protein is involved in the degradation of L-histidine to L-glutamate and catalyzes the second step to form 4-imidazolone-5-propanoate from trans-urocanate and water. It uses NAD^+ as possible electron acceptor cofactor for

the hydratization of trans-urocanate. The protein is localized in the cytoplasm and is encoded in an operon along with *hutH*, *hutI*, *hutG,* and *hutM.* Here, *hutH*, *hutI,* and *hutG* encode enzymes that catalyze the remaining reactions required to form L-glutamate from L-histidine and *hutM* encodes a histidine permease. The whole operon is induced by histidine and repressed by CodY and CcpA (Wray and Fisher, 1994; Fisher *et al.*, 1996; Zalieckas *et al.*, 1999).

Fbp is a protein of the gluconeogenesis and catalyzes the hydrolysis of 1,6-fructose-bisphosphate to phosphate and fructose-6-phosphate. It uses manganese as a cofactor and is constitutively expressed. The activity of Fbp is repressed by polyphosphorylated nucleotides like (p)ppGpp or nucleotide triphosphates, and monophosphorylated nucleotides, denatured RNA or denatured DNA. PEP and monovalent cations are stimulating factors for it. While the localization of Fbp is not described, it is known to be part of the SigA regulon (Fujita and Freese, 1979; Fujita *et al.*, 1998).

Mfd is the transcription-repair-coupling factor that releases stalled RNA polymerase (RNAP) from the damaged DNA strand and probably recruits the nuclear-excision-repair (NER) to the lesion. A known cofactor is ATP, but Mfd can also bind other nucleotides. The protein is localized in the cytoplasm and encoded in an operon with *fin* and *spoVT*. These are involved in the regulation of the sigma factors SigF and SigG that are important for early and late spore formation genes, respectively (Roberts and Park, 2004; Robleto *et al.*, 2012).

Buk is a probable butyrate kinase and involved in the utilization of branched-chain keto acids. It is encoded in a seven-gene operon focused on the processing of branched-chain keto acids, yet they do not work in succession like the *hut*-operon, but individually on different substrates. The protein is cytosolic, and expression is stimulated by BkdR the transcription activator for the entire operon that is repressed by CodY (Debarbouille *et al.*, 1999; Nickel *et al.*, 2004).

YerA has similarity to adenine deaminases and could convert adenine into hypoxanthine. This would place it in the nucleotide salvage pathway. The regulation and localization of YerA are unknown, however, it is encoded in the operon *yerA*-*yerB*-*yerC*. *yerB* codes for an interaction protein of PcrA which is an essential ATP-dependent helicase. *yerC* has similarity to a putative Trp repressor of *Staphylococcus aureus*. Although, it is not defined in *B. subtilis*, dysfunctionality of *yerC* reduces sporulation by 90 % (Noirot-Gros *et al.*, 2002; Macek *et al.*, 2007).

AcsA is an acetyl CoA-synthetase, hence catalyzing the reaction of acetate and CoA with ATP to acetyl-CoA and AMP. This is a vital reaction for the usage of fatty acids and links anabolic and catabolic

pathways. The known cofactors for AcsA are ATP, CoA and magnesium. *acsA* is in an operon with *ytzK* and *tyrS*, this operon is repressed by CodY, CcpA, and glucose. YtzK is a 5.7 kDa protein with unknown function. TyrS is the major tyrosyl-tRNA-synthetase, therefore essential (Starai and Escalante-Semerena, 2004; Gardner *et al.*, 2006).

Lastly, YqfE is a protein that is similar to PhoH from *E. coli* which is a cytosolic, ATP binding protein induced under phosphate limiting conditions. YqfE contains conserved regions that are associated with nucleotide binding, nevertheless, the regulation and function of the protein is unknown (Kazakov *et al.*, 2002).

5. DISCUSSION

5.1. The RicAF: A necessary tetramer?

The genes encoding RicA and RicF are common in facultative anaerobic bacteria (Tanner *et al.*, 2017). The proteins were first discovered in a genetic screen identifying genes required for biofilm formation and sporulation. Deletion of either gene led to smooth, unstructured biofilms (Tortosa *et al.*, 2000; Branda *et al.*, 2004). These phenotypes were later attributed to an insufficiently working phosphorelay or an RNase Y-dependent lack of maturation of mRNAs (Carabetta *et al.*, 2013; DeLoughery *et al.*, 2016; Dubnau *et al.*, 2016; DeLoughery *et al.*, 2018). Moreover, a third protein, RicT, is involved in the same pathway causing similar phenotypes and was shown to form a complex with RicA and RicF (Carabetta *et al.*, 2013; DeLoughery *et al.*, 2016). Yet, only the structure of *Bs*RicA as a dimer and *Bs*RicAF as a heterodimer have been solved (Adusei-Danso *et al.*, 2019).

The available structures were solved using constructs with truncated C-termini, as these are unstructured, thereby hindering the crystallization process. However, the C-termini are important for the binding of a second [4Fe-4S] cluster in conjunction with RicT (Tanner *et al.*, 2017; Adusei-Danso *et al.*, 2019) thus it is unfortunate they are not resolved. A complete structure of RicA and RicF would give further insight into the binding and coordination of the [4Fe-4S] cluster.

As demonstrated earlier, RicA was successfully produced in full-length and purified from *E. coli* (see 4.1.1). The following crystallization experiment yielded the structure shown in Figure 12. The structure represents the amino acids from M1 to G131, the C-terminus relevant for the coordination is not represented. Due to the unstructured nature of the C-terminus, no secondary structure is formed and the electron density is too dispersed, hence a precise reconstruction is unattainable. Nevertheless, some additional amino acids were mapped in comparison to the previously available structure and they were *in toto* comparable. Despite not completing the full-length structure of RicA with the C-terminus, a deeper insight into the interactions of RicA and RicF and their complex formation was achieved. The structure of the RicAF heterodimer was resolved with four molecules in the asymmetric unit, representing two heterodimers. Previously, the size for the complex observed by analytical ultracentrifugation was 30.5 kDa which would correspond to a dimer (Adusei-Danso *et al.*, 2019). In 4.1.2 the RicAF complex has been purified without any large solubility tag, e.g., a SUMO-

or GST-tag, where it was demonstrated to be present at least partially as heterotetramers by analytical size exclusion. Nevertheless, the majority of the complex is present as a heterodimer in solution. This is confirmed by the mass photometry results, showing a 68 kDa peak, which is in accordance with the predicted size of two heterodimers of 64 kDa. However, the resolution limit of the mass photometry method is around 50 kDa, therefore the smaller dimer with a size of 32 kDa is possibly not detected.

The mutation studies performed in 4.2.2 provide further support for the naturally occurring oligomerization state of the RicAF complex, which is presumably the RicAF heterotetramer. The mutation K65A in RicF inhibited the formation of the RicAF complex in solution. This mutation is not at the interaction interface of the RicA and RicF dimer but rather on the protruding hinge at the end of α_3, as shown in Figure 32, close to the position of the other RicAF dimer in a tetrameric organization. It is worth mentioning that the results of the analytical size exclusion chromatography, which suggest that most of the complex is present as a dimer, not as a tetramer, might be explained by the shape of the heterotetramer. Since the heterotetramer has a vent of 38 Å in length and 32 Å in diameter (Figure 16) there could be an alteration in the hydration shell radius, which could lead to changes in the retention volume.

Nonetheless, this inability of the RicF K65A mutant to form the RicAF complex might arise from the lack of acetylation. Analogously, the RicA K64A mutant leads to a phenotype that resembled the deletion of either RicA or RicF, therefore, a similar effect could be expected of the RicF K65A mutant. However, acetylation of RicF in *B. subtilis* has not been reported (Reverdy *et al.*, 2018) and the mutations are not in the same location. In a RicAF dimer, RicA K64 would be positioned on the opposite hinge of RicF K65. In a tetrameric RicAF complex, it would be located on an outermost location. However, Reverdy *et al*. did not study the effect of the mutation biochemically and hence, there is no evidence that the complex still forms when the acetylation or lysine is absent. The RicF K65A mutation is shown to prevent complex formation, thereby the mutant protein could be used to study the importance of the complex formation. As prior studies only used deletions of the genes, additional effects may be present, as it is claimed that RicA and RicF have additional functions in the cell (Carabetta *et al.*, 2013; DeLoughery *et al.*, 2016; Dubnau *et al.*, 2016; DeLoughery *et al.*, 2018).

5.2. The oligomerizing RicAFT complex

5.2.1. RicT is a labile and oligomerizing monomer

Genes for RicT homologues are found in all domains of life (see Table 1). In Firmicutes it is often concomitantly conserved with RicAF, while no homologues of RicAF can be found in the other phyla. As RicT forms a complex with RicAF, it is found to have similar phenotypes and appears to be involved in the same pathways: RNA maturation, sporulation, and genetic competence (Hosoya *et al.*, 2002; Carabetta *et al.*, 2013; DeLoughery *et al.*, 2016; Dubnau *et al.*, 2016; DeLoughery *et al.*, 2018). Taken together, this underlines the importance of RicT for the resilience of *B. subtilis*. Other studies have shown that it carries a [4Fe-4S] cluster that is coordinated by four cysteines (Tanner *et al.*, 2017; Adusei-Danso *et al.*, 2019). Nonetheless, the protein was never purified without a solubility tag or in absence of RicAF (Carabetta *et al.*, 2013; DeLoughery *et al.*, 2016; Adusei-Danso *et al.*, 2019). In this work it was proven that the RicT homologue of *G. thermodenitrificans* can be purified as a monomer with a His_6-tag (see 4.1.3). Additionally, it could be assumed that it carries an ISC as well, by the brownish color of the eluate. The iron-sulfur cluster and the RicT protein itself are labile in the absence of RicAF. RicT was observed to have distinct degradation products, yet were negligible in a purification of the complete complex. By analytical size exclusion chromatography, it was shown that RicT in solution is present as a monomer. However, analytical size exclusion and mass photometry analysis showed that a small fraction of *Gt*RicT can dimerize, which can potentially further oligomerize into tetramers (see Figure 19 and Figure 20). Despite employing different conditions and protocols to crystallize *Gt*RicT, no structure could be resolved. This could be caused by the oxygen-sensitive [4Fe-4S] cluster whose degradation might disrupt the secondary structure of the protein and affect the crystallization process. Another reason might be the possible self-degradation of *Gt*RicT, which would prevent the formation of a crystallization seed.

5.2.2. The RicAFT complex oligomerizes

Recent studies showed RicAF and RicT form a heterotrimeric complex in *B. subtilis* with two [4Fe-4S] clusters. RicT coordinates the clusters and is essential for functionality of the complex (Adusei-Danso *et al.*, 2019). The stoichiometry of the reconstituted complex has been described as 1:1:1 with a molecular weight of 65 kDa (Carabetta *et al.*, 2013; Dubnau *et al.*, 2016; Tanner *et al.*, 2017; Adusei-Danso *et al.*, 2019). The components of the RicAFT complex are conserved in Bacilli, while RicT is more widely found (Tanner *et al.*, 2017, see Table 1).

In this work these observations were confirmed by analytical size exclusion, MALS, and mass photometry, as these methods detected a complex with a size of around 65 kDa. This corresponds to a stoichiometry of 1:1:1 of each component in the complex (see 4.2.1). This complex was also detectable with the proteins from *G. thermodenitrificans* and even a combination of *Gt*RicT and *Bs*RicAF, producing a chimeric complex with the same stoichiometry (see Figure 22, Figure 23, Figure 25, Figure 26, Figure 27). However, in these experiments the RicAFT complex also appeared with a size of 130 kDa with a possible stoichiometry of 1:1:1. As deducted from the intensity of protein bands on SDS-PAGEs or possible stoichiometry options calculated from the sizes of the individual proteins. This complex has never been observed before in any of the RicAFT preparations and it was concluded that this is a dimer of the 1:1:1 RicAFT complex. The 65 kDa and the 130 kDa RicAFT complex could be interconverted into one another, and both complexes formed from *Bs*RicAF and *Gt*RicT when the separate components were mixed (see 4.2.1). This suggests the physiological feasibility of the complex and its formation, as it forms spontaneously and without the need or addition of other components. Thereby, excluding the possibility that the second [4Fe-4S] cluster, that is ligated at the interface by RicA, RicF, and RicT, is responsible for the dimerization of the RicAFT complex. This is in agreement with previous studies that no iron-sulfur cluster is needed for the formation of the 65 kDa RicAFT complex (Tanner *et al.*, 2017). This larger complex was not more stable than the smaller 65 kDa RicAFT complex, and crystallization experiments were not successful. Nevertheless, the 130 kDa RicAFT complex is large enough for a structure determination by cryo-EM, which requires proteins to be at least 50 kDa in size. As RicAFT is a complex, larger particles are beneficial for the final resolution of the structure by cryo-EM. Nonetheless, the addition of crosslinkers to stabilize this larger complex was not sufficient to get an atomic resolution (see 4.2.4).

It was, however, possible to stabilize the complex on the cryo-grids and to obtain single particles, which had a recurring disk-like feature (Figure 41). From these pictures a schematic representation of the 130 kDa RicAFT complex was drawn and is presented in Figure 43 including the predicted positions of the iron-sulfur clusters. The location of the cluster that is coordinated by RicA, RicF, and RicT must be towards the C-termini according to data provided by Tanner *et al.* (2017) and Adusei-Danso *et al.* (2019) therefore, its location is quite certain. However, the location of the cluster bound by RicT is only estimated (Tanner *et al.*, 2017; Adusei-Danso *et al.*, 2019). RicT is located on top of the RicAF heterodimers overlapping from their C-termini to the location of the [4Fe-4S] cluster coordinated by all three proteins. It is possible that RicT interacts with a RicT from another RicAFT heterotrimer.

Such a dimerization of the complex might be conferred by the [4Fe-4S] cluster that is coordinated by RicT. As shown here, *Gt*RicT has a tendency to dimerize (Figure 19) and is known to carry a [4Fe-4S] cluster, which could have an impact on the structural integrity of the protein or its oligomerization state depending on its degradation. This effect of ISCs has already been observed for FNR or phosphoribosylpyrophosphate amidotransferase (Grandoni *et al.*, 1989; Smith *et al.*, 1994; Khoroshilova *et al.*, 1997; Popescu *et al.*, 1998; Kiley and Beinert, 1998; Mettert and Kiley, 2015). The importance of the state of the [4Fe-4S] cluster is further supported by the fact that in previous studies the proteins were purified in an anoxic, reducing environment, and because the [4Fe-4S] cluster of

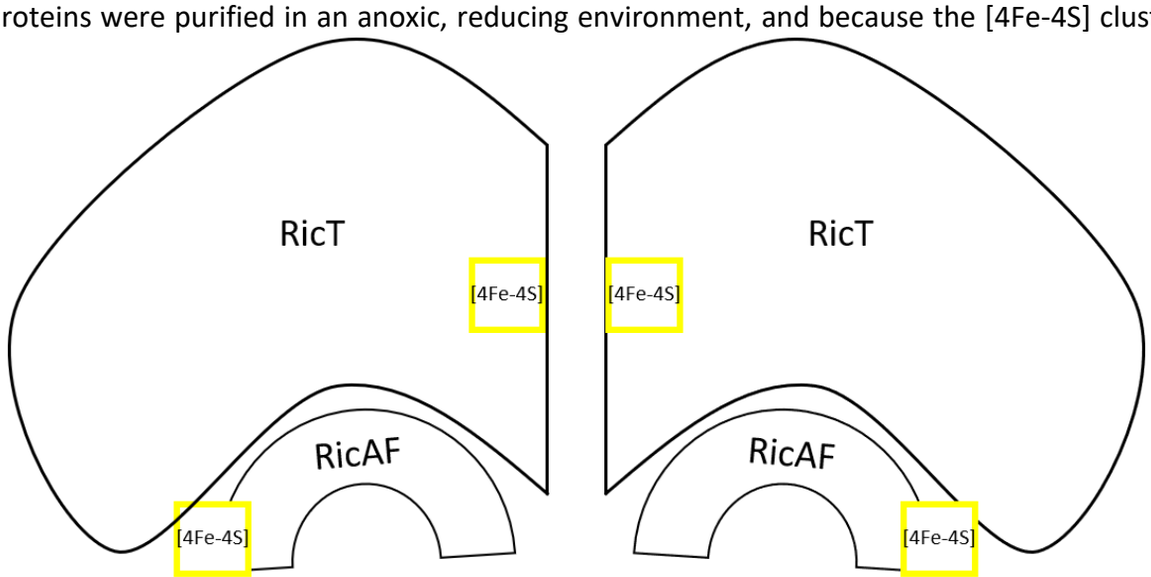

Figure 43: Schematic reconstruction of the dimerized RicAFT complex.
The RicAF heterodimer is located at the bottom of the complex. RicT is located a top of the heterodimer. One [4Fe-4S] cluster is located at the interface of the C-termini of RicAF and somewhere on RicT. The other one is coordinated solely by RicT. A possible oxidation of the [4Fe-4S] cluster could lead to a dimerization of the complex.

RicT is coordinated by four cysteines (Carabetta *et al.*, 2013; Dubnau *et al.*, 2016; Tanner *et al.*, 2017; Adusei-Danso *et al.*, 2019). In this work the proteins were purified in an oxidizing environment, which might lead to the degradation of the [4Fe-4S] cluster into a [2Fe-2S] or a [3Fe-4S] cluster. Such clusters are more linear and possibly enable a connection to the other complex, allowing dimerization.

Nevertheless, the presence of the dimer of RicAFT heterotrimers in the cell is purely speculative, and therefore, its role unknown. One possibility is that the complex, like FNR, senses the oxygen content inside the cell and therefore, the reductive potential. In a cell with high oxygen availability the [4Fe-4S] cluster would be oxidized, leading to the dimerized state and possibly affecting the regulation of RNase Y, thus, directly altering the maturation of mRNAs (Khoroshilova *et al.*, 1997; Popescu *et al.*, 1998; Kiley and Beinert, 1998; Mettert and Kiley, 2015; DeLoughery *et al.*, 2016; DeLoughery *et al.*, 2018). Another possibility could be that the dimerization is a protection startegy to counter further oxidation of the iron-sulfur cluster, which would cause further damage to the cell. Additionally, the interaction of *Bs*RicAF with *Gt*RicT was investigated. To this purpose, HDX was employed to observe changes in the deuteration pattern at the interaction sites of the subunits (4.2.2). While reduction in the deuteration along the whole protein was observed for RicA and RicF, specifically in α_1, α_3, and α_5 for RicA, and $\alpha_{1\text{-}4}$ for RicF, the precise locations required for the interaction could not be determined (see Figure 30). Mutational analysis of RicA and RicF (see Figure 32) failed to locate the sites required for interaction, however, it did exclude some sites from being essential for the interaction. Although, it is also possible that the mutated sites confer the interaction but were overall too insignificant to inhibit the formation of the complex, since the interaction takes place along nearly the entire protein (Figure 30; Adusei-Danso *et al.*, 2019). Sites of reduced and increased deuteration were observed for *Gt*RicT, implying a larger structural change upon binding to *Bs*RicAF. To date, no structure is available for *Gt*RicT, hence, it is impossible to ascribe these changes to any structural feature or specific amino acids.

5.3. The RicAFT interactions with the RNase Y

The cell-wall association of the RicAFT complex is dependent on RNase Y, while regulating its activity. Nonetheless, this had only been supported by bacterial two-hybrid analysis and CoIP data of RicF (Tortosa *et al*., 2000; DeLoughery *et al.*, 2016; DeLoughery *et al.*, 2018). Therefore, an *in vitro* reconstitution for the RicAFT + RNase Y complex was attempted analogously to the reconstitution of the RicAFT complex in this work (see 4.2.1 and 4.2.3). RNase Y from *G. thermodenitrificans* was purified lacking the first 22 amino acids, which are involved in the membrane anchoring of the complex, and then mixed with the purified *Bs*RicAF + *Gt*RicT complex or *Gt*RicT (see 4.2.3; Mora *et al*., 2018). However, no complex formation could be observed by analytical size exclusion chromatography or during co-purification of the proteins (see 4.2.3). In contrast, CoIP experiments performed with a tagged RicT led to co-elution of RicA, RicF, and RNase Y. The proteins of the RicAFT complex were found in equimolar amounts, emphasizing the hypothesis that the complete complex is needed for interaction with RNase Y (DeLoughery *et al.*, 2016; DeLoughery *et al.*, 2018). Hence, a discrepancy between the *in vitro* and *in vivo* data is observed, since no interaction of RNase Y and the RicAFT complex could be established *in vitro* (see Figure 34) but was possible *in vivo* (see Table 8). This might be due to several reasons 1) the heterologous production of the proteins led to missing or additional modifications of the proteins, inhibiting the interaction of RicAFT with RNase Y. 2) The interaction requires RNA or the RNase Y in a working conformation to interact. 3) The N-terminal domain of RNase Y is required for the interaction. These are all requisites that are present in the *in vivo* CoIP but missing in the heterologous production and reconstitution of the complex. It could be that the RicAFT directly interacts with mRNA and thus is transiently interacting with RNase Y as the mRNA is processed. However, the RicAFT complex was never observed to directly interact with RNA *in vitro*, yet this might be due to the heterologous production as well.

Overall, the reasons for the interaction of the RicAFT complex and RNase Y as well as its function remain elusive, and a topic of debate (Dubnau, 2020; Losick, 2020). The complex is either involved in the phosphorelay for Spo0A by interaction of KinA, Spo0B, and SpoF (Carabetta *et al.*, 2013; Dubnau *et al.*, 2016; see Figure 6) and/or is an accessory protein complex of RNase Y that regulates mRNA maturation and degradation (DeLoughery *et al.*, 2016; DeLoughery *et al.*, 2018; Adusei-Danso *et al.*, 2019).

In this work, evidence is presented that more factors might have an influence in the regulation of the RicAFT complex and its regulating functions. It was shown that RicAF and RicT can form a complex spontaneously (see 4.2.1) and that it appears in two states: a 65 kDa and a 130 kDa state (see 4.2.1). This possible oligomerization could be caused by the [4Fe-4S] cluster coordinated by RicT, as is the case for FNR (Khoroshilova *et al.*, 1997; Popescu *et al.*, 1998; Kiley and Beinert, 1998; Mettert and Kiley, 2015). Nonetheless, the function of the two [4Fe-4S] clusters is yet to be determined. The coordination of the cluster bound by RicT which is coordinated by four cysteines, rules out some possibilities, as a function similar to radical SAM enzymes requires only three coordinated irons (Johnson and Smith, 2011; Broderick *et al.*, 2014; Adusei-Danso *et al.*, 2019). The cysteines required for the coordination of the [4Fe-4S] cluster are highlighted in Figure 44, where it can be seen that the section is well conserved among all shown organisms, underlining its importance.

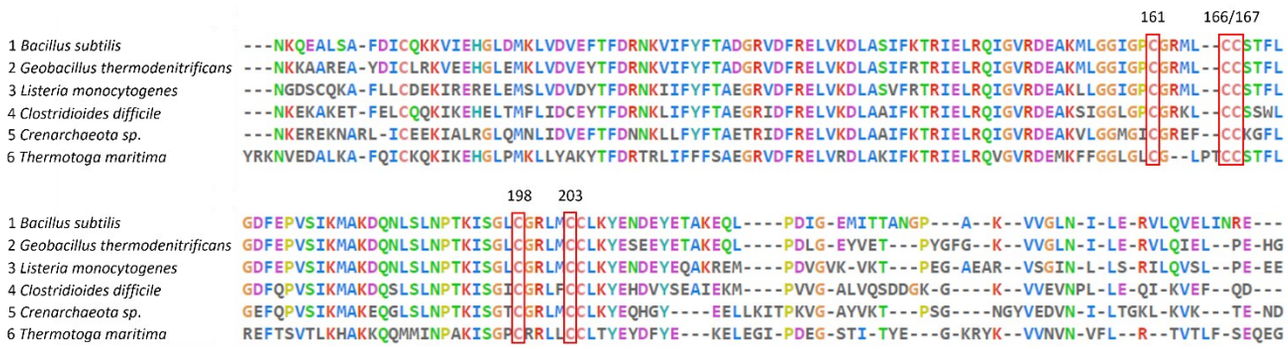

Figure 44: RicT protein alignment of various species.
The proteins aligned from amino acids 100 to 300. The cysteines required for [4Fe-4S] cluster coordination are highlighted. The species of origin are in the header of the row. Positively charged amino acids are colored red, negatively charged purple, neutral polar green, non-polar blue, glycine is orange, cyclic polar are turquoise, proline is yellow, and cysteine is salmon colored.

Moreover, the binding of $FADH_2$ hints towards a role in electron transfer, as $FADH_2$ is used to reduce the oxidized iron-sulfur cluster to perform another electron transfer (Hubbard *et al.*, 2003; van den Heuvel *et al.*, 2004; Johnson and Smith, 2011). Contradicting this is the unusual coordination of the [4Fe-4S] cluster which is not in line with the common pattern observed for ferredoxins (Johnson and Smith, 2011; Adusei-Danso *et al.*, 2019). The role of the second iron-sulfur cluster is unknown as well, yet at least three cysteines are involved in its coordination (Tanner *et al.*, 2017; Adusei-Danso *et al.*, 2019). Its role is of special interest, since RicAF is only present in species with genes encoding RicT (see Table 1). These species often have in common that they are facultative anaerobe and spore forming, therefore a possible involvement in oxygen sensing and/or protection is suggested. Moreover, the second [4Fe-4S] cluster could satisfy a requirement for a higher redox potential or

more transferred electrons, which is common in ferredoxins (Lamotte and Mouesca, 1997; Sticht and Rösch, 1998; Beinert, 2000; Johnson and Smith, 2011; Tanner *et al.*, 2017). Additionally, species like *Listeria monocytogenes* encode for the RicAFT proteins, yet lack RNase Y, or else encode only RicT and RNase Y, like *Clostridioides difficile* does. Their function and interactions are of interest, as they could shed additional light onto the function of the RicAFT complex and on whether or not they are involved in similar pathways (see Table 1). Furthermore, the interaction of RicAF and RicT affects the heterodimer along the entire structure, yet the precise interaction sites cannot be pinpointed to specific amino acids (see Figure 32). The performed CoIP experiments demonstrated that the RicAFT complex interacts with RNase Y, however, this cannot be replicated *in vitro* (see 4.2.3). This emphasizes the requirement of additional factors that induce the interaction of the RicAFT complex and RNase Y, that are yet unknown, but evidently present in the *in vivo* analysis (Adusei-Danso *et al.*, 2019; see 4.3). It appears highly likely that the RicAFT is a specificity factor for RNase Y that allows for the maturation of certain mRNAs under specific conditions (DeLoughery *et al*., 2016; DeLoughery *et al*., 2018).

In conclusion, the exact function of the RicAFT complex is challenging to determine and remains elusive. Nevertheless, this study has laid a groundwork for the structural characterization of the complex via cryo-EM that will allow for a better understanding of its mechanism and function.

5.4. CoIP experiments reveal potential new interaction partners of the RicAFT complex

CoIP experiments are an established method to potentially identify new *in vivo* interaction partners, especially when used in combination with other tagged proteins to exclude false positives and generate high confidence results. However, the results are never absolutely accurate, since the protein overproduction may lead to false positives. This should be taken into account when analyzing the data obtained through this type of experiment.

For the proof of concept, the first CoIP experiment was performed with a Strep-tagged RicT in *B. subtilis*. The expected interaction partners RicA and RicF were found with high confidence, thereby confirming the concept (see Table 8). Additionally, RNase Y was detected, which was reported before to associate with the RicAFT complex (Carabetta *et al.*, 2013; DeLoughery *et al.*, 2016; DeLoughery *et al.*, 2018). Although this is the first time RNase Y association was detected with RicT as bait protein, it is a protein previously implicated to interact with RNase Y (see Table 8; Branda *et al.*, 2001; Adusei-Danso *et al.*, 2019). The repercussions of such an interaction have already been discussed above (5.3). Additional proteins that were detected are YmfH, SufA, and YuaB. YmfH is a possible zinc protease that possibly degrades RicT (Miethke *et al.*, 2008). As RicT is overproduced in the cell, too much unbound RicT could prove toxic. To counter this, degradation by YmfH, or specific regulation by RicA and RicF is required in *B. subtilis*. The observation of a specific degradation product of RicT (see Figure 18) is in agreement with this. As are previous observations that a *ricT* deletion is less harmful to the lifestyle switch than either a *ricA* or *ricF* deletion (Carabetta *et al.*, 2013; DeLoughery *et al.*, 2016). The interaction with SufA probably arises from the incorporation of the [4Fe-4S] cluster into RicT. SufA is an iron-sulfur carrier protein and probably traffics [2Fe-2S] clusters from their generation point to RicT and helps with their maturation into [4Fe-4S] (Lu *et al.*, 2008; Albrecht *et al.*, 2010). The connection of YuaB and the RicAFT complex might be in the phosphorelay, as both supposedly interact with KinA (Dubnau *et al.*, 2016) however no KinA was found in the CoIP experiment performed here (Table 8). As the complex should accelerate the phosphorelay and YuaB inhibits it, RicAFT could bind YuaB to prevent the protein from inhibiting KinA (Carabetta *et al.*, 2013; Garti-Levi *et al.*, 2013; Dubnau *et al.*, 2016). In Figure 45, a schematic of the novel findings for the RicAFT complex and its interaction with RNase Y is presented.

The second protein analyzed by CoIP experiments was YjbN, the essential NAD-kinase in *B. subtilis* required for the transformation of NAD to NADP, or from a catabolite electron carrier to an anabolite electron carrier (Garavaglia *et al.*, 2003). Several proteins were found with relative confidence amongst which several share a common theme. For example, YhdR, Fbp, and AcsA are all proteins located at junctions in the metabolism of catabolism and anabolism. YhdR as a producer of oxaloacetate is located at the starting point of the citric acid cycle (Nakai *et al.*, 1999). The same is true for AcsA as this enzyme produces acetyl-CoA (Starai and Escalante-Semerena, 2004; Gardner *et al.*, 2006). Fbp is involved in the switch between glycolysis to gluconeogenesis (Fujita and Freese, 1979; Fujita *et al.*, 1998). Thus, as a group of anabolite electron carriers, these proteins could signal the need for more or less NADP and could crosstalk with YjbN.

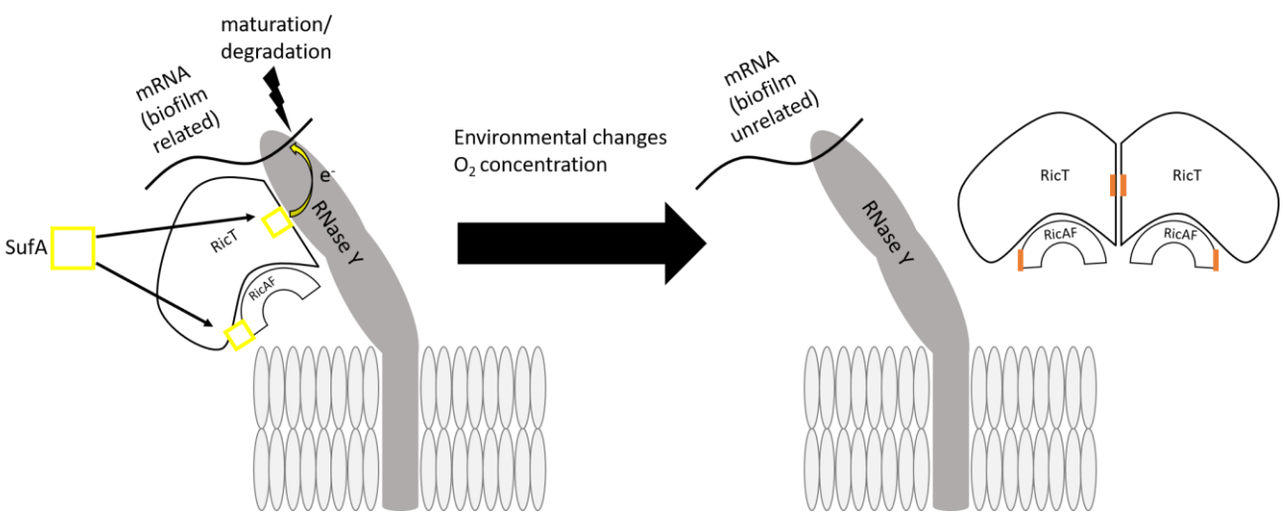

Figure 45: Schematic for RicAFT complex interaction with RNase Y
When oxygen is limited and the ISCs are not oxidized, RicAFT is present as heterotrimer. It supplies the RNase Y with electrons from its ISCs (yellow), that are possibly needed for certain mRNA degradation events. The ISCs are supplied by SufA. Upon oxygen influx, a greater number of ISCs are oxidized (orange) and RicAFT cannot supply electrons to RNase Y anymore, hence RNase Y is unable to perform certain degradation events. Moreover, the RicAFT complex dimerizes, to possibly protect the oxidized ISCs from further oxidation.

The other detected proteins are more diverse. HutU uses NAD^+ as an electron acceptor, hence YjbN could be interacting to acquire NAD^+ for phosphorylation (Wray and Fisher, 1994; Fisher *et al.*, 1996; Zalieckas *et al.*, 1999). YerA is involved in the salvage pathway for adenine and in which it requires electrons to form hypoxanthine. YerA is also a junction for the catabolic process of adenine or the anabolite process of hypoxanthine (Noirot-Gros *et al.*, 2002; Macek *et al.*, 2007).

Buk, Mfd, and YqfE share the ability to bind ATP, which also delivers the phosphate group in YjbN for the phosphorylation of NAD^+. However, these are highly diverse and a sufficient conclusion for their

supposed interaction with YjbN could not be drawn (Debarbouille *et al.*, 1999; Kazakov *et al.*, 2002; Roberts and Park, 2004; Nickel *et al.*, 2004; Robleto *et al.*, 2012).

Lastly YmcB, a tRNA methyltransferase encoded in the same operon as *ricA* (Anton *et al.*, 2010) was analyzed for potential interaction partners. Firstly, proteins that are involved in the export or production of molecules that are exported out of the cell were identified. Amongst these, the phage-derived proteins SunT and SunS, responsible for the production and export of sublancin (Quentin *et al.*, 1999; Dorenbos *et al.*, 2002; Oman *et al.*, 2011; Wang and van der Donk, 2011) or DhbE involved in the production of a siderophore (May *et al.*, 2001; May *et al.*, 2002) or GltT a Na^+/H^+ coupled glutamate/aspartate symporter (Reyes *et al.*, 2013; Jensen *et al.*, 2013). The possible connection of DhbE with YmcB could be that YmcB is a [4Fe-4S] cluster radical SAM enzyme, hence it requires iron to perform its reaction, the iron for which is acquired by siderophores (May *et al.*, 2001; Anton *et al.*, 2010). Additionally, sporulation and biofilm formation could be associated with the methylation pattern of tRNAs. These switches in lifestyles are often associated with the switch in the production of antimicrobial compounds, hence explaining the interaction with SunS and SunT, as YmcB could act as a mediator (Vold, 1973; Vold, 1978; Quentin *et al.*, 1999; Dorenbos *et al.*, 2002; Oman *et al.*, 2011; Wang and van der Donk, 2011). The change in lifestyle might require a change in the uptake of amino acids and explain the interaction with GltT. Soj is involved in the regulation of sporulation, another lifestyle change, and thereby could be connected to YmcB. When YmcB and RicA were simultaneously overproduced, SipS was detected as a potential interaction partner. The protein is involved in the maturation of proteins that are then exported. This is again growth-phase-dependent and might be an ideal junction for crosstalk between the different growth states (Bolhuis *et al.*, 1996; Tjalsma *et al.*, 1997; Tjalsma *et al.*, 1998; Hastie *et al.*, 2014; Zalucki and Jennings, 2017; Castro *et al.*, 2018).

This study shone light on the interaction network of interesting, yet not well-investigated proteins, and confirmed several previous observations. These results lay the foundation for future interaction studies, that may elucidate on the convoluted and complicated network of intracellular dependencies and regulations.

6. A GLIMPSE INTO THE FUTURE

The mode of action of the RicAFT complex could not be explored in this study as requires an atomic resolution structure. The discovery of a novel RicAFT complex dimer presents a solid basis for future work and the possible structure elucidation by cryo-EM. With a resolved atomic structure, the functions of the two [4Fe-4S] clusters can be determined and the matter of their requirement for structural integrity or electron transfer resolved, further exploring the mode of action of the RicAFT complex. The coordination of the [4Fe-4S] cluster in the interface of all three proteins will be of special interest for future analysis, as it has possible additional functions in comparison to those from the cluster coordinated by RicT (Tanner *et al.*, 2017). In this regard, analysis of RicT from organisms lacking RNase Y or RicAF might be enlightening, since such studies explore the role of the RicAF heterodimer. Primarily their suspected role as shields against oxygen in aerobic bacteria (see Table 1). In species lacking RNase Y but encoding the RicAFT complex or just RicT, the phenotypic analysis will be compelling, as these might regulate other pathways. These proteins could have an alternative mode of action, yet act in a similar pathway, while possibly interacting with different endoribonucleases and enabling certain mRNA maturation events. The conservation of RicT in all domains of life emphasizes its importance (see Table 1). Moreover, a precise description of its mechanism might settle the hen-egg dispute of whether the RicAFT complex regulates the phosphorelay and thereby changes the RNA maturation, or *vice versa* (Dubnau, 2020; Losick, 2020). For this, using a RicAFT complex unable to bind the iron-sulfur clusters or a reconstituted complex with only one iron-sulfur cluster is highly convenient. Additionally, the K65A mutation of RicF described in this work will be advantageous for future studies as it allows for expression of all three proteins without complex formation (4.2.2).

Most importantly, if RicT mutants cause similar phenotypes in all species encoding the protein, such as the observed lack of biofilm formation or sporulation in *B. subtilis*, it might be a prime target for an inhibitor. Most human bacterial pathogens are becoming increasingly dangerous due to biofilm formation or sporulation, as they boost antibiotic resistance and persistence in the human body. RicT is then an ideal target as it has no homologue in humans, yet is present in various pathogenic bacteria, highlighting the importance of future research of the RicAFT complex.

7. REFERENCES

1. Adams, P.D., Afonine, P. V., Bunkóczi, G., Chen, V.B., Davis, I.W., Echols, N., Headd, J.J., Hung, L.-W., Kapral, G.J., Grosse-Kunstleve, R.W., McCoy, A.J., Moriarty, N.W., Oeffner, R., Read, R.J., Richardson, D.C., Richardson, J.S., Terwilliger, T.C., and Zwart, P.H. **PHENIX : a comprehensive Python-based system for macromolecular structure solution**. *Acta Crystallogr Sect D Biol Crystallogr*. 2010, **66**: 2: 213–221.
2. Adusei-Danso, F., Khaja, F.T., DeSantis, M., Jeffrey, P.D., Dubnau, E., Demeler, B., Neiditch, M.B., and Dubnau, D. **Structure-function studies of the *Bacillus subtilis* RIC proteins identify the Fe-S cluster-ligating residues and their roles in development and RNA processing**. *MBio*. 2019, **10**: 5: e01841-19.
3. Agaisse, H., and Lereclus, D. **STAB-SD: a Shine–Dalgarno sequence in the 5′ untranslated region is a determinant of mRNA stability**. *Mol Microbiol*. 1996, **20**: 3: 633–43.
4. Albrecht, A.G., Netz, D.J.A., Miethke, M., Pierik, A.J., Burghaus, O., Peuckert, F., Lill, R., and Marahiel, M.A. **SufU Is an Essential Iron-Sulfur Cluster Scaffold Protein in *Bacillus subtilis***. *J Bacteriol*. 2010, **192**: 6: 1643–51.
5. Alen, C., and Sonenshein, A.L. ***Bacillus subtilis* aconitase is an RNA-binding protein**. *Proc Natl Acad Sci*. 1999, **96**: 18: 10412–7.
6. Anton, B.P., Russell, S.P., Vertrees, J., Kasif, S., Raleigh, E.A., Limbach, P.A., and Roberts, R.J. **Functional characterization of the YmcB and YqeV tRNA methylthiotransferases of *Bacillus subtilis***. *Nucleic Acids Res*. 2010, **38**: 18: 6195–205.
7. Arnaouteli, S., MacPhee, C.E., and Stanley-Wall, N.R. **Just in case it rains: building a hydrophobic biofilm the *Bacillus subtilis* way**. *Curr Opin Microbiol*. 2016, **34**: 7–12.
8. Bai, U., Mandic-Mulec, I., and Smith, I. **SinI modulates the activity of SinR, a developmental switch protein of *Bacillus subtilis*, by protein-protein interaction.** *Genes Dev*. 1993, **7**: 1: 139–48.
9. Baichoo, N., Wang, T., Ye, R., and Helmann, J.D. **Global analysis of the Bacillus subtilis Fur regulon and the iron starvation stimulon**. *Mol Microbiol*. 2002, **45**: 6: 1613–29.
10. Balk, J., and Pilon, M. **Ancient and essential: the assembly of iron–sulfur clusters in plants**. *Trends Plant Sci*. 2011, **16**: 4: 218–26.
11. Balueva, K.E., Malygin, A.A., Karpova, G.G., Nevinsky, G.A., and Zharkov, D.O. **Interactions of human ribosomal protein S3 with intact and damaged DNA**. *Mol Biol*. 2008, **42**: 2: 277–84.
12. Beinert, H. **Iron-sulfur proteins: ancient structures, still full of surprises**. *JBIC J Biol Inorg Chem*. 2000, **5**: 1: 2–15.
13. Beinert, H., Holm, R.H., and Münck, E. **Iron-Sulfur Clusters: Nature's Modular, Multipurpose Structures**. *Science*. 1997, **277**: 5326: 653–9.
14. Beinert, H., Kennedy, M.C., and Stout, C.D. **Aconitase as Iron–Sulfur Protein, Enzyme, and Iron-Regulatory Protein**. *Chem Rev*. 1996, **96**: 7: 2335–2374.
15. Bepler, T., Morin, A., Rapp, M., Brasch, J., Shapiro, L., Noble, A.J., and Berger, B. **Positive-unlabeled convolutional neural networks for particle picking in cryo-electron micrographs**. *Nat Methods*. 2019, **16**: 11: 1153–1160.
16. Berka, R.M., Hahn, J., Albano, M., Draskovic, I., Persuh, M., Cui, X., Sloma, A., Widner, W., and Dubnau, D. **Microarray analysis of the *Bacillus subtilis* K-state: genome-wide expression changes dependent on ComK**. *Mol Microbiol*. 2002, **43**: 5: 1331–45.
17. Berkovitch, F. **Crystal Structure of Biotin Synthase, an S-Adenosylmethionine-Dependent Radical Enzyme**. *Science*. 2004, **303**: 5654: 76–9.
18. Bird, J.G., Zhang, Y., Tian, Y., Panova, N., Barvík, I., Greene, L., Liu, M., Buckley, B., Krásný, L., Lee, J.K., Kaplan, C.D., Ebright, R.H., and Nickels, B.E. **The mechanism of RNA 5′ capping with NAD+, NADH and desphospho-CoA**. *Nature*. 2016, **535**: 7612: 444–7.
19. Bochner, B.R., Lee, P.C., Wilson, S.W., Cutler, C.W., and Ames, B.N. **AppppA and related adenylylated nucleotides are synthesized as a consequence of oxidation stress**. *Cell*. 1984, **37**: 1: 225–32.
20. Bolhuis, A., Sorokin, A., Azevedo, V., Ehrlich, S.D., Braun, P.G., Jong, A. De, Venema, G., Bron, S., and Maarten van Dijl, J. ***Bacillus subtilis* can modulate its capacity and specificity for protein secretion through temporally controlled expression of the *sipS* gene for signal peptidase I**. *Mol Microbiol*. 1996, **22**: 4: 605–18.
21. Bradford, M. **A Rapid and Sensitive Method for the Quantitation of Microgram Quantities of Protein Utilizing the Principle of Protein-Dye Binding**. *Anal Biochem*. 1976, **7**: 72: 248–54.

22. Bramucci, M.G., Green, B.D., Ambulos, N., and Youngman, P. **Identification of a *Bacillus subtilis spo0H* allele that is necessary for suppression of the sporulation-defective phenotype of a *spo0A* mutation.** *J Bacteriol*. 1995, **177**: 6: 1630–3.
23. Branda, S.S., Gonzalez-Pastor, J.E., Ben-Yehuda, S., Losick, R., and Kolter, R. **Fruiting body formation by *Bacillus subtilis***. *Proc Natl Acad Sci*. 2001, **98**: 20: 11621–11626.
24. Branda, S.S., González-Pastor, J.E., Dervyn, E., Ehrlich, S.D., Losick, R., and Kolter, R. **Genes Involved in Formation of Structured Multicellular Communities by *Bacillus subtilis***. *J Bacteriol*. 2004, **186**: 12: 3970–9.
25. Britton, R.A., Eichenberger, P., Gonzalez-Pastor, J.E., Fawcett, P., Monson, R., Losick, R., and Grossman, A.D. **Genome-Wide Analysis of the Stationary-Phase Sigma Factor (Sigma-H) Regulon of *Bacillus subtilis***. *J Bacteriol*. 2002, **184**: 17: 4881–90.
26. Broderick, J.B., Duffus, B.R., Duschene, K.S., and Shepard, E.M. **Radical S -Adenosylmethionine Enzymes**. *Chem Rev*. 2014, **114**: 8: 4229–4317.
27. Burbulys, D., Trach, K.A., and Hoch, J.A. **Initiation of sporulation in *B. subtilis* is controlled by a multicomponent phosphorelay**. *Cell*. 1991, **64**: 3: 545–52.
28. Campos-Guillén, J., Bralley, P., Jones, G.H., Bechhofer, D.H., and Olmedo-Alvarez, G. **Addition of Poly(A) and Heteropolymeric 3' Ends in *Bacillus subtilis* Wild-Type and Polynucleotide Phosphorylase-Deficient Strains**. *J Bacteriol*. 2005, **187**: 14: 4698–706.
29. Carabetta, V.J., Tanner, A.W., Greco, T.M., Defrancesco, M., Cristea, I.M., and Dubnau, D. **A complex of YlbF, YmcA and YaaT regulates sporulation, competence and biofilm formation by accelerating the phosphorylation of Spo0A**. *Mol Microbiol*. 2013, **88**: 2: 283–300.
30. Castro, A.N., Lewerke, L.T., Hastie, J.L., and Ellermeier, C.D. **Signal Peptidase Is Necessary and Sufficient for Site 1 Cleavage of RsiV in *Bacillus subtilis* in Response to Lysozyme**. *J Bacteriol*. 2018, **200**: 11: e00663-17.
31. Chai, Y., Kolter, R., and Losick, R. **Reversal of an epigenetic switch governing cell chaining in *Bacillus subtilis* by protein instability**. *Mol Microbiol*. 2010, **78**: 1: 218–29.
32. Cheek, J., and Broderick, J.B. **Adenosylmethionine-dependent iron-sulfur enzymes: versatile clusters in a radical new role**. *JBIC J Biol Inorg Chem*. 2001, **6**: 3: 209–26.
33. Chumsakul, O., Takahashi, H., Oshima, T., Hishimoto, T., Kanaya, S., Ogasawara, N., and Ishikawa, S. **Genome-wide binding profiles of the *Bacillus subtilis* transition state regulator AbrB and its homolog Abh reveals their interactive role in transcriptional regulation**. *Nucleic Acids Res*. 2011, **39**: 2: 414–28.
34. Collins, J.A., Irnov, I., Baker, S., and Winkler, W.C. **Mechanism of mRNA destabilization by the *glmS* ribozyme**. *Genes Dev*. 2007, **21**: 24: 3356–68.
35. Commichau, F.M., Rothe, F.M., Herzberg, C., Wagner, E., Hellwig, D., Lehnik-Habrink, M., Hammer, E., Völker, U., and Stülke, J. **Novel Activities of Glycolytic Enzymes in *Bacillus subtilis***. *Mol Cell Proteomics*. 2009, **8**: 6: 1350–60.
36. Coste H, Brevet A, Plateau P, and Blanquet S **Non-adenylylated bis(5'-nucleosidyl) tetraphosphates occur in *Saccharomyces cerevisiae* and in *Escherichia coli* and accumulate upon temperature shift or exposure to cadmium**. *J Biol Chem*. 1987, **5**: 262: 12096–103.
37. Costerton, J.W. **Bacterial Biofilms: A Common Cause of Persistent Infections**. *Science*. 1999, **284**: 5418: 1318–22.
38. Crane, B.R., Siegel, L.M., and Getzoff, E.D. **Sulfite Reductase Structure at 1.6 : Evolution and Catalysis for Reduction of Inorganic Anions**. *Science*. 1995, **270**: 5233: 59–67.
39. Crane, B.R., Siegel, L.M., and Getzoff, E.D. **Structures of the Siroheme- and [Fe 4 S 4] -Containing Active Center of Sulfite Reductase in Different States of Oxidation: Heme Activation via Reduction-Gated Exogenous Ligand Exchange**. *Biochemistry*. 1997, **36**: 40: 12101–19.
40. Cutting, S.M., and Ricca, E. **Bacterial spore-formers: friends and foes**. *FEMS Microbiol Lett*. 2014, **358**: 2: 107–109.
41. Czerwoniec, A., Dunin-Horkawicz, S., Purta, E., Kaminska, K.H., Kasprzak, J.M., Bujnicki, J.M., Grosjean, H., and Rother, K. **MODOMICS: a database of RNA modification pathways. 2008 update**. *Nucleic Acids Res*. 2009, **37**: Database: 118–21.
42. D'Souza, C., Nakano, M.M., and Zuber, P. **Identification of comS, a gene of the *srfA* operon that regulates the establishment of genetic competence in *Bacillus subtilis*.** *Proc Natl Acad Sci*. 1994, **91**: 20: 9397–9401.
43. Dai, S., Schwendtmayer, C., Johansson, K., Ramaswamy, S., Schürmann, P., and Eklund, H. **How does light regulate chloroplast enzymes? Structure–function studies of the ferredoxin/thioredoxin system**. *Q Rev*

Biophys. 2000, **33**: 1: 67–108.
44. Darnault, C., Volbeda, A., Kim, E.J., Legrand, P., Vernède, X., Lindahl, P.A., and Fontecilla-Camps, J.C. **Ni-Zn-[Fe4-S4] and Ni-Ni-[Fe4-S4] clusters in closed and open α subunits of acetyl-CoA synthase/carbon monoxide dehydrogenase**. *Nat Struct Mol Biol*. 2003, **10**: 4: 271–9.
45. Davies, D. **Understanding biofilm resistance to antibacterial agents**. *Nat Rev Drug Discov*. 2003, **2**: 2: 114–22.
46. Deana, A., Celesnik, H., and Belasco, J.G. **The bacterial enzyme RppH triggers messenger RNA degradation by 5′ pyrophosphate removal**. *Nature*. 2008, **451**: 7176: 355–8.
47. Debarbouille, M., Gardan, R., Arnaud, M., and Rapoport, G. **Role of BkdR, a Transcriptional Activator of the SigL-Dependent Isoleucine and Valine Degradation Pathway in *Bacillus subtilis***. *J Bacteriol*. 1999, **181**: 7: 2059–66.
48. DeLoughery, A., Dengler, V., Chai, Y., and Losick, R. **Biofilm formation by *Bacillus subtilis* requires an endoribonuclease-containing multisubunit complex that controls mRNA levels for the matrix gene repressor SinR**. *Mol Microbiol*. 2016, **99**: 2: 425–37.
49. DeLoughery, A., Lalanne, J.-B., Losick, R., and Li, G.-W. **Maturation of polycistronic mRNAs by the endoribonuclease RNase Y and its associated Y-complex in *Bacillus subtilis***. *Proc Natl Acad Sci*. 2018, **115**: 24: E5585–E5594.
50. Deng, X., Chen, K., Luo, G.-Z., Weng, X., Ji, Q., Zhou, T., and He, C. **Widespread occurrence of N 6 - methyladenosine in bacterial mRNA**. *Nucleic Acids Res*. 2015, **43**: 13: 6557–6567.
51. Dijl, J.M. van, and Hecker, M. ***Bacillus subtilis*: from soil bacterium to super-secreting cell factory**. *Microb Cell Fact*. 2013, **12**: 1: 3–9.
52. Dorenbos, R., Stein, T., Kabel, J., Bruand, C., Bolhuis, A., Bron, S., Quax, W.J., and Dijl, J.M. van **Thiol-Disulfide Oxidoreductases Are Essential for the Production of the Lantibiotic Sublancin 168**. *J Biol Chem*. 2002, **277**: 19: 16682–8.
53. Dorléans, A., Li de la Sierra-Gallay, I., Piton, J., Zig, L., Gilet, L., Putzer, H., and Condon, C. **Molecular Basis for the Recognition and Cleavage of RNA by the Bifunctional 5′–3′ Exo/Endoribonuclease RNase J**. *Structure*. 2011, **19**: 9: 1252–61.
54. Doukov, T.I. **A Ni-Fe-Cu Center in a Bifunctional Carbon Monoxide Dehydrogenase/ Acetyl-CoA Synthase**. *Science*. 2002, **298**: 5593: 567–72.
55. Dubnau, D. **Reply to losick, "concerns about continuing claims that a protein complex interacts with the phosphorelay"**. *MBio*. 2020, **11**: 2: e00154-20.
56. Dubnau, D., and Losick, R. **Bistability in bacteria**. *Mol Microbiol*. 2006, **61**: 3: 564–72.
57. Dubnau, E.J., Carabetta, V.J., Tanner, A.W., Miras, M., Diethmaier, C., and Dubnau, D. **A protein complex supports the production of Spo0A-P and plays additional roles for biofilms and the K-state in *Bacillus subtilis***. *Mol Microbiol*. 2016, **101**: 4: 606–624.
58. Durand, S., Braun, F., Lioliou, E., Romilly, C., Helfer, A.-C., Kuhn, L., Quittot, N., Nicolas, P., Romby, P., and Condon, C. **A Nitric Oxide Regulated Small RNA Controls Expression of Genes Involved in Redox Homeostasis in *Bacillus subtilis***. *PLOS Genet*. 2015, **11**: 2: e1004957-81.
59. Durand, S., Gilet, L., Bessières, P., Nicolas, P., and Condon, C. **Three Essential Ribonucleases—RNase Y, J1, and III—Control the Abundance of a Majority of *Bacillus subtilis* mRNAs**. *PLoS Genet*. 2012, **8**: 3: e1002520-34.
60. Earl, A.M., Losick, R., and Kolter, R. **Ecology and genomics of *Bacillus subtilis***. *Trends Microbiol*. 2008, **16**: 6: 269–75.
61. Emsley, P., and Cowtan, K. **Coot : model-building tools for molecular graphics**. *Acta Crystallogr Sect D Biol Crystallogr*. 2004, **60**: 12: 2126–32.
62. Eschbach, S., Hofmann, C., Maerz, M., Maier, U.-G., and Sitte, P. **Molecular Cloning. A Laboratory Manual. 2. Auflage. Hrsg. von J. Sambrook, E. F. Fritsch, T. Maniatis, Cold Spring Harbor Laboratory Press, Cold Spring Harbour 1989**. *Biol unserer Zeit*. 1990, **20**: 6.
63. Evans, P.R., and Murshudov, G.N. **How good are my data and what is the resolution?** *Acta Crystallogr Sect D Biol Crystallogr*. 2013, **69**: 7: 1204–1214.
64. Feller, G. **Protein stability and enzyme activity at extreme biological temperatures**. *J Phys Condens Matter*. 2010, **22**: 32: 323101–323118.
65. Figaro, S., Durand, S., Gilet, L., Cayet, N., Sachse, M., and Condon, C. ***Bacillus subtilis* Mutants with Knockouts of the Genes Encoding Ribonucleases RNase Y and RNase J1 Are Viable, with Major Defects in Cell Morphology, Sporulation, and Competence**. *J Bacteriol*. 2013, **195**: 10: 2340–8.

66. Fisher, S.H., Rohrer, K., and Ferson, A.E. **Role of CodY in regulation of the *Bacillus subtilis hut* operon.** *J Bacteriol*. 1996, **178**: 13: 3779–84.
67. Friedrich, T., and Böttcher, B. **The gross structure of the respiratory complex I: a Lego System**. *Biochim Biophys Acta - Bioenerg*. 2004, **1608**: 1: 1–9.
68. Frindert, J., Zhang, Y., Nübel, G., Kahloon, M., Kolmar, L., Hotz-Wagenblatt, A., Burhenne, J., Haefeli, W.E., and Jäschke, A. **Identification, Biosynthesis, and Decapping of NAD-Capped RNAs in *B. subtilis***. *Cell Rep*. 2018, **24**: 7: 1890–1901.
69. Fujita, M., González-Pastor, J.E., and Losick, R. **High- and Low-Threshold Genes in the Spo0A Regulon of *Bacillus subtilis***. *J Bacteriol*. 2005, **187**: 4: 1357–68.
70. Fujita, Y., and Freese, E. **Purification and Properties of Fructose-1,6-bisphosphatase of *Bacillus subtilis***. *J Biol Chem*. 1979, **254**: 12: 5340–5349.
71. Fujita, Y., Yoshida, K.-I., Miwa, Y., Yanai, N., Nagakawa, E., and Kasahara, Y. **Identification and Expression of the *Bacillus subtilis* Fructose-1,6-Bisphosphatase Gene (*fbp*)**. *J Bacteriol*. 1998, **180**: 16: 4309–13.
72. Garavaglia, S., Galizzi, A., and Rizzi, M. **Allosteric Regulation of *Bacillus subtilis* NAD Kinase by Quinolinic Acid**. *J Bacteriol*. 2003, **185**: 16: 4884–50.
73. Gardner, J.G., Grundy, F.J., Henkin, T.M., and Escalante-Semerena, J.C. **Control of Acetyl-Coenzyme A Synthetase (AcsA) Activity by Acetylation/Deacetylation without NAD+ Involvement in *Bacillus subtilis***. *J Bacteriol*. 2006, **188**: 15: 5460–8.
74. Garti-Levi, S., Eswara, A., Smith, Y., Fujita, M., and Ben-Yehuda, S. **Novel Modulators Controlling Entry into Sporulation in *Bacillus subtilis***. *J Bacteriol*. 2013, **195**: 7: 1475–83.
75. Geromanos, S.J., Vissers, J.P.C., Silva, J.C., Dorschel, C.A., Li, G.-Z., Gorenstein, M. V., Bateman, R.H., and Langridge, J.I. **The detection, correlation, and comparison of peptide precursor and product ions from data independent LC-MS with data dependant LC-MS/MS**. *Proteomics*. 2009, **9**: 6: 1683–95.
76. Gout, I. **Coenzyme A: a protective thiol in bacterial antioxidant defence**. *Biochem Soc Trans*. 2019, **47**: 1: 469–476.
77. Grandoni, J.A., Switzers, R.L., Makarofq, C.A., and Zalkin, H. **Evidence That the Iron-Sulfur Cluster of B*acillus subtilis* Glutamine Phosphoribosylpyrophosphate Amidotransferase Determines Stability of the Enzyme to Degradation *in vivo***.
78. Green, M.R., and Sambrook, J. **Preparation of plasmid DNA by alkaline lysis with sodium dodecyl sulfate: Minipreps**. *Cold Spring Harb Protoc*. 2016, **2016**: 10: 911–916.
79. Gruner, I., Frädrich, C., Böttger, L.H., Trautwein, A.X., Jahn, D., and Härtig, E. **Aspartate 141 Is the Fourth Ligand of the Oxygen-sensing [4Fe-4S] 2+ Cluster of *Bacillus subtilis* Transcriptional Regulator Fnr**. *J Biol Chem*. 2011, **286**: 3: 2017–2021.
80. Haile, D.J., Rouault, T.A., Harford, J.B., Kennedy, M.C., Blondin, G.A., Beinert, H., and Klausner, R.D. **Cellular regulation of the iron-responsive element binding protein: disassembly of the cubane iron-sulfur cluster results in high-affinity RNA binding.** *Proc Natl Acad Sci*. 1992, **89**: 24: 11735–11739.
81. Hall-Stoodley, L., and Stoodley, P. **Evolving concepts in biofilm infections**. *Cell Microbiol*. 2009, **11**: 7: 1034–43.
82. Hambraeus, G., Wachenfeldt, C. von, and Hederstedt, L. **Genome-wide survey of mRNA half-lives in *Bacillus subtilis* identifies extremely stable mRNAs**. *Mol Genet Genomics*. 2003, **269**: 5: 706–14.
83. Hamoen, L.W., Eshuis, H., Jongbloed, J., Venema, G., and Sinderen, D. **A small gene, designated *comS*, located within the coding region of the fourth amino acid-activation domain of *srfA*, is required for competence development in *Bacillus subtilis***. *Mol Microbiol*. 1995, **15**: 1: 55–63.
84. Hamoen, L.W., Smits WK, Jong A, de, Holsappel S, and Kuipers OP **Improving the predictive value of the competence transcription factor (ComK) binding site in *Bacillus subtilis* using a genomic approach**. *Nucleic Acids Res*. 2002, **30**: 24: 5517–28.
85. Hamon, M.A., Stanley, N.R., Britton, R.A., Grossman, A.D., and Lazazzera, B.A. **Identification of AbrB-regulated genes involved in biofilm formation by *Bacillus subtilis***. *Mol Microbiol*. 2004, **52**: 3: 847–860.
86. Hanahan, D. **Studies on transformation of *Escherichia coli* with plasmids**. *J Mol Biol*. 1983, **166**: 4: 557–80.
87. Hanahan, D., Jessee, J., and Bloom, F.R. **Plasmid transformation of *Escherichia coli* and other bacteria**. *Methods Enzym*. 1991, **204**: 63–113.
88. Hanzelmann, P., and Schindelin, H. **Crystal structure of the S-adenosylmethionine-dependent enzyme MoaA and its implications for molybdenum cofactor deficiency in humans**. *Proc Natl Acad Sci*. 2004, **101**: 35: 12870–12875.

89. Hastie, J.L., Williams, K.B., Sepúlveda, C., Houtman, J.C., Forest, K.T., and Ellermeier, C.D. **Evidence of a Bacterial Receptor for Lysozyme: Binding of Lysozyme to the Anti-σ Factor RsiV Controls Activation of the ECF σ Factor σV**. *PLoS Genet*. 2014, **10**: 10: e100463.
90. Healy, J., Weir, J., Smith, I., and Losick, R. **Post-transcriptional control of a sporulation regulatory gene encoding transcription factor H in *Bacillus subtilis***. *Mol Microbiol*. 1991, **5**: 2: 477–87.
91. Hedderich, R., Albracht, S.P.J., Linder, D., Koch, J., and Thauer, R.K. **Isolation and characterization of polyferredoxin from *Methanobacterium thermoautotrophicum* The *mvhb* gene product of the methylviologen-reducing hydrogenase operon**. *FEBS Lett*. 1992, **298**: 1: 65–68.
92. Hentze, M.W., and Kuhn, L.C. **Molecular control of vertebrate iron metabolism: mRNA-based regulatory circuits operated by iron, nitric oxide, and oxidative stress.** *Proc Natl Acad Sci*. 1996, **93**: 16: 8175–8182.
93. Heuvel, R.H.H. van den, Curti, B., Vanoni, M.A., and Mattevi, A. **Glutamate synthase: a fascinating pathway from L-glutamine to L-glutamate**. *Cell Mol Life Sci*. 2004, **61**: 6: 669–681.
94. Hobley, L., Ostrowski, A., Rao, F. V., Bromley, K.M., Porter, M., Prescott, A.R., MacPhee, C.E., Aalten, D.M.F. van, and Stanley-Wall, N.R. **BslA is a self-assembling bacterial hydrophobin that coats the *Bacillus subtilis* biofilm**. *Proc Natl Acad Sci*. 2013, **110**: 33: 13600–5.
95. Hölscher, T., Bartels, B., Lin, Y.-C., Gallegos-Monterrosa, R., Price-Whelan, A., Kolter, R., Dietrich, L.E.P., and Kovács, Á.T. **Motility, Chemotaxis and Aerotaxis Contribute to Competitiveness during Bacterial Pellicle Biofilm Development**. *J Mol Biol*. 2015, **427**: 23: 3695–3708.
96. Holtmann, G., Bakker, E.P., Uozumi, N., and Bremer, E. **Uptake Systems in *Bacillus subtilis* and Their Role in Adaptation to Hypertonicity**. *J Bacteriol*. 2003, **185**: 4: 1289–1298.
97. Hoseki, J., Okamoto, A., Masui, R., Shibata, T., Inoue, Y., Yokoyama, S., and Kuramitsu, S. **Crystal Structure of a Family 4 Uracil-DNA Glycosylase from *Thermus thermophilus* HB8**. *J Mol Biol*. 2003, **333**: 3: 515–26.
98. Hosoya, S., Asai, K., Ogasawara, N., Takeuchi, M., and Sato, T. **Mutation in *yaaT* Leads to Significant Inhibition of Phosphorelay during Sporulation in *Bacillus subtilis***. *J Bacteriol*. 2002, **184**: 20: 5545–53.
99. Hubbard, P.A., Liang, X., Schulz, H., and Kim, J.-J.P. **The Crystal Structure and Reaction Mechanism of *Escherichia coli* 2,4-Dienoyl-CoA Reductase**. *J Biol Chem*. 2003, **278**: 39: 37553–60.
100. Hue, K.K., and Bechhofer, D.H. **Effect of ermC leader region mutations on induced mRNA stability.** *J Bacteriol*. 1991, **173**: 12: 3732–40.
101. Huen, J., Lin, C.-L., Golzarroshan, B., Yi, W.-L., Yang, W.-Z., and Yuan, H.S. **Structural Insights into a Unique Dimeric DEAD-Box Helicase CshA that Promotes RNA Decay**. *Structure*. 2017, **25**: 3: 469–481.
102. Huntzinger, E., Boisset, S., Saveanu, C., Benito, Y., Geissmann, T., Namane, A., Lina, G., Etienne, J., Ehresmann, B., Ehresmann, C., Jacquier, A., Vandenesch, F., and Romby, P. ***Staphylococcus aureus* RNAIII and the endoribonuclease III coordinately regulate *spa* gene expression**. *EMBO J*. 2005, **24**: 4: 824–35.
103. Imamura, D., Zhou, R., Feig, M., and Kroos, L. **Evidence That the *Bacillus subtilis* SpoIIGA Protein Is a Novel Type of Signal-transducing Aspartic Protease**. *J Biol Chem*. 2008, **283**: 22: 15287–99.
104. Ingle, S., Chhabra, S., Laspina, D., Salvo, E., Liu, B., and Bechhofer, D.H. **Polynucleotide phosphorylase and RNA helicase CshA cooperate in *Bacillus subtilis* mRNA decay**. *RNA Biol*. 2020, **Accepted**.
105. Inoue, H., Nojima, H., and Okayama, H. **High efficiency transformation of *Escherichia coli* with plasmids**. *Gene*. 1990, **96**: 1: 23–8.
106. Jang, Y.-J., Won, M., Chung, K.-S., Kim, D.-U., Hoe, K.-L., Park, C., and Yoo, H.-S. **A Novel Protein, Psp1, Essential for Cell Cycle Progression of Schizosaccharomyces pombe Is Phosphorylated by Cdc2-Cdc13 upon Entry into G 0 -like Stationary Phase of Cell Growth**. *J Biol Chem*. 1997, **272**: 32: 19993–20002.
107. Jarrett, J. **The generation of 5'-deoxyadenosyl radicals by adenosylmethionine-dependent radical enzymes**. *Curr Opin Chem Biol*. 2003, **7**: 2: 174–82.
108. Jensen, S., Guskov, A., Rempel, S., Hänelt, I., and Slotboom, D.J. **Crystal structure of a substrate-free aspartate transporter**. *Nat Struct Mol Biol*. 2013, **20**: 10: 1224–6.
109. Jindal, L., and Emberly, E. **DNA segregation under Par protein control**. *PLoS One*. 2019, **14**: 7: e0218520.
110. Johnson, D.C., Dean, D.R., Smith, A.D., and Johnson, M.K. **Structure, function, and formation of biological iron-sulfur clusters**. *Annu Rev Biochem*. 2005, **74**: 1: 247–81.
111. Johnson, M.K., and Smith, A.D. **Iron-Sulfur Proteins**. In *Encyclopedia of Inorganic and Bioinorganic Chemistry*. John Wiley & Sons, Ltd, Chichester, UK. pp. 1–31.
112. Jonas, R.M., Weaver, E.A., Kenney, T.J., Moran, C.P., and Haldenwang, W.G. **The *Bacillus subtilis spoIIG* operon encodes both sigma E and a gene necessary for sigma E activation.** *J Bacteriol*. 1988, **170**: 2: 507–511.

113. Kabsch, W. **XDS**. *Acta Crystallogr Sect D Biol Crystallogr*. 2010, **66**: 2: 125–32.
114. Kazakov, A., Vassieva, O., Gelfand, M., Osterman, A., and Overbeek, R. **Bioinformatics classification and functional analysis of PhoH homologs.** *In Silico Biol*. 2002, **3**: (1-2): 3–15.
115. Kearns, D.B., Chu, F., Branda, S.S., Kolter, R., and Losick, R. **A master regulator for biofilm formation by *Bacillus subtilis***. *Mol Microbiol*. 2004, **55**: 3: 739–49.
116. Khemici, V., Prados, J., Linder, P., and Redder, P. **Decay-Initiating Endoribonucleolytic Cleavage by RNase Y Is Kept under Tight Control via Sequence Preference and Sub-cellular Localisation**. *PLOS Genet*. 2015, **11**: 10: e1005577.
117. Khoroshilova, N., Popescu, C., Munck, E., Beinert, H., and Kiley, P.J. **Iron-sulfur cluster disassembly in the FNR protein of *Escherichia coli* by O2: [4Fe-4S] to [2Fe-2S] conversion with loss of biological activity**. *Proc Natl Acad Sci*. 1997, **94**: 12: 6087–92.
118. Kiley, P.J., and Beinert, H. **Oxygen sensing by the global regulator, FNR: the role of the iron-sulfur cluster**. *FEMS Microbiol Rev*. 1998, **22**: 5: 341–52.
119. Kiley, P.J., and Beinert, H. **The role of Fe–S proteins in sensing and regulation in bacteria**. *Curr Opin Microbiol*. 2003, **6**: 2: 181–5.
120. Kim, K., Manasherob, R., and Cohen, S.N. **YmdB: a stress-responsive ribonuclease-binding regulator of *E. coli* RNase III activity**. *Genes Dev*. 2008, **22**: 24: 3497–508.
121. Kimura, S., and Waldor, M.K. **The RNA degradosome promotes tRNA quality control through clearance of hypomodified tRNA**. *Proc Natl Acad Sci*. 2019, **116**: 4: 1394–1403.
122. Kobayashi, K., and Iwano, M. **BslA(YuaB) forms a hydrophobic layer on the surface of *Bacillus subtilis* biofilms**. *Mol Microbiol*. 2012, **85**: 1: 51–66.
123. Kolter, R., and Greenberg, E.P. **The superficial life of microbes**. *Nature*. 2006, **441**: 7091: 300–2.
124. Kowtoniuk, W.E., Shen, Y., Heemstra, J.M., Agarwal, I., and Liu, D.R. **A chemical screen for biological small molecule-RNA conjugates reveals CoA-linked RNA**. *Proc Natl Acad Sci*. 2009, **106**: 19: 7768–7773.
125. Kuo, C., McRee, D., Fisher, C., O'Handley, S., Cunningham, R., and Tainer, J. **Atomic structure of the DNA repair [4Fe-4S] enzyme endonuclease III**. *Science*. 1992, **258**: 5081: 434–40.
126. Laemmli, U.K. **Cleavage of Structural Proteins during the Assembly of the Head of Bacteriophage T4**. *Nature*. 1970, **227**: 5259: 680–685.
127. Lamotte, B., and Mouesca, J.-M. **Iron-sulfur clusters: fascinating magnetic structures at the heart of ubiquitous proteins**. *Comptes Rendus l'Académie des Sci - Ser IIB - Mech*. 1997, **324**: 2: 117–132.
128. Landgraf, B.J., Arcinas, A.J., Lee, K.-H., and Booker, S.J. **Identification of an Intermediate Methyl Carrier in the Radical S -Adenosylmethionine Methylthiotransferases RimO and MiaB**. *J Am Chem Soc*. 2013, **135**: 41: 15404–15416.
129. Layer, G. **Crystal structure of coproporphyrinogen III oxidase reveals cofactor geometry of Radical SAM enzymes**. *EMBO J*. 2003, **22**: 23: 6214–24.
130. LeDeaux, J.R., Yu, N., and Grossman, A.D. **Different roles for KinA, KinB, and KinC in the initiation of sporulation in *Bacillus subtilis*.** *J Bacteriol*. 1995, **177**: 3: 861–863.
131. Lehnik-Habrink, M., Pförtner, H., Rempeters, L., Pietack, N., Herzberg, C., and Stülke, J. **The RNA degradosome in *Bacillus subtilis*: identification of CshA as the major RNA helicase in the multiprotein complex**. *Mol Microbiol*. 2010, **77**: 4: 958–71.
132. Lehnik-Habrink, M., Schaffer, M., Mäder, U., Diethmaier, C., Herzberg, C., and Stülke, J. **RNA processing in *Bacillus subtilis*: identification of targets of the essential RNase Y**. *Mol Microbiol*. 2011, **81**: 6: 1459–73.
133. Leroy, M., Piton, J., Gilet, L., Pellegrini, O., Proux, C., Coppée, J., Figaro, S., and Condon, C. **Rae1/YacP, a new endoribonuclease involved in ribosome-dependent mRNA decay in *Bacillus subtilis***. *EMBO J*. 2017, **36**: 9: 1167–1181.
134. Li, G.-Z., Vissers, J.P.C., Silva, J.C., Golick, D., Gorenstein, M. V., and Geromanos, S.J. **Database searching and accounting of multiplexed precursor and product ion spectra from the data independent analysis of simple and complex peptide mixtures**. *Proteomics*. 2009, **9**: 6: 1167–1181.
135. Li, Z., Pandit, S., and Deutscher, M.P. **Polyadenylation of stable RNA precursors in vivo**. *Proc Natl Acad Sci*. 1998, **95**: 21: 12158–12162.
136. Liang, W., and Deutscher, M.P. **Transfer-messenger RNA-SmpB Protein Regulates Ribonuclease R Turnover by Promoting Binding of HslUV and Lon Proteases**. *J Biol Chem*. 2012, **287**: 40: 33472–33479.
137. Lill, R. **Function and biogenesis of iron–sulphur proteins**. *Nature*. 2009, **460**: 7257: 831–8.

138. Liou, G.-G., Chang, H.-Y., Lin, C.-S., and Lin-Chao, S. **DEAD Box RhlB RNA Helicase Physically Associates with Exoribonuclease PNPase to Degrade Double-stranded RNA Independent of the Degradosome-assembling Region of RNase E**. *J Biol Chem*. 2002, **277**: 43: 41157–62.
139. Lodish, H., Berk, A., Zipursky Lawrence S., Matsudaira, P., Baltimore David, and Darnell, J. **Molecular Cell Biology** . 4th ed., W. H. Freeman, New York.
140. Lopez, D., Vlamakis, H., and Kolter, R. **Generation of multiple cell types in *Bacillus subtilis***. *FEMS Microbiol Rev*. 2009, **33**: 1: 152–63.
141. Losick, R. **Concerns about Continuing Claims that a Protein Complex Interacts with the Phosphorelay**. *MBio*. 2020, **11**: 2: e03371-19.
142. Lu, J., Yang, J., Tan, G., and Ding, H. **Complementary roles of SufA and IscA in the biogenesis of iron–sulfur clusters in *Escherichia coli***. *Biochem J*. 2008, **409**: 2: 535–43.
143. Luciano, D.J., Levenson-Palmer, R., and Belasco, J.G. **Stresses that Raise Np4A Levels Induce Protective Nucleoside Tetraphosphate Capping of Bacterial RNA**. *Mol Cell*. 2019, **75**: 5: 957–966.
144. Macek, B., Mijakovic, I., Olsen, J. V., Gnad, F., Kumar, C., Jensen, P.R., and Mann, M. **The Serine/Threonine/Tyrosine Phosphoproteome of the Model Bacterium *Bacillus subtilis***. *Mol Cell Proteomics*. 2007, **6**: 4: 697–707.
145. Madeira, F., Park, Y. mi, Lee, J., Buso, N., Gur, T., Madhusoodanan, N., Basutkar, P., Tivey, A.R.N., Potter, S.C., Finn, R.D., and Lopez, R. **The EMBL-EBI search and sequence analysis tools APIs in 2019**. *Nucleic Acids Res*. 2019, **47**: W1.
146. Mah, T.-F.C., and O'Toole, G.A. **Mechanisms of biofilm resistance to antimicrobial agents**. *Trends Microbiol*. 2001, **9**: 1: 34–9.
147. Mansy, S.S., and Cowan, J.A. **Iron–Sulfur Cluster Biosynthesis: Toward an Understanding of Cellular Machinery and Molecular Mechanism**. *Acc Chem Res*. 2004, **37**: 9: 719–25.
148. Marbaniang, C.N., and Vogel, J. **Emerging roles of RNA modifications in bacteria**. *Curr Opin Microbiol*. 2016, **30**: 50–57.
149. Mari, J.F., and Bechhofer, D.H. **Initiation of mRNA decay in *Bacillus subtilis***. *Mol Microbiol*. 1993, **7**: 5: 705–17.
150. Marincola, G., and Wolz, C. **Downstream element determines RNase Y cleavage of the *saePQRS* operon in *Staphylococcus aureus***. *Nucleic Acids Res*. 2017, **45**: 10: 5980–5994.
151. Marolda, C.L., Li, B., Lung, M., Yang, M., Hanuszkiewicz, A., Rosales, A.R., and Valvano, M.A. **Membrane topology and identification of critical amino acid residues in the Wzx O-antigen translocase from E*scherichia coli O157:H4***. *J Bacteriol*. 2010, **192**: 23: 6160–6171.
152. Mathy, N., Bénard, L., Pellegrini, O., Daou, R., Wen, T., and Condon, C. **5'-to-3' Exoribonuclease Activity in Bacteria: Role of RNase J1 in rRNA Maturation and 5' Stability of mRNA**. *Cell*. 2007, **129**: 4: 681–92.
153. May, J.J., Kessler, N., Marahiel, M.A., and Stubbs, M.T. **Crystal structure of DhbE, an archetype for aryl acid activating domains of modular nonribosomal peptide synthetases**. *Proc Natl Acad Sci*. 2002, **99**: 19: 12120–12125.
154. May, J.J., Wendrich, T.M., and Marahiel, M.A. **The *dhb* Operon of *Bacillus subtilis* Encodes the Biosynthetic Template for the Catecholic Siderophore 2,3-Dihydroxybenzoate-Glycine-Threonine Trimeric Ester Bacillibactin**. *J Biol Chem*. 2001, **276**: 10: 7209–17.
155. Mettert, E.L., and Kiley, P.J. **Fe–S proteins that regulate gene expression**. *Biochim Biophys Acta - Mol Cell Res*. 2015, **1853**: 6: 1284–1293.
156. Miethke, M., Schmidt, S., and Marahiel, M.A. **The major facilitator superfamily-type transporter YmfE and the multidrug-efflux activator Mta mediate bacillibactin secretion in *Bacillus subtilis***. *J Bacteriol*. 2008, **190**: 15: 5143–52.
157. Miller, J.P., Hussain, Z., and Schweizer, M.P. **The involvement of the anticodon adjacent modified nucleoside N-[9-(-D-ribofuranosyl) purine-6-ylcarbamoyl]-threonine in the biological function of *E.coli* tRNAile**. *Nucleic Acids Res*. 1976, **3**: 5: 1185–1202.
158. Mirouze, N., Prepiak, P., and Dubnau, D. **Fluctuations in *spo0A* Transcription Control Rare Developmental Transitions in *Bacillus subtilis***. *PLoS Genet*. 2011, **7**: 4: e1002048.
159. Molle, V., Fujita, M., Jensen, S.T., Eichenberger, P., González-Pastor, J.E., Liu, J.S., and Losick, R. **The Spo0A regulon of *Bacillus subtilis***. *Mol Microbiol*. 2003, **50**: 5: 1683–701.
160. Mora, L., Ngo, S., Laalami, S., and Putzer, H. ***In Vitro* Study of the Major *Bacillus subtilis* Ribonucleases Y and J**. *Methods Enzym*. 2018, **612**: 343–359.

161. Murray, H., and Errington, J. **Dynamic Control of the DNA Replication Initiation Protein DnaA by Soj/ParA**. *Cell*. 2008, **135**: 1: 74–84.
162. Nakai, T., Okada, K., Akutsu, S., Miyahara, I., Kawaguchi, S., Kato, R., Kuramitsu, S., and Hirotsu, K. **Structure of *Thermus thermophilus* HB8 Aspartate Aminotransferase and Its Complex with Maleate**. *Biochemistry*. 1999, **38**: 8: 2413–2424.
163. Newman, J.A., Hewitt, L., Rodrigues, C., Solovyova, A., Harwood, C.R., and Lewis, R.J. **Unusual, Dual Endo- and Exonuclease Activity in the Degradosome Explained by Crystal Structure Analysis of RNase J1**. *Structure*. 2011, **19**: 9: 1241–51.
164. Nickel, M., Homuth, G., Böhnisch, C., Mäder, U., and Schweder, T. **Cold induction of the *Bacillus subtilis bkd* operon is mediated by increased mRNA stability**. *Mol Genet Genomics*. 2004, **272**: 1: 98–107.
165. Nicolas, P., Mader, U., Dervyn, E., Rochat, T., Leduc, A., Pigeonneau, N., Bidnenko, E., Marchadier, E., Hoebeke, M., Aymerich, S., Becher, D., Bisicchia, P., Botella, E., Delumeau, O., Doherty, G., Denham, E.L., Fogg, M.J., Fromion, V., Goelzer, A., Hansen, A., Noirot, P. *et al.* **Condition-Dependent Transcriptome Reveals High-Level Regulatory Architecture in *Bacillus subtilis***. *Science*. 2012, **335**: 6072: 1103–6.
166. Nishimura S, and Schimmel PR **Transfer RNA: Structure, Properties, and Recognition**. NY Col Spring Harbor Laboratory, New York.
167. Noirot-Gros, M.-F., Soultanas, P., Wigley, D., Ehrlich, S., Noirot, P., and Petit, M.-A. **The beta-propeller protein YxaL increases the processivity of the PcrA helicase**. *Mol Genet Genomics*. 2002, **267**: 3: 391–400.
168. Oguro, A., Kakeshita, H., Nakamura, K., Yamane, K., Wang, W., and Bechhofer, D.H. ***Bacillus subtilis* RNase III Cleaves Both 5′- and 3′-Sites of the Small Cytoplasmic RNA Precursor**. *J Biol Chem*. 1998, **273**: 31: 19542–7.
169. Ohlsen, K.L., Grimsley, J.K., and Hoch, J.A. **Deactivation of the sporulation transcription factor Spo0A by the Spo0E protein phosphatase.** *Proc Natl Acad Sci*. 1994, **91**: 5: 1756–1760.
170. Oman, T.J., Boettcher, J.M., Wang, H., Okalibe, X.N., and Donk, W.A. van der **Sublancin is not a lantibiotic but an S-linked glycopeptide**. *Nat Chem Biol*. 2011, **7**: 2: 78–80.
171. Osorio-Valeriano, M., Altegoer, F., Steinchen, W., Urban, S., Liu, Y., Bange, G., and Thanbichler, M. **ParB-type DNA Segregation Proteins Are CTP-Dependent Molecular Switches**. *Cell*. 2019, **179**: 7: 1512–1524.
172. Oussenko, I.A., Abe, T., Ujiie, H., Muto, A., and Bechhofer, D.H. **Participation of 3′-to-5′ Exoribonucleases in the Turnover of *Bacillus subtilis* mRNA**. *J Bacteriol*. 2005, **187**: 8: 2758–67.
173. Pechter, K.B., Meyer, F.M., Serio, A.W., Stulke, J., and Sonenshein, A.L. **Two Roles for Aconitase in the Regulation of Tricarboxylic Acid Branch Gene Expression in *Bacillus subtilis***. *J Bacteriol*. 2013, **195**: 7: 1525–1537.
174. Perego, M., and Hoch, J.A. **Negative regulation of *Bacillus subtilis* sporulation by the *spo0E* gene product.** *J Bacteriol*. 1991, **173**: 8: 2514–20.
175. Piggot PJ, and Coote JG **Genetic aspects of bacterial endospore formation**. *Rev*. 1976, **40**: 4: 908–962.
176. Popescu, C. V., Bates, D.M., Beinert, H., Munck, E., and Kiley, P.J. **Mossbauer spectroscopy as a tool for the study of activation/inactivation of the transcription regulator FNR in whole cells of *Escherichia coli***. *Proc Natl Acad Sci*. 1998, **95**: 23: 13431–5.
177. Punjani, A., Rubinstein, J.L., Fleet, D.J., and Brubaker, M.A. **cryoSPARC: algorithms for rapid unsupervised cryo-EM structure determination**. *Nat Methods*. 2017, **14**: 3: 290–296.
178. Quentin, Y., Fichant, G., and Denizot, F. **Inventory, assembly and analysis of *Bacillus subtilis* ABC transport systems**. *J Mol Biol*. 1999, **287**: 3: 467–84.
179. Quisel, J.D., and Grossman, A.D. **Control of Sporulation Gene Expression in *Bacillus subtilis* by the Chromosome Partitioning Proteins Soj (ParA) and Spo0J (ParB)**. *J Bacteriol*. 2000, **182**: 12: 3446–51.
180. Ravikumar, V., Nalpas, N.C., Anselm, V., Krug, K., Lenuzzi, M., Šestak, M.S., Domazet-Lošo, T., Mijakovic, I., and Macek, B. **In-depth analysis of *Bacillus subtilis* proteome identifies new ORFs and traces the evolutionary history of modified proteins**. *Sci Rep*. 2018, **8**: 1: 17246.
181. Reents, H., Gruner, I., Harmening, U., Bottger, L.H., Layer, G., Heathcote, P., Trautwein, A.X., Jahn, D., and Hartig, E. ***Bacillus subtilis* Fnr senses oxygen via a [4Fe-4S] cluster coordinated by three cysteine residues without change in the oligomeric state**. *Mol Microbiol*. 2006, **60**: 6: 1432–45.
182. Reeve, J.N., Beckler, G.S., Cram, D.S., Hamilton, P.T., Brown, J.W., Krzycki, J.A., Kolodziej, A.F., Alex, L., Orme-Johnson, W.H., and Walsh, C.T. **A hydrogenase-linked gene in *Methanobacterium thermoautotrophicum* strain delta H encodes a polyferredoxin.** *Proc Natl Acad Sci*. 1989, **86**: 9: 3031–3035.

183. Reverdy, A., Chen, Y., Hunter, E., Gozzi, K., and Chai, Y. **Protein lysine acetylation plays a regulatory role in *Bacillus subtilis* multicellularity**. *PLoS One*. 2018, **13**: 9: e0204687.
184. Reyes, N., Oh, S., and Boudker, O. **Binding thermodynamics of a glutamate transporter homologue**. *Nat Struct Mol Biol*. 2013, **20**: 5: 634–640.
185. Richards, J., Liu, Q., Pellegrini, O., Celesnik, H., Yao, S., Bechhofer, D.H., Condon, C., and Belasco, J.G. **An RNA Pyrophosphohydrolase Triggers 5'-Exonucleolytic Degradation of mRNA in *Bacillus subtilis***. *Mol Cell*. 2011, **43**: 6: 940–9.
186. Roberts, J., and Park, J.-S. **Mfd, the bacterial transcription repair coupling factor: translocation, repair and termination**. *Curr Opin Microbiol*. 2004, **7**: 2: 120–5.
187. Robleto, E. A., Martin, H., A., and Pedraza-Reyes, M. **Mfd and transcriptional derepression cause genetic diversity in *Bacillus subtilis***. *Front Biosci*. 2012, **E4**: 1: 1246–54.
188. Romero, D., Aguilar, C., Losick, R., and Kolter, R. **Amyloid fibers provide structural integrity to *Bacillus subtilis* biofilms**. *Proc Natl Acad Sci*. 2010, **107**: 5: 2230–2234.
189. Romero, D., Vlamakis, H., Losick, R., and Kolter, R. **An accessory protein required for anchoring and assembly of amyloid fibres in *B. subtilis* biofilms**. *Mol Microbiol*. 2011, **80**: 5: 1155–68.
190. Salvo, E., Alabi, S., Liu, B., Schlessinger, A., and Bechhofer, D.H. **Interaction of *Bacillus subtilis* Polynucleotide Phosphorylase and RNase Y**. *J Biol Chem*. 2016, **291**: 13: 6655–6663.
191. Sanger, F., Nicklen, S., and Coulson, A.R. **DNA sequencing with chain-terminating inhibitors**. *Proc Natl Acad Sci*. 1977, **74**: 12: 5463–5467.
192. Scholefield, G., Errington, J., and Murray, H. **Soj/ParA stalls DNA replication by inhibiting helix formation of the initiator protein DnaA**. *EMBO J*. 2012, **31**: 6: 1542–55.
193. Schostag, M.D., Albers, C.N., Jacobsen, C.S., and Priemé, A. **Low Turnover of Soil Bacterial rRNA at Low Temperatures**. *Front Microbiol*. 2020, **11**: 962.
194. Seid, C.A., Smith, J.L., and Grossman, A.D. **Genetic and biochemical interactions between the bacterial replication initiator DnaA and the nucleoid-associated protein Rok in *Bacillus subtilis***. *Mol Microbiol*. 2017, **103**: 5: 798–817.
195. Serio, A.W., Pechter, K.B., and Sonenshein, A.L. ***Bacillus subtilis* Aconitase Is Required for Efficient Late-Sporulation Gene Expression**. *J Bacteriol*. 2006, **188**: 17: 6396–405.
196. Shahbabian, K., Jamalli, A., Zig, L., and Putzer, H. **RNase Y, a novel endoribonuclease, initiates riboswitch turnover in *Bacillus subtilis***. *EMBO J*. 2009, **28**: 22: 3523–33.
197. Sinderen, D., Luttinger, A., Kong, L., Dubnau, D., Venema, G., and Hamoen, L. ***comK* encodes the competence transcription factor, the key regulatory protein for competence development in *Bacillus subtilis***. *Mol Microbiol*. 1995, **15**: 3: 455–62.
198. Sinderen, D. van, and Venema, G. ***comK* acts as an autoregulatory control switch in the signal transduction route to competence in *Bacillus subtilis*.** *J Bacteriol*. 1994, **176**: 18: 5762–5770.
199. Smith, J., Zaluzec, E., Wery, J., Niu, L., Switzer, R., Zalkin, H., and Satow, Y. **Structure of the allosteric regulatory enzyme of purine biosynthesis**. *Science*. 1994, **264**: 5164: 1427–33.
200. Sofia, H.J. **Radical SAM, a novel protein superfamily linking unresolved steps in familiar biosynthetic pathways with radical mechanisms: functional characterization using new analysis and information visualization methods**. *Nucleic Acids Res*. 2001, **29**: 5: 1097–106.
201. Sogin, M.L., and Pace, N.R. **In vitro maturation of precursors of 5S ribosomal RNA from *Bacillus subtilis***. *Nature*. 1974, **252**: 5484: 589–600.
202. Song, L., Wang, G., Malhotra, A., Deutscher, M.P., and Liang, W. **Reversible acetylation on Lys501 regulates the activity of RNase II**. *Nucleic Acids Res*. 2016, **44**: 5: 1979–88.
203. Starai, V.J., and Escalante-Semerena, J.C. **Acetyl-coenzyme A synthetase (AMP forming)**. *Cell Mol Life Sci*. 2004, **61**: 16: 2020–30.
204. Stead, M.B., Marshburn, S., Mohanty, B.K., Mitra, J., Castillo, L.P., Ray, D., Bakel, H. van, Hughes, T.R., and Kushner, S.R. **Analysis of *Escherichia coli* RNase E and RNase III activity *in vivo* using tiling microarrays**. *Nucleic Acids Res*. 2011, **39**: 8: 3188–203.
205. Sticht, H., and Rösch, P. **The structure of iron–sulfur proteins**. *Prog Biophys Mol Biol*. 1998, **70**: 2: 95–136.
206. Stragier, P., Bonamy, C., and Karmazyn-Campelli, C. **Processing of a sporulation sigma factor in *Bacillus subtilis:* How morphological structure could control gene expression**. *Cell*. 1988, **52**: 5: 697–704.

207. Svetlitchnyi, V., Dobbek, H., Meyer-Klaucke, W., Meins, T., Thiele, B., Romer, P., Huber, R., and Meyer, O. **A functional Ni-Ni-[4Fe-4S] cluster in the monomeric acetyl-CoA synthase from *Carboxydothermus hydrogenoformans***. *Proc Natl Acad Sci*. 2004, **101**: 2: 446–451.
208. Tanner, A.W., Carabetta, V.J., Martinie, R.J., Mashruwala, A.A., Boyd, J.M., Krebs, C., and Dubnau, D. **The RicAFT (YmcA-YlbF-YaaT) complex carries two [4Fe-4S]2+ clusters and may respond to redox changes**. *Mol Microbiol*. 2017, **104**: 5: 837–850.
209. Tjalsma, H., Bolhuis, A., Roosmalen, M.L. van, Wiegert, T., Schumann, W., Broekhuizen, C.P., Quax, W.J., Venema, G., Bron, S., and Dijl, J.M. van **Functional analysis of the secretory precursor processing machinery of *Bacillus subtilis*: identification of a eubacterial homolog of archaeal and eukaryotic signal peptidases**. *Genes Dev*. 1998, **12**: 15: 2318–31.
210. Tjalsma, H., Noback, M.A., Bron, S., Venema, G., Yamane, K., and Dijl, J.M. van ***Bacillus subtilis* Contains Four Closely Related Type I Signal Peptidases with Overlapping Substrate Specificities**. *J Biol Chem*. 1997, **272**: 41: 25983–92.
211. Tortosa, P., Albano, M., and Dubnau, D. **Characterization of *ylbF*, a new gene involved in competence development and sporulation in *Bacillus subtilis***. *Mol Microbiol*. 2000, **35**: 5: 1110–9.
212. Toymentseva, A.A., Schrecke, K., Sharipova, M.R., and Mascher, T. **The LIKE system, a novel protein expression toolbox for *Bacillus subtilis* based on the *liaI* promoter**. *Microb Cell Fact*. 2012, **11**: 1: 143–156.
213. Trinquier, A., Durand, S., Braun, F., and Condon, C. **Regulation of RNA processing and degradation in bacteria**. *Biochim Biophys Acta - Gene Regul Mech*. 2020, **1863**: 5.
214. Turgay, K., Hamoen, L.W., Venema, G., and Dubnau, D. **Biochemical characterization of a molecular switch involving the heat shock protein ClpC, which controls the activity of ComK, the competence transcription factor of *Bacillus subtilis*.** *Genes Dev*. 1997, **11**: 1: 119–28.
215. Turgay K, Hahn J, Burghoorn J, and Dubnau D **Competence in *Bacillus subtilis* is controlled by regulated proteolysis of a transcription factor**. *EMBO J*. 1998, **17**: 22: 6730–6738.
216. Vieille, C., and Zeikus, G.J. **Hyperthermophilic Enzymes: Sources, Uses, and Molecular Mechanisms for Thermostability**. *Microbiol Mol Biol Rev*. 2001, **65**: 1: 1–43.
217. Vlamakis, H., Chai, Y., Beauregard, P., Losick, R., and Kolter, R. **Sticking together: building a biofilm the *Bacillus subtilis way***. *Nat Rev Microbiol*. 2013, **11**: 3: 157–68.
218. Vold, B.S. **Analysis of isoaccepting transfer ribonucleic acid species of *Bacillus subtilis*: Changes in chromatography of transfer ribonucleic acids associated with stage of Dvelopment**. *J Bacteriol*. 1973, **114**: 1: 178–82.
219. Vold, B.S. **Post-transcriptional modifications of the anticodon loop region: Alterations in isoaccepting species of tRNA's during development in *Bacillus subtilis***. *J Bacteriol*. 1978, **135**: 1: 124–32.
220. Wales, T.E., Fadgen, K.E., Gerhardt, G.C., and Engen, J.R. **High-Speed and High-Resolution UPLC separation at zero degrees celsius**. *Anal Chem*. 2008, **80**: 17: 6815–20.
221. Walters, E.M., and Johnson, M.K. **Ferredoxin:thioredoxin reductase: Disulfide reduction catalyzed via novel site-specific [4Fe–4S] cluster chemistry**. *Photosynth Res*. 2004, **79**: 3: 249–264.
222. Wang, H., and Donk, W.A. van der **Substrate selectivity of the sublancin S-Glycosyltransferase**. *J Am Chem Soc*. 2011, **133**: 41: 16394–16397.
223. Weissenbach, J., and Grosjean, H. **Effect of threonylcarbamoyl modification (t6A) in yeast tRNAArgIII on codon-anticodon and anticodon-anticodon interactions. A thermodynamic and kinetic evaluation**. *Eur J Biochem*. 1981, **116**: 1: 207–13.
224. Winn, M.D., Ballard, C.C., Cowtan, K.D., Dodson, E.J., Emsley, P., Evans, P.R., Keegan, R.M., Krissinel, E.B., Leslie, A.G.W., McCoy, A., McNicholas, S.J., Murshudov, G.N., Pannu, N.S., Potterton, E.A., Powell, H.R., Read, R.J., Vagin, A., and Wilson, K.S. **Overview of the CCP 4 suite and current developments**. *Acta Crystallogr Sect D Biol Crystallogr*. 2011, **67**: 4: 235–42.
225. Wray, L. V, and Fisher, S.H. **Analysis of *Bacillus subtilis hut* operon expression indicates that histidine-dependent induction is mediated primarily by transcriptional antitermination and that amino acid repression is mediated by two mechanisms: regulation of transcription initiation** . *J Bacteriol*. 1994, **176**: 17: 5466–73.
226. Yankovskaya, V., Horsefield R, Tönroth S, Luna-Chavez C, Miyoshi H, Léger C, Byrne B, Cecchini G, and Iwata S **Architecture of succinate dehydrogenase and reactive oxygen species generation**. *Science*. 2003, **299**: 5607: 700–4.

227. Zalieckas, J.M., Wray, L. V., and Fisher, S.H. **Trans-acting factors affecting carbon catabolite repression of the hut Operon in *Bacillus subtilis***. *J Bacteriol*. 1999, **181**: 9: 2883–8.
228. Zalucki, Y.M., and Jennings, M.P. **Signal peptidase I processed secretory signal sequences: Selection for and against specific amino acids at the second position of mature protein**. *Biochem Biophys Res Commun*. 2017, **483**: 3: 972–977.
229. Zhang, W., Wang, C., Song, Y., Shao, C., Zhang, X., and Zang, J. **Structural insights into the mechanism of *Escherichia coli* YmdB: A 2'- O -acetyl-ADP-ribose deacetylase**. *J Struct Biol*. 2015, **192**: 3: 478–486.

8. LIST OF FIGURES

9. LIST OF TABLES

10. APPENDIX

10.1. Materials

10.1.1. Chemicals

All chemicals used in this study were purchased from Roth (Germany), Sigma Aldrich (Germany), VWR (Germany) and AppliChem (Germany). Plastic consumable ware (reaction, falcon tubes, pipette tips, syringes) were obtained from Sarstedt and Braun.

10.1.2. Equipment

The equipment used in this thesis is listed in Table 10.

Table 10: Equipment

Equipment	Manufacturer
Azure c280	Azure Biosystems, USA
Centrifuges	Thermo Scientific, USA
	Heraeus Christ, Osterode
	Hubbard Systems, UK
Wisd Shaking Incubator WIS-20	witeg, Germany
INCUCELL 222 Comfort	MMM Group, USA
ChemiDoC™ MP Imaging System (170-8280)	Bio-Rad, USA
T100™ Thermocycler	Bio-Rad, USA
PerfectBlue 'Semi-Dry'-Blotter	VWR, USA
Power Supply EV2310	Carl-Roth, Germany
Nanodrop® Lite	Thermo Scientific, USA
M-110L Microfluidizer® Materials Processor	Microfluidics, USA
LLG-uni THERMIX 2 pro	LLG, Germany
300kV Titan Krios	FEI company, USA
PERIMAX 12	SPETEC, Germany
Crystal Gryphon	Art Robbins, USA
PN3150 RI Detector	Postnova Analytics, Germany
Kern PCB 6000	KERN, Germany
Denver Instruments S-203	Denver Instruments, USA
Denver Instruments SI-234	Denver Instruments, USA
ÄKTA pure	Cytiva, USA
ÄKTA Purifier	Cytiva, USA
ÄKTA Prime	Cytiva, USA
Refeyn One	Refeyn, UK
Retsch MM400	Retsch, Germany

10.1.3. Commercial systems

Commercials systems (kits) used, can be seen in Table 11.

Table 11: Commercial systems

Commercial system	Manufacturer
GeneRuler™ 1kb Plus DNA Ladder	Thermo Scientific, USA
Q5®Site-Directed Mutagenesis Kit	NEB, USA
StrepTactin® HRP	IBA, Germany
GeneJET Miniprep Plasmid Kit	Thermo Scientific, USA
GeneJET Gelextraction Kit	Thermo Scientific, USA
PageRuler™ Plus Prestaiend Protein Ladder 10 to 250 kDa	Thermo Scientific, USA
ROTI® Blue	Thermo Scientific, USA
Amicon® Ultra Centrifugal Filters	Merck, Germany
Pierce™ Crosslinking Magnetic IP/CoIP-Kit	Thermo Scientific, USA
Pierce™ ECL Western Blotting Substrate	Thermo Scientific, USA
Pierce™ Unstained Protein MW Marker	Thermo Scientific, USA

10.1.4. Enzymes

Enzymes used in this research were purchased from NEB.

10.2. Bacterial strains

All bacterial strains used can be seen in Table 12.

Table 12: Bacterial strains used in this work

Name	Genotype	Reference / received from
E. coli		
BL 21 (DE3)	B(834)-derivate *F-lon ompT hsdS($r_B m_B$) gal dcm[DE3]*	Sambrook *et al*., 1989, Novagen
DH5α	F^- Φ80*lacZ*ΔM15 Δ(*lacZYA-argF*) U169 *recA1 endA1 hsdR*17(r_K^-,m_K^+) *phoA supE*44 *thi*-1 *gyrA*99 *relA*1 λ	Taylor *et al*., 1993
B. subtilis		
NCIB3610	"Wilde type", prototrophic	Cohn 1930, Laboratory strain collection
PB39	NCIB3610 pPB39 (pLIKErep erm P_{lial-} *yaaT*-strep)	This work
PB72	NCIB3610 pPB72 (pLIKErep erm P_{lial} -*ymcB*-strep)	This work
PB74	NCIB3610 pPB74 (pLIKErep erm P_{lial} -*ymcB*-strep-*ricA*)	This work
GH11	NCIB3610 pGH11 (pLIKErep erm P_{lial} -*yjbN*-strep)	This work

10.3. Plasmids

Plasmids constructed in this work are listed in Table 13 and plasmids used in this work are listed in Table 14.

Table 13: Plasmids constructed in this work

Backbone	Insert	Tag	Name
pLIKErep	*yjbN*^{Bs}	C-Strep	pGH11
pET24d	*ricT*^{Gt}	NH_6	pGH67
pET24d	*ricT*^{Gt}	-	pGH68
pETduet	1. *ricA*^{Gt} 2. *ricF*^{Gt}	NH_6-RicA	pGH69
pET24d	ΔN1-25 *rny*^{Gt}	C-Strep	pGH72
pETduet	1. *ricA*^{Bs} E80A 2. *ricF*^{Bs}	NH_6-RicA	pGH77
pETduet	1. *ricA*^{Bs} E81A 2. *ricF*^{Bs}	NH_6-RicA	pGH78
pETduet	1. *ricA*^{Bs} E83A 2. *ricF*^{Bs}	NH_6-RicA	pGH79
pETduet	1. *ricA*^{Bs} 2. *ricF*^{Bs} K65A	NH_6-RicA	pGH80
pETduet	1. *ricA*^{Bs} 2. *ricF*^{Bs} R71A	NH_6-RicA	pGH81
pETduet	1. *ricA*^{Bs} 2. *ricF*^{Bs} R78A	NH_6-RicA	pGH82
pETduet	1. *ricA*^{Bs} E80A E81A 2. *ricF*^{Bs}	NH_6-RicA	pGH84
pETduet	1. *ricA*^{Bs} E81A E83A 2. *ricF*^{Bs}	NH_6-RicA	pGH85
pETduet	1. *ricA*^{Bs} E80A E83A 2. *ricF*^{Bs}	NH_6-RicA	pGH86
pETduet	1. *ricA*^{Bs} E80A E81A E83A 2. *ricF*^{Bs}	NH_6-RicA	pGH89

Table 14: Plasmids used in this work

Backbone	Insert	Tag	Name
pLIKErep	*yjbN*^{Bs}	C-Sterp	pGH11
pET24d	*ricT*^{Gt}	N-H_6	pGH67
pET24d	*ricT*^{Gt}	-	pGH68
pETduet	1. *ricA*^{Gt} 2. *ricF*^{Gt}	N-H_6-RicA	pGH69
pET24d	ΔN1-22 *rny*^{Gt}	C-Strep	pGH72
pETduet	1. *ricA*^{Bs} E80A 2. *ricF*^{Bs}	N-H_6-RicA	pGH77
pETduet	1. *ricA*^{Bs} E81A 2. *ricF*^{Bs}	N-H_6-RicA	pGH78
pETduet	1. *ricA*^{Bs} E83A 2. *ricF*^{Bs}	N-H_6-RicA	pGH79
pETduet	1. *ricA*^{Bs} 2. *ricF*^{Bs} K65A	N-H_6-RicA	pGH80
pETduet	1. *ricA*^{Bs} 2. *ricF*^{Bs} R71A	N-H_6-RicA	pGH81
pETduet	1. *ricA*^{Bs} 2. *ricF*^{Bs} R78A	N-H_6-RicA	pGH82
pETduet	1. *ricA*^{Bs} E80A E81A 2. *ricF*^{Bs}	N-H_6-RicA	pGH84
pETduet	1. *ricA*^{Bs} E81A E83A 2. *ricF*^{Bs}	N-H_6-RicA	pGH85
pETduet	1. *ricA*^{Bs} E80A E83A 2. *ricF*^{Bs}	N-H_6-RicA	pGH86
pETduet	1. *ricA*^{Bs} E80A E81A E83A 2. *ricF*^{Bs}	N-H_6-RicA	pGH89
pETduet	1. *ricA*^{Bs} 2. *ricF*^{Bs}	N-H_6-RicA	pPB65
pLIKErep	*ricT*^{Bs}	C-Strep	pPB39
pLIKErep	*ymcB*^{Bs}	C-Strep	pPB72
pLIKErep	*ymcB*^{Bs}-*ricA*^{Bs}	C-Strep-YmcB	pPB74
pET24d	*ricT*^{Bs}	-	pPB6

10.4. Oligonucleotides

All oligonucleotides used in this work were purchased from Sigma-Aldrich, Hamburg, Germany and are listed in Table 15.

Table 15: Oligonucleotides. Restriction sites are underlined and mentioned, promoters are in italics, ribosomal binding sites are in bold and italics, translation start codons are in bold and underlined and translation stop codons are in italics and underlined.

Name	Sequence (5'→3')[1]	Description
GH13	ttaaTCTAG**ATG**CAAAACAGAATCGAAATTT	Fwd C-Strep *yjbN*^{Bs}
GH14	ttaaAAGCTT*TTA***CTTTTCGAACTGCGGGTGGCTCCATCCTGC**TAAAAACACGC GTTTCAC	Rev C-Strep *yjbN*^{Bs}
GH131	ttaaGGTCTCCC**ATG**Ggc**CATCATCACCATCACCAC**TATACTGTAGTCGGCGTC C	Fwd H_6-*ricT*^{Gt}
GH132	ttaaCTCGAGGAGACC*TTA*ATCTGCGACACGAATCG	Rev *ricT*^{Gt}
GH133	ttaaGGTCTCCC**ATG**GgcTATACTGTAGTCGGCGTCC	Fwd *ricT*^{Gt}
GH134	ttaaCC**ATG**Ggc**CATCATCACCATCACCAC**GCAAAATATACGCGGGATG	Fwd H_6-*ricA*^{Bs}
GH135	ttaaGGATCC*TTA*ATGGCAACCACCCTG	Rev *ricA*^{Bs}
GH136	ttaaCATATGAGGATTGCTACTCTCGAGC	Fwd *ricF*^{Bs}
GH137	ttaaGATATC*TTA*TGTGCGGCAACCGC	Rev *ricF*^{Bs}
GH138	ttaaCC**ATG**GgcGCAAAATATACGCGGGATG	Fwd *ricA*^{Bs}
GH139	ttaaGGTCTCCC**ATG**GcCGCAAATCGATTGCCG	Fwd ΔN1-22 *rny*^{Gt}
GH140	ttaaCTCGAGGAGACC*TTA***CTTTTCGAACTGCGGGTG**GCTCCATTTCGCATATT CGACCGC	Rev *rny*^{Gt}-Strep
GH146	aggagGGTCTCaa**GCA**GAGCTTGAAGAGATTCCTGTTATC	Fwd *ricA*^{Bs} E80A
GH147	aggagGGTCTCc**TGC**TTGCAGCGCGTCAATT	Rev *ricA*^{Bs} E80A
GH148	aggagGGTCTCaa**GCA**CTTGAAGAGATTCCTGTTATCCAG	Fwd *ricA*^{Bs} E81A
GH149	aggagGGTCTCg**TGC**TTCTTGCAGCGCGTCAA	Rev *ricA*^{Bs} E81A
GH150	aggagGGTCTCtt**GCA**GAGATTCCTGTTATCCAGGAATTC	Fwd *ricA*^{Bs} E83A
GH151	aggagGGTCTCc**TGCA**AGCTCTTCTTGCAGCG	Rev *ricA*^{Bs} E83A

GH152	aggagGGTCTCgc**GCA**TATCATCCTGACTATAGAGAAATATCCC	Fwd *ricF*^{Bs} K65A
GH153	aggagGGTCTCa**TGC**GCCAAAACGCTGTACATC	Rev *ricF*^{Bs} K65A
GH154	aggagGGTCTCat**GCA**GAAATATCCCGGAAAATGAGGG	Fwd *ricF*^{Bs} R71A
GH155	aggagGGTCTCc**TGC**ATAGTCAGGATGATATTTGCCAAAAC	Rev *ricF*^{Bs} R71A
GH156	aggagGGTCTCtg**GCA**GAGATCAAACGTGAGCTGG	Fwd *ricF*^{Bs} R78A
GH157	aggagGGTCTCt**TGC**CCGGGATATTTCTCTATAGTCAGG	Rev *ricF*^{Bs} R78A
GH158	aggaGGTCTCca**GCA**CTTGAAGAGATTCCTGTTATCCAG	Fwd *ricA*^{Bs} E80A E81A
GH159	aggaGGTCTCg**TGC**TGCtTGCAGCGCG	Rev *ricA*^{Bs} E80A E81A
GH160	aggaGGTCTCaa**GCA**GAGCTtGCAGAGATTCCTG	Fwd *ricA*^{Bs} E80A E83A
GH161	aggaGGTCTCc**TGC**TTGCAGCGCGTCAAT	Rev *ricA*^{Bs} E80A E83A
GH162	aggaGGTCTCaa**GCA**CTtGCAGAGATTCCTGTTATCC	Fwd *ricA*^{Bs} E81A E83A
GH163	aggaGGTCTCg**TGC**TTCTTGCAGCGCGTC	Rev *ricA*^{Bs} E81A E83A
GH168	ttaaGGTCTCtt**GCA**GAGATTCCTGTTATCCAGGAATTC	Fwd *ricA*^{Bs} E80A E81A E83A
GH169	ttaaGGTCTCc**TGC**AAGTGCTGCtTGCAG	Rev *ricA*^{Bs} E80A E81A E83A

10.5. Bioinformatic tools and software

Used tools and software products are listed in Table 16 and Table 17.

Table 16: Used bioinformatic tools and web pages

Tool / URL	Provider	Application
Google Scholar https://scholar.google.de/	Google Inc.	Literature research
PubMed https://www.ncbi.nlm.nih.gov/pubmed/	National Institutes of Health, USA	Literature research
SubtiWiki http://subtiwiki.uni-goettingen.de/	General Microbiology, Georg-August-Universität, Göttingen	Information about genes and proteins from *B. subtilis*
UniProt http://www.uniprot.org/	UniProt consortium EMBL-EBI, SIB, PIR	Information about protein functions, sequences and domains
NCBI https://www.ncbi.nlm.nih.gov/	National Institutes of Health, USA	Literature research and information about genomes
MUSCLE https://www.ebi.ac.uk/Tools/msa/muscle/	Madeira *et al.*, 2019, EMBL	Alignment of nucleotide and peptide sequences

Table 17: Software products

Program	Producer	Application
SnapGene V 5.08	Biomatters Ltd.	Genetic analysis, primer design, analysis of sequence data, information on proteins
Mendeley Desktop 1.17.11	Mendeley Ltd.	Reference management
CryoSPARC	Punjani *et al.*, 2017	Analysis and reconstruction of cryo-EM data
Image Lab™	Bio-Rad	Analysis of UV-Vis signals and image processing of agar plates and imaging of SDS-PAGE
Image J 1.49 t	National Institutes of Health, USA	Processing of microscopic images
Perseus v1.6.14.0	Tyanova, Max-Planck-Institute, Germany	Evaluation of mass spectroscopy data of CoIP experiments
PyMOL 2.4	Schrödinger Inc., USA	Depiction of crystallographic data and analysis
CCP4	Collaborative Computational Project Number 4, 1993, UK	MR, data processing of crystal data and follow up evaluation
COOT	GNU General Public License	Molecular modeling
UNICORN 7	cytiva Global Life Sciences Solutions, USA	Programming and control of ÄKTAs
NovaMALS software	Postnova Analytics, Germany	Analysis and acquisition of the MALS data
AcquireMP v2.3.0	Refeyn, UK	Acquisition of mass photometry data
DiscoverM v2.2.0	Refeyn, UK	Evaluation of mass photometry data
DynamX HDX Data Analysis Software 3.0	Waters Corporation, USA	Analysis of HDX data
GraphPad Prism 8.4.3	GraphPad Software, USA	Plotting of MALS and SEC data
Microsoft® Office	Microsoft® Inc	Processing of images, text and data

10.6. Supplementary data

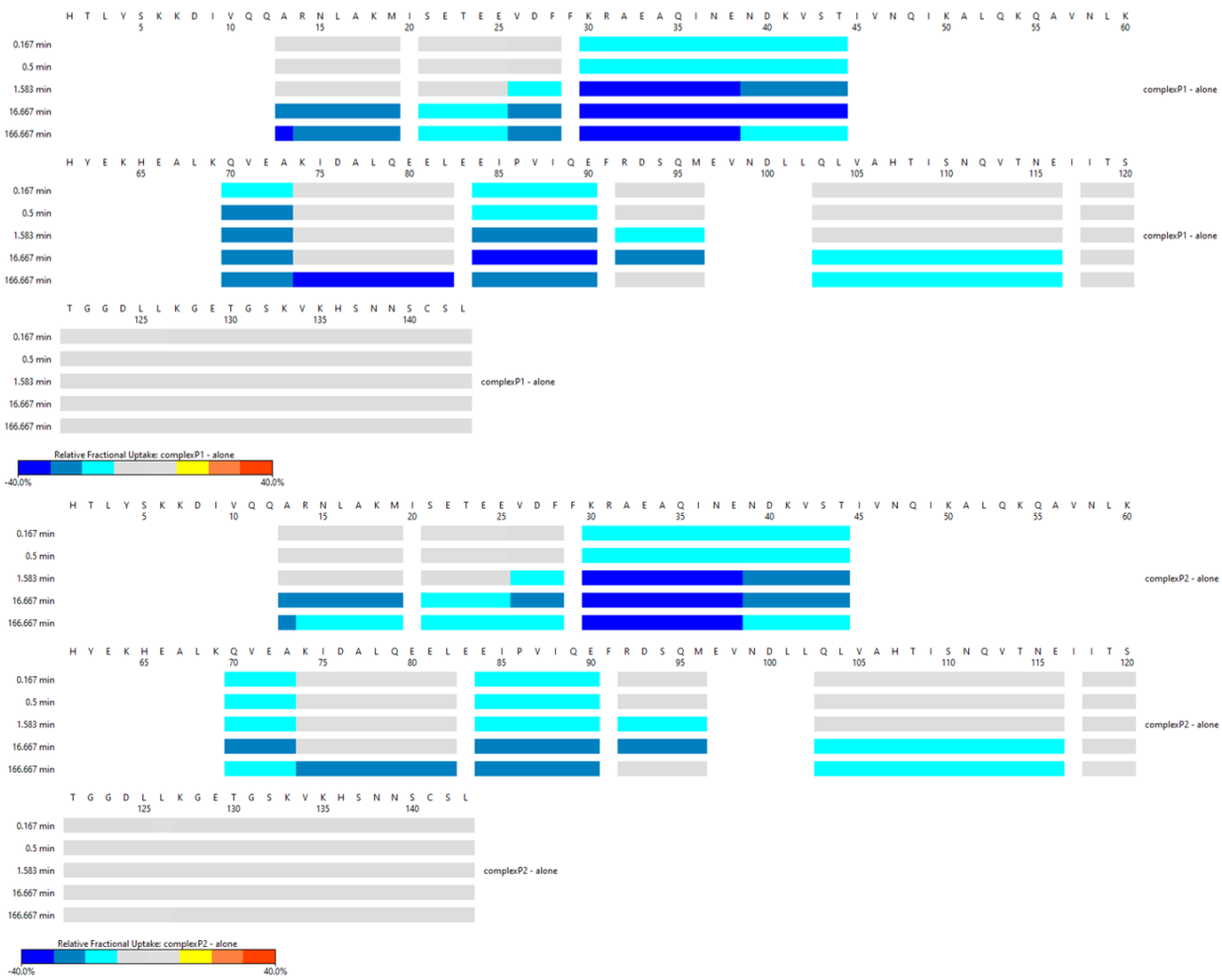

Figure 46: HDX data of *Bs*RicA of the RicAFT complex peak 1 and peak 2 in comparison to the *Bs*RicAF complex
*Bs*RicA peptides relative deuterium exchange. The darker the fewer deuterium was incorporated in the RicAFT complex, the brighter the areas the more the deuterium exchange.

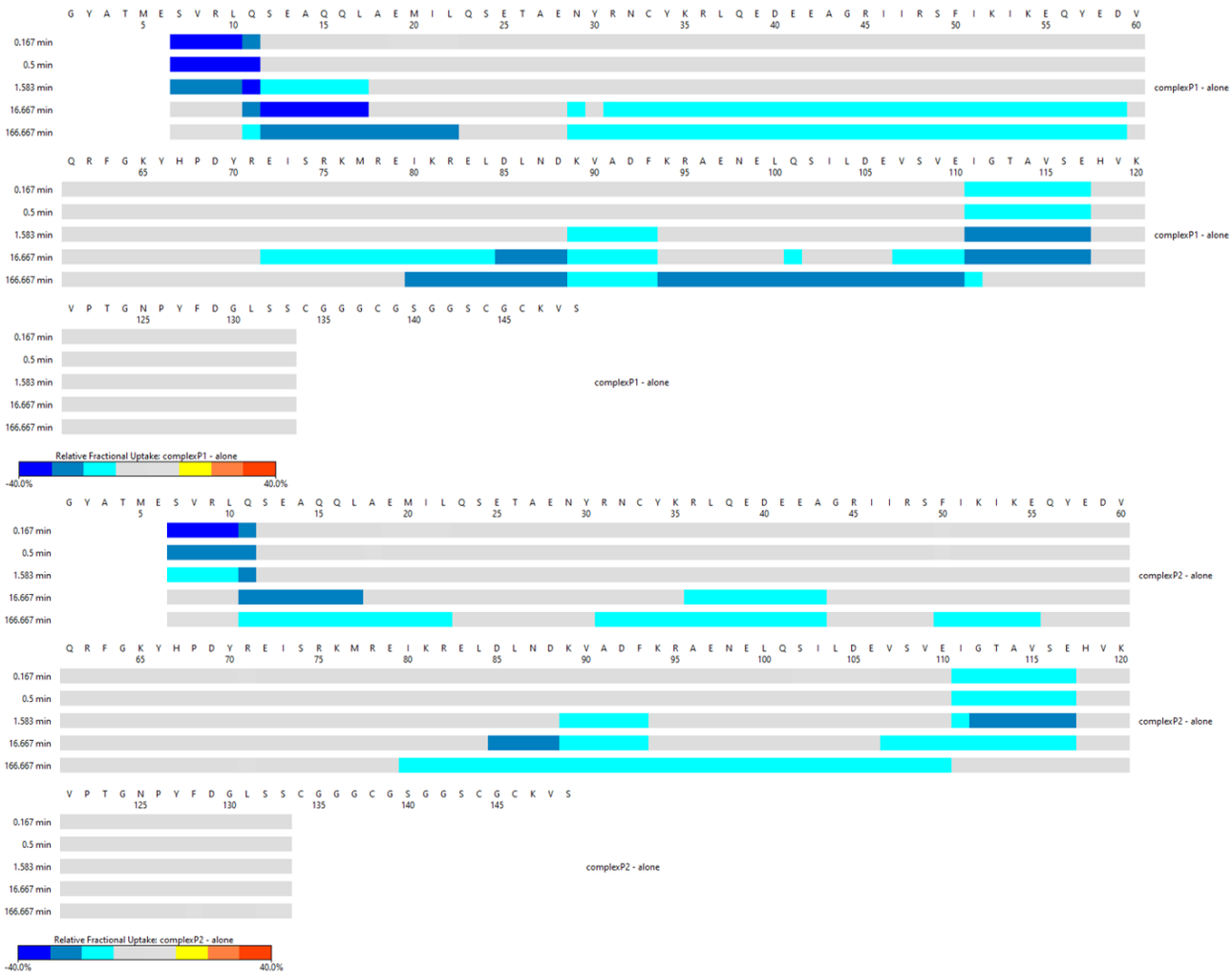

Figure 47: HDX data of *Bs*RicF of the RicAFT complex peak 1 and peak 2 in comparison to the *Bs*RicAF complex
*Bs*RicF peptides relative deuterium exchange. The darker the fewer deuterium was incorporated in the RicAFT complex, the brighter the areas the more the deuterium exchange.

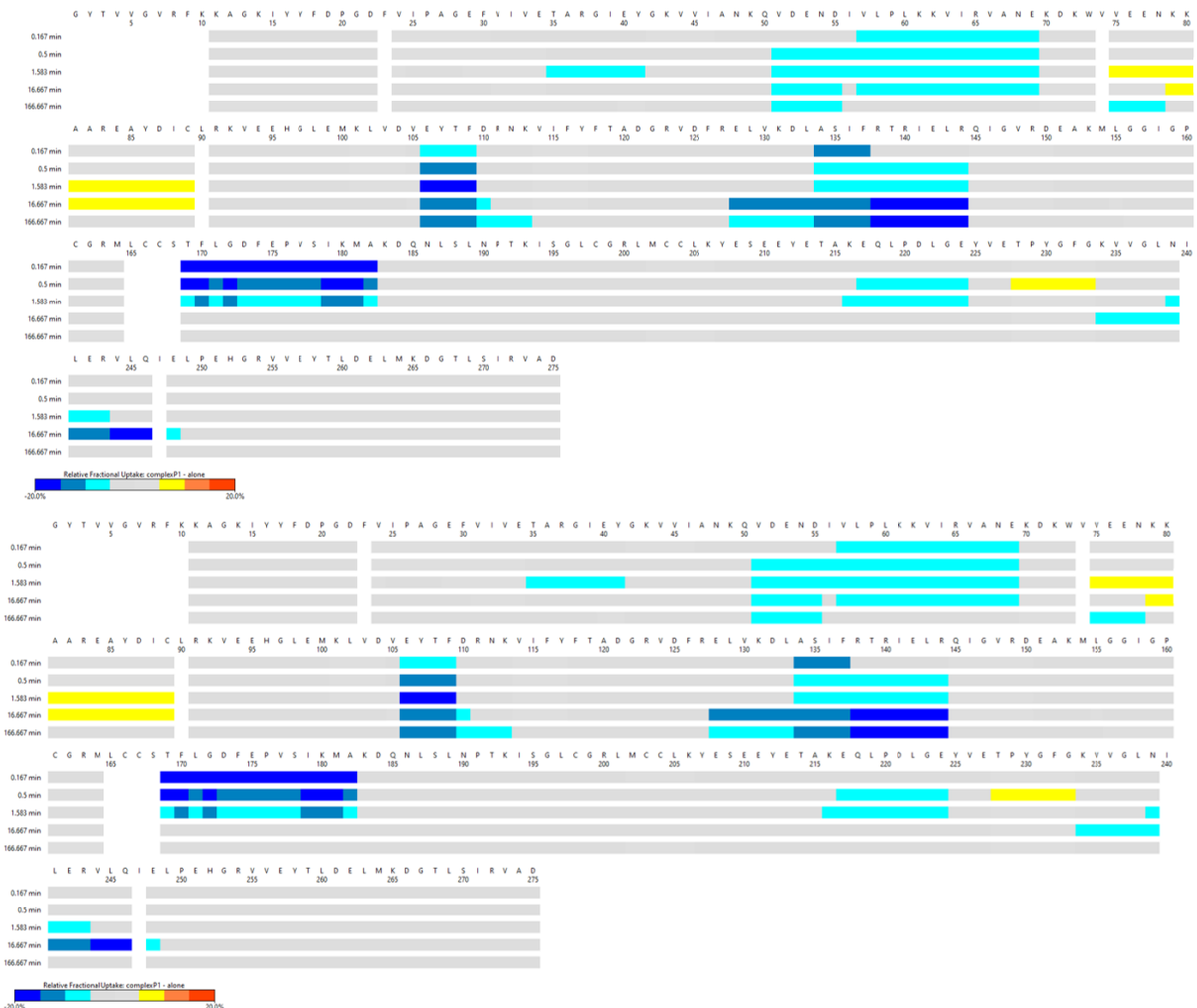

Figure 48: HDX data of *Gt*RicT of the RicAFT complex peak 1 and peak 2 in comparison to individual protein
*Gt*RicT peptides relative deuterium exchange. The darker the fewer deuterium was incorporated in the RicAFT complex, the brighter the areas the more the deuterium exchange.

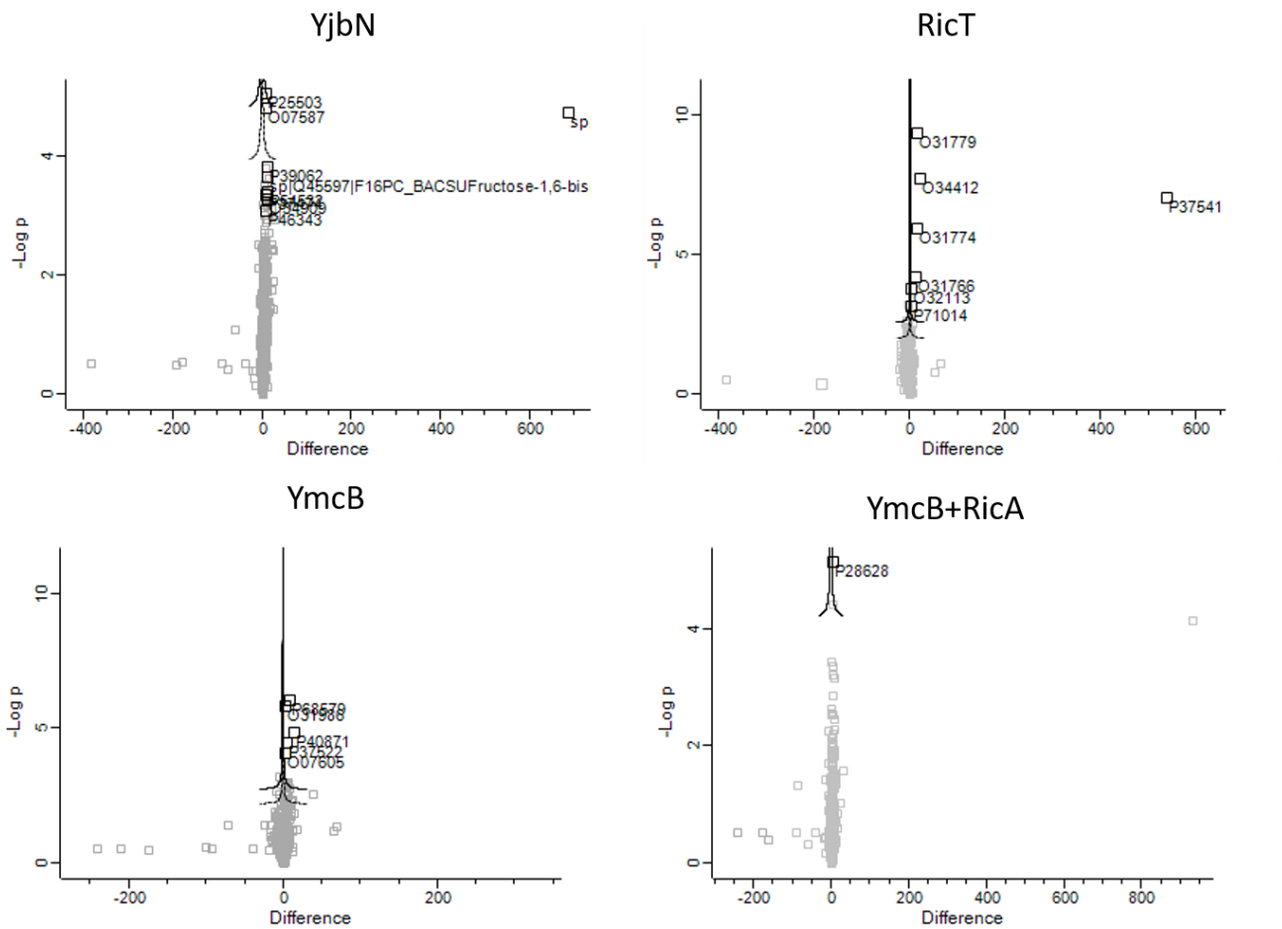

Figure 49: Volcano plots of the CoIP experiments.

The proteins designation of the bate protein is shown above the respective plot. The solid line is the 5 % confidence interval and the dotted line the 10 % confidence interval. The proteins chosen for the tables of the CoIP experiments are marked as solid black squares and denoted with their accession number.

Wissenschaflicher Werdegang

Gregor Hoffmann

Geboren am 9. September 1993 in Hann. Münden

E-Mail: hoffmann.gregor@googlemail.com

Ausbildung:

01/2018 - 12/2020	Doktorarbeit SYNMIKRO, Philipps-Universität Marburg, Deutschland Betreuer: Prof. Dr. Gert Bange
10/2015-11/2017	Master of Science, MSc (Biochemie und Molekularbiologie) Georg-August Universität Göttingen, Deutschland Betreuer: Dr. Fabian Commichau
09/2012-09/2015	Bachelor of Science, BSc (Biologie) Georg-August Universität Göttingen, Deutschland Betreuer: Prof. Dr. Gerhard Braus
07/2012	Allgemeine Hochschulreife Grotefend-Gymnasium, Hann. Münden, Deutschland

Beteiligungen an Konferenzen und Meetings:

09/2018	How microorganisms view their world, Marburg, Konferenzzentrum Erwin-Piscator-Haus, Deutschland TÜBINGEN SFB
11/2018	SFB987 Spotlight meeting, Marburg, Deutschland
11/2019	Posterpräsentation, SFB987 Spotlight meeting, Marburg, Deutschland

Erklärung der selbstständigen Erarbeitung der Dissertation

Hiermit erkläre ich, dass ich die vorliegende Dissertation:

"Structural and biochemical analysis of the RicAFT complex"

Selbständig und ohne unerlaubte Hilfsmittel angefertigt habe. Es wurden keine anderen, als der von mir ausdrücklich angegebenen Hilfsmittel verwendet. Die Dissertation wurde in der jetzigen oder in einer ähnlichen Form noch bei keiner Hochschule eigereicht.

Es handelt sich bei den heute von mir eingereichten Exemplaren um in Wort und Bild völlig übereinstimmende Exemplare.

Des Weiteren erkläre ich, dass die digitalen Abbildungen ausschließlich originale Daten enthalten und in keinem Fall inhaltsverändernde Bildbearbeitung vorgenommen wurde.

Marburg, den

_____

Gregor Hoffmann